

**Computational Studies, using Density Functional
Theory, of Proton Transfer through Polymer
Electrolyte Membrane in Fuel Cells, as well as of
Hydrogenation and Dehydrogenation Reactions using
Frustrated Lewis Pairs**

Thesis Submitted to AcSIR for the Award of
the Degree of

DOCTOR OF PHILOSOPHY
In Chemical Sciences



By

MANOJ VASISHT MANE

Registration Number: **10CC11J26029**

Under the Guidance of
DR. KUMAR VANKA

**Physical and Materials Chemistry Division
CSIR-NATIONAL CHEMICAL LABORATORY
PUNE – 411008, INDIA**

September 2015



सीएसआयआर-राष्ट्रीय रासायनिक प्रयोगशाला

(वैज्ञानिक तथा औद्योगिक अनुसंधान परिषद)

डॉ. होमी भाभा मार्ग, पुणे - 411 008, भारत

CSIR-NATIONAL CHEMICAL LABORATORY

(Council of Scientific & Industrial Research)

Dr. Homi Bhabha Road, Pune - 411008, India



Certificate

This is to certify that the work incorporated in this Ph.D. thesis entitled “*Computational Studies, using Density Functional Theory, of Proton Transfer through Polymer Electrolyte Membrane in Fuel Cells, as well as of Hydrogenation and Dehydrogenation Reactions using Frustrated Lewis Pairs*” submitted by **Mr. Manoj V. Mane** to Academy of Scientific and Innovative Research (AcSIR) in fulfillment of the requirements for the award of the Degree of **Doctor of Philosophy In Chemical Sciences**, embodies original research work under my supervision. I further certify that this work has not been submitted to any other University or Institution in part or full for the award of any degree or diploma. Research material obtained from other sources has been duly acknowledged in the thesis. Any text, illustration, table etc., used in the thesis from other sources, have been duly cited and acknowledged.

Mr. Manoj V. Mane
(Student)

Dr. Kumar Vanka
(Supervisor)

Communications Channels	☎	FAX	WEBSITE
	NCL Level DID : 2590	Director's Office : +91-20-25902601	www.ncl-india.org
	NCL Board No. : +91-20-25902000	COA's Office : +91-20-25902660	
Four PRI Lines : +91-20-25902000	SPO's Office : +91 20 25902664		

DECLARATION BY RESEARCH SCHOLAR

I hereby declare that the work incorporated in this thesis entitled "*Computational Studies, using Density Functional Theory, of Proton Transfer through Polymer Electrolyte Membrane in Fuel Cells, as well as of Hydrogenation and Dehydrogenation Reactions using Frustrated Lewis Pairs*" submitted by me for the degree of Doctor of Philosophy in Chemical Sciences to the AcSIR is the record of the work I have carried out under the supervision of Dr. Kumar Vanka, is original and has not formed the basis of award of any degree or diploma. Such material as has been obtained from other sources has been duly acknowledged in this thesis.

Date: 15/09/2015



Manoj Vasisht Mane

Physical Chemistry Division

CSIR- National Chemical Laboratory

Pune-411008

Dedicated to
My Beloved Parents
And
Wife Manisha and Daughter Manasvini ...

ACKNOWLEDGEMENTS

It is my great pleasure to thank all the people who have helped and supported me throughout my Ph.D life.

I especially thank my research supervisor, **Dr. Kumar Vanka**, for his valuable guidance and scholarly inputs. I feel extremely fortunate to have worked under his supervision. He has given me a continuous flow of freedom, support, guidance and encouragement throughout the whole research period. I believe that he has been a fantastic advisor, who taught me how to do research and to think independently. Also, he motivated me to enjoy books and movies along with research, which has allowed me to know about so many new things. I am really thankful to him for making my research life smooth and enjoyable.

I express warm thanks to my DAC members Dr. Neelanjana Sengupta, Dr. Sarika Bhattacharyya, Dr. Mugdha Gadgil and my external expert Dr. Arun Venkatnathan (IISER, Pune) whose contribution in stimulating suggestions and encouragement has helped me to improve my work.

I would also like to thank Dr. Vijayamohan K. Pillai, Director, CSIR-NCL and Dr. Anil Kumar, Head and Chairman of the Physical and Materials Chemistry division for providing me with all the infrastructural facilities. I am grateful to CSIR, New Delhi, for the research fellowship and to the Academy of Scientific & Innovative Research (AcSIR) for giving me an opportunity to pursue my doctoral degree.

I also want to thank Dr. Sourav Pal (former director CSIR – NCL) for his wonderful and inspiring classroom lectures, as well as Dr. Nayana Vaval, Dr. Kavita Joshi, Dr. Durba Sengupta and Dr. Ajithkumar for the course work classes.

I am grateful to all collaborators, including Dr. Rahul Banerjee, Dr. Nitin T. Patil, Dr. Akkattu Biju, Dr. Ashutosh A. Kelkar, Dr. Soumen Mukherjee, Dr. Bhahwal Shah. My heartiest thanks go to all my school, college and university teachers, whose teaching, encouragement and suggestions helped me a lot. I especially wish to thank Dr. R. A. Mane, Dr. Chondekar, Dr. Arbad, Dr. Shingare, Dr. Lande, Mr. Autade, Mr. Dhotare, Mr. Mote, Mr. Khose, Mr. Jagdale, Mr. Munde, Mr. Jagtap and Mr. Gopalkar. I also had the fortune of interacting with the new scientists of in the computational chemistry group: Dr. Debashree Ghosh and Dr. Suman Chakrabarty. I also want to thank my all seniors and colleagues who have offered unconditional support and help during my Ph.D. study. I can never for the assistance

and helpful advice from my seniors Dr. Bhaskar Sathe, Dr. Kishor Harale, Dr. Ravi Jagtap, Dr. Rahul Patil, Dr. Prakash Chavan, Santosh Chavan, Dr. Satish Biradar, Dr. Dhanaraj Shinde, Dr. Rahul Kavthe, Dr. Valmik Shinde and many more.

A special thanks goes to all labmates Shantanu Kadam, Nishamol Kuriakose, Yuvraj Dangat, Amrita Pal, Jugal Kumawat, Jaya C. Jose, Himadri Pathak, Prathit Chatterjee, Tamal Das, Subrashish Banerjee, Kamalika Ghatak, Lalita, Subrata, Sayali, Anagha, Deepti, Sneha Menon, Aryya, Nupur Bansal, Sumantra, Susanta, Achintya, Turbasu, Sudip, Manzoor, Anil, Chandan, Prithvi, Swagata, Souvik, Vidhika, Madhulita, Saba, Baljinder, Vaibhav, Samik, Rahul, Mukunda, Mudit, Deepak, Dr. Masood, Vipin Raj and Shailaja for sharing their truthful and illuminating views on a number of issues related to my work. I would like to thank all my beloved friends: Suhas Bhosale, Dr. Govind Pawar, Sunil, Amar, Sambhaji Dhumal, Nagnath, Ishwar, Sandip, Ganesh, Harshal, Kilash, Dr. Nagesh, Manik, Satej, Anil, Sharad, Shekhar, Dr. Ravi G., Shrikant, Vijay, Nilesh, Balasaheb, Sunil, Rupesh, Shridhar, Tukaram, Mangesh, Dr. Ketan, Dr. Shilpi, and many more, also Marathi@ncl friends and all my juniors from Aurangabad.

I also acknowledge my grandmother for her encouragement to me for completing higher education. I am very lucky to get kind and unwavering support from both my families. I owe a lot to my mother, father, and mother-in-law, and father-in-law, who have encouraged and helped me at every stage of my personal and academic life, and longed to see this achievement come true. My sincere thanks to my beloved sister *Mangal* and brother *Vaibhav* for their endless support. I also thank my cousin sisters and brothers *Manisha*, *Swati*, *Mukeshand Sudarshan* for being there since my childhood and niece *Sharvari* and nephew *Advay*. I would like to express my deepest appreciation to my better half *Mrs. Manisha* for her love, kindness, aspiration and for her unconditional encouragement and the adjustment which she has shown during the past one and a half year that it has taken me to finalize this thesis and to our dearest daughter *Manasvini*, who completes our life in every way. I am very much indebted to my whole family, my family that has supported me in every possible way to see the completion of this research work.

Manoj Vasisht Mane

TABLE OF CONTENTS

Abstract	v
Abbreviations	viii
List of publications	x

1	Introduction to Fuel Cell and Frustrated Lewis Pairs	1
	1A: Proton Transfer in Fuel cells	4
1.1	Polymer electrolyte or proton exchange membrane fuel cells (PEMFCs)	6
1.2	Proton Conducting Materials	7
1.3	The Proton Transfer Mechanism	9
	1B: Frustrated Lewis Pairs (FLP)	10
1.4	FLPs Activation of H ₂	12
1.5	Reactions of Frustrated Lewis Pairs with Saturated/Unsaturated Compounds	
	i) Dehydrogenation of Alcohols	14
	ii) Hydrogenation of imines and oximes	15
	iii) Hydrogenation of ketone and aldehyde	16
1.6	Scope of the thesis	17
1.7	References	18

2	Theoretical Methods and Computational Details	29
2.1	The many-body problem or (Basic Quantum Mechanics)	31
2.2	Density Functional Theory (DFT)	32
	2.2.1 Thomas-Fermi Theorem	32
	2.2.2 Hohenberg-Kohn Theorem	33

2.2.3	Kohn-Sham Equations	35
2.2.4	Exchange-Correlation Functionals	36
	a) The local-density approximation (LDA)	37
	b) The generalized-gradient approximation (GGA)	37
	c) The meta-GGA	38
	d) The hybrid functionals	38
2.3	RI-J and MARI-J approximations	39
2.4	Solvent Correction	39
2.5	Energetic Span Model	40
2.6	References	42

3 Exploring the Potential of Doped Zero-Dimensional Cages for Proton Transfer in Fuel Cells 47

3.1	Introduction	49
3.2	Computational Details	51
3.3	Results and Discussion	53
	3.3.1 Proton Transfer through <i>N-cage</i> in Tandem with H ₃ PO ₄	53
	3.3.2 Proton Conduction Studies	59
	3.3.3 Proton Transfer with 1,2,4 triazole	62
3.4	Conclusions	65
3.5	References	66

4 Proposing Efficient New Pendant Group Polymer Electrolyte Membranes for Fuel Cells 69

4.1	Introduction	71
4.2	Computational Details	75
4.3	Results and Discussion	76

4.3.1	The Mono-aza Crown Ether Case	76
4.3.2	The Di-aza Crown Ether Case	80
4.3.3	The Tri aza-crown Ether Case	84
4.4	The Relative Efficiencies of the Different PEMs Considered: Overall Picture	87
4.5	Conclusion	88
4.6	References	89

5 Computational Study of Metal Free Alcohol Dehydrogenation Employing Frustrated Lewis Pairs 93

5.1	Introduction	95
5.2	Computational Details	97
5.3	Results and Discussion	98
5.3.1	Strategy I	103
5.3.2	Strategy II	105
5.3.3	Strategy III	108
5.3.4	Strategy IV	112
5.5	Conclusion	116
5.6	References	116

6 A Computational Study of the Hydrogenation of Unsaturated Substrates (C=O, C=N, C=C) Catalyzed by Frustrated Lewis Pairs 121

6.1	Introduction	123
6.2	Computational Details	126
6.3	Results and Discussion	127
6.3.1	Hydrogen Splitting	128

6.3.2 Hydrogenation by B/N pairs	129
6.3.3 Hydrogenation by HB(C ₆ F ₅) ₂ and P/B FLP pairs	138
6.5 Conclusion	143
5.6 References	143
<hr/>	
7 Summary	149
<hr/>	

Abstract of the Thesis

The production of molecular hydrogen (H_2) through electrochemically, photochemically, or thermal means offers an obvious way to capture energy and thus provide “greener” energy for the future. Hydrogen itself is not only a fuel but also can be processed to produce other fuels, and it is an essential material for chemical production, metal refining, food processing and electronics manufacturing. It is not freely available. It is produced by the chemical conversion of fuels such as hydrocarbons and alcohols. The present research work is thus focused on the possibilities of chemistry with dihydrogen: the efficient proton transfer from anode to cathode through the polymer electrolyte membrane (PEM) in fuel cells and the mechanistic study of hydrogenation-dehydrogenation reactions by using transition metal free catalysts. In this thesis, to solve the difficulties existing in current high temperature PEM systems based on H_3PO_4 and imidazole, particularly with regard to the “reorientation barrier”, new types of proton conducting species, like triazole, tetrazole and pendant crown ethers have been explored, and have been shown computationally to have high proton conductivity and also effectively transfer protons through the membrane.

The other aspect of the chemistry of dihydrogen that has been considered in this thesis is the investigation of new designs of transition metal free systems towards catalyzing hydrogenation-dehydrogenation reactions. The study of the kinetics and thermodynamics of chemical reaction mechanisms has been investigated using density functional theory (DFT).

This thesis, entitled “Computational Studies, using Density Functional Theory, of Proton Transfer through Polymer Electrolyte Membrane in Fuel Cells, as well as of Hydrogenation and Dehydrogenation Reactions using Frustrated Lewis Pairs” is organized into six chapters.

Chapter 1: This chapter is divided into two parts: fuel cell (1A) and frustrated Lewis pairs (1B). The first section starts with a brief history of fuel cells and polymer electrolyte membranes along with the motivation for working on PEM fuel cells that can operate at higher temperatures. This is followed by the discussion on the proton

conducting materials widely used in PEMs, as well as proton transfer mechanisms, with the literature survey of previous experimental and theoretical studies in this area. The second section of this chapter provides an introduction to frustrated Lewis Pairs (FLPs) that typically consist of main-group Lewis acids and bases, and can be used to effect a variety of small molecule activations. The modulation of FLP based catalysts is of high interest as this affords the reduction-oxidation of systems, with the efficacy varying with the varying electronic properties of catalysts. The review of the literature showcasing the development of the hydrogenation-dehydrogenation of imines, oximes, ketones, enamines alcohol and C=C bonds has been provided. The chapter ends with the scope of the thesis.

Chapter 2: This chapter focuses on the theoretical background and the computational details used in the present work. Initially, we discuss the density functional theory (DFT) approach, which includes the Hohenberg-Kohn theorems, Kohn-Sham equations and Exchange-Correlation functionals. This is followed by a discussion of the resolution of identity (RI), and with the multipole accelerated resolution of identity (MARIJ) approximations. The chapter ends with the solvent corrections and the Energetic Span Model (ESM) to calculate the Turn Over Frequency (TOF) from a theoretically obtained energy profile.

Chapter 3: In this chapter is described the recently synthesized zero-dimensional (0D) nitrogen-based porous structures that have been experimentally found to be stable at high temperatures. A hydrogenated 0D cage can be easily doped with hydrogen bonding bases such as phosphoric acid, imidazole, and 1,2,3- and 1,2,4-triazoles. Chapter 3 discussed investigations with DFT that have been done to determine the feasibility of each of these dopants acting as an effective counterpart to the hydrogenated 0D cage for proton transfer at high temperature. Therefore, it is likely that the effectiveness of the proposed fuel cell membrane would also be high at the higher temperatures.

Chapter 4: The need for low-cost, clean, efficient future energy has stimulated a great amount of interest in the modern age. There is a need to develop new membranes for fuel cells that can conduct protons with high efficiency and at high temperatures. This chapter discussed the computational study of newly proposed

proton transfer PEMs, having pendant nitrogen containing crown ether groups on an alkyl backbone. What is proposed is a new design of nitrogen containing pendant group PEMs that can eliminate the need for a reorientation barrier during the proton transfer process.

Chapter 5: This chapter focuses on dihydrogen generation chemistry. The catalysis of alcohol dehydrogenation is an important area of research. Transition metals are known to be effective catalysts for this reaction, but developing metal free catalytic systems would lead to highly desirable cheaper and greener alternatives. In this regard, the chapter describes investigations of new design strategies that can be employed for alcohol dehydrogenations by using metal free frustrated Lewis pairs (FLPs). A careful study of 36 different proposed FLP candidates reveals that several new FLPs can be designed from existing, experimentally synthesized FLPs, candidates that can rival or be even better than state-of-the-art transition metal based systems in catalyzing the alcohol dehydrogenation process.

Chapter 6: The advent of FLPs reactivity has brought up new perspectives in the realm of small molecule activation and their application in hydrogenation reactions. In this chapter, we have investigated the mechanism of metal-free catalytic hydrogenation by less frustrated and less sterically hindered FLPs, denoted as modified FLPs (MFLPs). In detail, mechanistic studies with DFT have been employed for a set of six MFLPs. In addition, a comparison of the turnover frequencies of FLPs and MFLPs has been done, with the results indicating that almost all the cases having MFLPs would have higher turnover frequency (TOF).

Chapter 7: Summary

ABBREVIATIONS

0D	Zero dimensional
AIMD	<i>Ab initio</i> molecular dynamics simulations
Ar ^F	2,4,6-tris(trifluoromethyl)phenyl
CC	Coupled cluster
CI	Configuration interaction
COSMO	Conductor-like screening model
CSM	Continuum solvation model
DFT	Density functional theory
DIBAL	Di-isobutylaluminum hydride
EF	Electric field
ESM	Energetic Span Model
ET	Electron transfer
FLP	Frustrated Lewis Pair
GGA	Generalized gradient approximation
HF	Hartree-Fock
HOMO	Highest occupied molecular orbital
KS	Kohn-Sham
LDA	Local density approximation
LUMO	Lowest unoccupied molecular orbital
LYP	Lee, Yang and Parr
MARIJ	Multipole accelerated resolution of identity
MFLP	Modified Frustrated Lewis Pair
MO	Molecular orbital
MP2	Second-order Møller–Plesset perturbation theory
MPV	Meerwein–Ponndorf–Verley
NBO	Natural bond orbital

PBE	Perdew, Burke and Ernzerhof
PCM	Polarizable continuum model
PEM	Polymer electrolyte membrane
PEMFC	Proton exchange or Polymer electrolyte membrane fuel cell
PW	Perdew and Wang
QM	Quantum mechanical
RI	Resolution of identity
SMD	Solvation Model Based on Solute Electron Density
^t Bu ₃ P	Tri-tert-butylphosphine
TDI	TOF determining intermediate
TDTS	TOF determining transition state
TF	Thomas-Fermi
TMP	2,2,6,6-tetramethylpiperidine
TM	Transition Metal
TS	Transition state
TST	Transition state theory
TOF	Turnover frequencies

List of Publications

1. **Manoj V. Mane**, Arun Venkatnathan, Kamalika Ghatak, and Kumar Vanka; Exploring the Potential of Doped Zero-Dimensional Cages for Proton Transfer in Fuel Cells: A Computational Study, *The Journal of Physical Chemistry B*, **2012**, 116 (32), 9803–9811.
2. Sharath Kandambeth, Arijit Mallick, Binit Lukose, **Manoj V. Mane**, Thomas Heine and Rahul Banerjee, Construction of crystalline 2D covalent organic frameworks with remarkable chemical (acid/base) stability via a combined reversible and irreversible route, *Journal of the American Chemical Society*, **2012**, 134, 19524-19527.
3. Kamalika Ghatak, **Manoj Mane**, and Kumar Vanka, Metal or Nonmetal Cooperation with a Phenyl Group: Route to Catalysis? A Computational Investigation, *ACS Catalysis*, **2013**, 3, 920-927.
4. Kamlesh N. Tayade, **Manoj V. Mane**, Suman Sen, C. N. Murthy, Gopal L. Tembe, S. Muthukumar Pillai, Kumar Vanka, Soumen Mukherjee, A catalytic and DFT study of selective ethylene oligomerization by nickel (II) oxime-based complexes, *Journal of Molecular Catalysis A: Chemical*, **2013**, 366, 238-246.
5. Santhivardhana Reddy Yetra, Anup Bhunia, Atanu Patra, **Manoj V. Mane**, Kumar Vanka, and Akkattu T. Bijua, Enantioselective N-Heterocyclic Carbene-Catalyzed Annulations of 2-Bromoaldehydes with 1,3-Dicarbonyl Compounds and Enamines via Chiral α,β -Unsaturated Acylazoliums, *Advanced Synthesis & Catalysis*, **2013**, 355, 1089 – 1097.
6. **Manoj V. Mane**, and Kumar Vanka, Proposing Efficient New Pendant Group Polymer Electrolyte Membranes for Fuel Cells: A Computational Study, *The Journal of Physical Chemistry C*, **2014**, 118 (2), 784–795.
7. Mudassir K. Munshi, Swapna M. Gade, **Manoj V. Mane**, Deepti Mishra, Sourav Pal, Kumar Vanka, Vilas H. Rane, Ashutosh A. Kelkar; 1, 8-Diazabicyclo [5.4. 0] undec-7-ene (DBU): A highly efficient catalyst in glycerol carbonate synthesis, *Journal of Molecular Catalysis A: Chemical*, **2014**, 391, 144-149.

8. Manjeet Kumar, Arvind Kumar, Masood Rizvi, **Manoj Mane**, Kumar Vanka, Subhash C. Taneja, Bhahwal Ali Shah, Synthesis of α , β -Unsaturated δ -Lactones by Vinyl Acetate Mediated Asymmetric Cross-Aldol Reaction of Acetaldehyde: Mechanistic Insights, *European Journal of Organic Chemistry*, **2014**, 5247–5255.
9. Masood Ahmad Rizvi, Mehvash Zaki, Mohd. Afzal, **Manoj Mane**, Manjeet Kumar, Bhahwal Ali Shah, Saurabh Srivastav, Saripella Srikrishna, Ghulam Mustafa Peerzada, Sartaj Tabassum, Nuclear blebbing of biologically active organoselenium compound towards human cervical cancer cell (HeLa): In vitro DNA/HSA binding, cleavage and cell imaging studies, *European Journal of Medicinal Chemistry*, **2015**, 90, 876–888.
10. Valmik S. Shinde, **Manoj V. Mane**, Kumar Vanka, Arijit Mallick, and Nitin T. Patil; Gold (I)/Chiral Brønsted Acid Catalyzed Enantioselective Hydroamination–Hydroarylation of Alkynes: The Effect of a Remote Hydroxyl Group on the Reactivity and Enantioselectivity, *Chemistry -A European Journal*, **2015**, 21(3), 975–979.
11. **Manoj V Mane**, Masood A Rizvi, Kumar Vanka, A Computational Study of Metal-free Alcohol Dehydrogenation Employing Frustrated Lewis Pairs, *The Journal of Organic Chemistry*, **2015**, 80 (4), pp 2081–2091.
12. Aslam C. Shaikh, S. Shalini, Ramanathan Vaidhyanathan, **Manoj V. Mane**, Ayan Kumar Barui, Chitta Ranjan Patra, Yeduru Venkatesh, Prakriti Ranjan Bangal and Nitin T. Patil,* , *European Journal of Organic Chemistry*, 2015, 22, 4860-4867.
13. **Manoj V Mane**, Kumar Vanka, A Computational Study of the Hydrogenation of Unsaturated Substrates (C=O, C=N, C=C) Catalyzed by Frustrated Lewis Pairs. (*Manuscript under preparation*)

Chapter 1

Introduction

Energy can be stored in different forms; as mechanical energy, as electrical energy and as the chemical energy of reactants and fuels, the utilization of which is one of the most important areas of research of the modern age of science. Storing chemical energy in the smallest molecule possible: dihydrogen, H₂, and unlocking the same in chemical reactions and in fuel cells is, therefore, a very extensive and important area of research. On the Earth, hydrogen is the most abundant element, but is present in the form of dihydrogen (H₂) in less than one percentage. H₂ is not freely available, so it has to be generated from H₂-rich fuels. It is generally generated by the chemical conversion of fuels such as hydrocarbons and alcohols. Dihydrogen is used in a range of industries, including chemical production, metal refining, food processing and electronics manufacturing.¹ The present thesis deals with this most important of molecules, and mainly consists of two parts. The first part contains a computational study of proton transfer barriers in newly proposed polymer electrolyte membranes (PEMs), in which dihydrogen is used as a basic source of fuel, converting chemical energy to electrical energy. The second part showcases the designing of new chemical systems that can do the important metal-free catalytic release of dihydrogen from alcohols, or catalyze the reaction of H₂ with ketones, imines, enamines and oximes to the corresponding hydrogenated products.

The first part, as mentioned in the previous paragraph, discusses polymer electrolyte membranes (PEMs) in fuel cells. Fuel cells are currently of great interest, because they are a key element in the emerging energy economy.² One of the most promising types of fuel cells is the proton exchange membrane fuel cell. The water in Nafion has been employed as a successful PEM in PEMFC,³ but it has some limitations. Therefore, in order to make the proton transfer more efficient, we need to propose new materials for use as PEMs and investigate their potential for efficient proton transfer through the membrane. This is the focus of the chapters 3 and 4 of this thesis.

The second part of the thesis discusses reactions involving dihydrogen. The oxidation-reduction of organic compounds are well-known and important reactions in organic chemistry. Among various methods, the widely used transition metal-catalyzed ones play a key role in these transformations of hydrogenation-dehydrogenation reactions.^{4,5} To overcome the disadvantages of transition metal based systems, the substitution of transition metal based systems with main group

systems such as frustrated Lewis pairs (FLPs)⁶ is an attractive option, because this can lead to cheap and green catalyst systems. The focus of the current work is to investigate these possibilities through the computational investigations using density functional theory (DFT). As the chapters 3 to 6 of the thesis will show, this will give a better understating of proton transfer in fuel cells and hydrogenation-dehydrogenation reactions using FLPs. A detailed background that has formed the basis of our research is discussed below in two parts: 1A for proton transfer in fuel cells and 1B for hydrogenation-dehydrogenation reactions using FLPs.

1A: Proton Transfer in Fuel cells

Sir William Grove in 1839 invented the basic principle of fuel cell and explored the utility of sulphuric acid as an electrolyte.⁷ According to him, a fuel cell is “an electrochemical device that continuously converts chemical energy into electrical energy (and some heat) as long as fuel and oxidant are supplied”. He spent most of his time searching for an appropriate electrolyte that produces constant current and observed many electrolytes that produced current with some difficulty, but could not get the consistent results. In the early 1960s, NASA, in collaboration with industrial partners, used a fuel cell in the Gemini Earth orbit space capsules and the Apollo moon landing missions. Willard Thomas Grubb (working at General Electric (GE)), who used a sulphonated polystyrene ion-exchange membrane, and GE chemist Leonard Niedrach devised a way of depositing platinum onto this membrane, which ultimately became known as the ‘Grubb-Niedrach fuel cell’. Meanwhile, General Electric (GE) developed another fuel cell technology called the proton exchange membrane (PEM) fuel cell, which was used on the Gemini missions.⁸ Initially, sulfonated polystyrene membrane was employed as the electrolyte but this was eventually replaced by Nafion[®] ionomers. This was the discovery of DuPont, and till date, the Nafion membrane is considered as a first choice for fuel cell membranes. Nafion proved to be superior in performance and durability compared to sulfonated polystyrene. In the 1990s, the phosphoric acid fuel cell (PAFC) plant, employing phosphoric acid and additives as the fuel cell membrane, also became commercially functional.

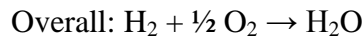
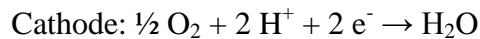
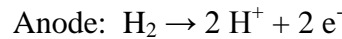
Fuel cell is a highly efficient and low-polluting promising energy source. In its basic form, it produces water and electricity from hydrogen and oxygen from the air, thus, making the fuel cell an environmentally friendly energy source. Notably, the most efficient heat engines, like internal combustion engines, normally show greater efficiency in comparison to traditional combustion devices (around 40-50 %), as such fuel cells are not constrained by Carnot limitations. Over the years, the fuel cell has advanced in structure and today several different types are available. These can be classified according to the electrolytes used in the fuel cell. The most widely used fuel cells classified by their types of electrolyte are given in Table 1.1. Each type of fuel cell has its own advantages and disadvantages. Phosphoric acid fuel cells (PAFC), molten carbonate fuel cells (MCFC), and solid oxide fuel cells (SOFC) are being used in larger power units, whereas the alkaline fuel cells (AFC), polymer electrolyte or proton exchange membrane fuel cells (PEMFC) and direct methanol fuel cells (DMFC) are being used for comparatively smaller power units. The high temperature fuel cells are MCFCs and SOFCs and the low temperature fuel cells are AFCs, PAFCs, PEMFCs and DMFCs. Out of these fuel cells, the most important is polymer electrolyte membrane fuel cells (PEMFCs). PEMFCs have attracted significant attention due to their high power density, higher energy conversion efficiency, low emission levels, and environmental friendliness.⁹

Table 1.1 Types of fuel cells.

Fuel Cells	Electrolyte	Mobile ion	Operating Temperature	Efficiency
Alkaline Fuel Cell (AFC)	Potassium Hydroxide	OH ⁻	60-90 °C	45-60 %
Phosphoric Acid Fuel Cell (PAFC)	Liquid Phosphoric Acid	H ⁺	100-200 °C	35-40 %
Molten Carbonate (MCFC)	Liquid Molten Carbonate	CO ₃ ²⁻	~650 °C	45-60 %
Solid Oxide Fuel Cell (SOFC)	Solid Oxide	O ²⁻	550-1000 °C	50-65 %
Polymer Electrolyte Membrane (PEM) Fuel Cell	Ion Exchange Polymer Membrane	H ⁺	60-130 °C	40-60 %
Direct Methanol Fuel Cell (DMFC)	Ion Exchange Polymer Membrane	H ⁺	60-130 °C	40 %

1.1 Polymer electrolyte or proton exchange membrane fuel cells (PEMFCs)

The Polymer electrolyte membrane fuel cell (PEMFC), also known as the proton exchange membrane (PEM) fuel cell, is a type of fuel cell that has been developed for transport, stationary and portable fuel cell applications. The PEMFCs convert chemical energy to electrical energy through chemical reactions of hydrogen with oxygen. The schematic diagram shows the basic operations of PEM fuel cells, as shown in Figure 1.1. The “heart” of the PEMFC is the proton-conducting membranes, or proton-exchange membranes (PEMs), which are separated by two electrodes: the anode and the cathode. PEMFC are an electrochemical device where the oxidation occurs at the anode and the reduction occurs at the cathode. When supplied with hydrogen and oxygen, electrochemical half-cell reactions take place at the anode and at the cathode.



On the anode side, hydrogen is oxidized to produce protons and electrons. The resulting protons are transported to the cathode through an aqueous environment, and the electron formed at the anode passes through external circuit to reach the cathode. At the cathode, oxygen taken from air is reduced and combined with protons and electrons to produce water as the final product.

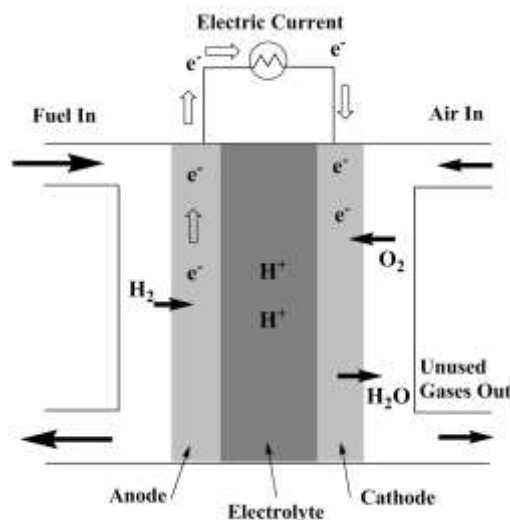


Figure 1.1 Schematic representations of the polymer electrolyte membrane fuel cells (PEMFCs).

In the PEMFC system, transporting the proton from anode to cathode through polymer electrolyte membrane (PEM) has to meet the following requirements for being practical for commercial usage:

1) chemical stability, 2) mechanical durability at high temperature for long times, 3) impermeability to gases, 4) resistance to dehydration, 5) high proton conductivity (especially at low relative humidity), and 6) low cost

1.2 Proton Conducting Materials

The success of PEMFCs technology is based on the effective transport proton through PEM. The PEM should possess good mechanical strength, high thermal stability and resistance to chemical attack and degradation.^{10,11} In 1960, the most widely used polymer electrolyte membranes are a class of perfluorosulfonic acid (PFSA) membranes such as Nafion[®] which were actually developed at DuPont by Walther Grot. The chemical structure of Nafion[®] is shown in the chapter 3. Nafion contains five to eleven repeat units of fluorocarbon (CF₂-CF₂), followed by a repeat unit with a pendent chain including a sulfonic acid group. The thickness of Nafion membranes are generally between 50-175 microns, which is used for fuel cell application. It has long-term stability due to the Teflon-like (copolymerization of tetrafluoroethylene, commercially known as Teflon[®]) backbone and also good mechanical properties with high conductivity, of around 0.1 S.cm⁻¹.¹² The practical application of PEMFCs has lots of problems. Typically, the operating temperature of 80 °C produces a large amount of heat with 40-50 % efficiency. However, a heat energy stack above 80 °C may have a chance of water evaporation, which would reduce the efficiency of Nafion. However, these polymers fail to operate at elevated temperatures. These types of systems are currently undergoing further developments in order to improve their favourable characteristics.^{13,14} Several reviews have been published throughout the world with in-depth research on the polymer electrolyte membrane fuel cell.^{12,15-23} Presently, a few most promising candidates for PEMs are based on high performance aromatic polymers such as polyimides,^{24,25} sulfonated polyetherketone (S-PEEK),²⁶⁻²⁹ poly-arylene ether sulfones (PAES),³⁰⁻³³

polybenzimidazoles (PBI)³⁴⁻³⁸ and many more.^{12,16,19,20,39-41} These materials improve the water uptake over a range of temperatures, easy recycling and low cost.

The Irvin group⁴² developed crown ethers as components in high temperature fuel cell membranes for which polyimides had been considered candidates. They prepared several polyimides comprising of hexafluoroisopropylidene (HFIP) groups, resulting in thermally stable polymers with 10% weight loss at 400 °C (*via* TGA). This stability range and the conductivity of 0.1 S.cm⁻¹, mentioned earlier, satisfy the high temperature requirements for fuel cell membranes. Also, Dukjoon Kim showed the combination of cerium, crown ether and s-PEEK to investigate one of the most important oxidation-promoting reagents (the anti-oxidation effect) in fuel cell membranes.⁴³ Some examples of polymeric structures used as PEMs are shown in Figure 1.2.

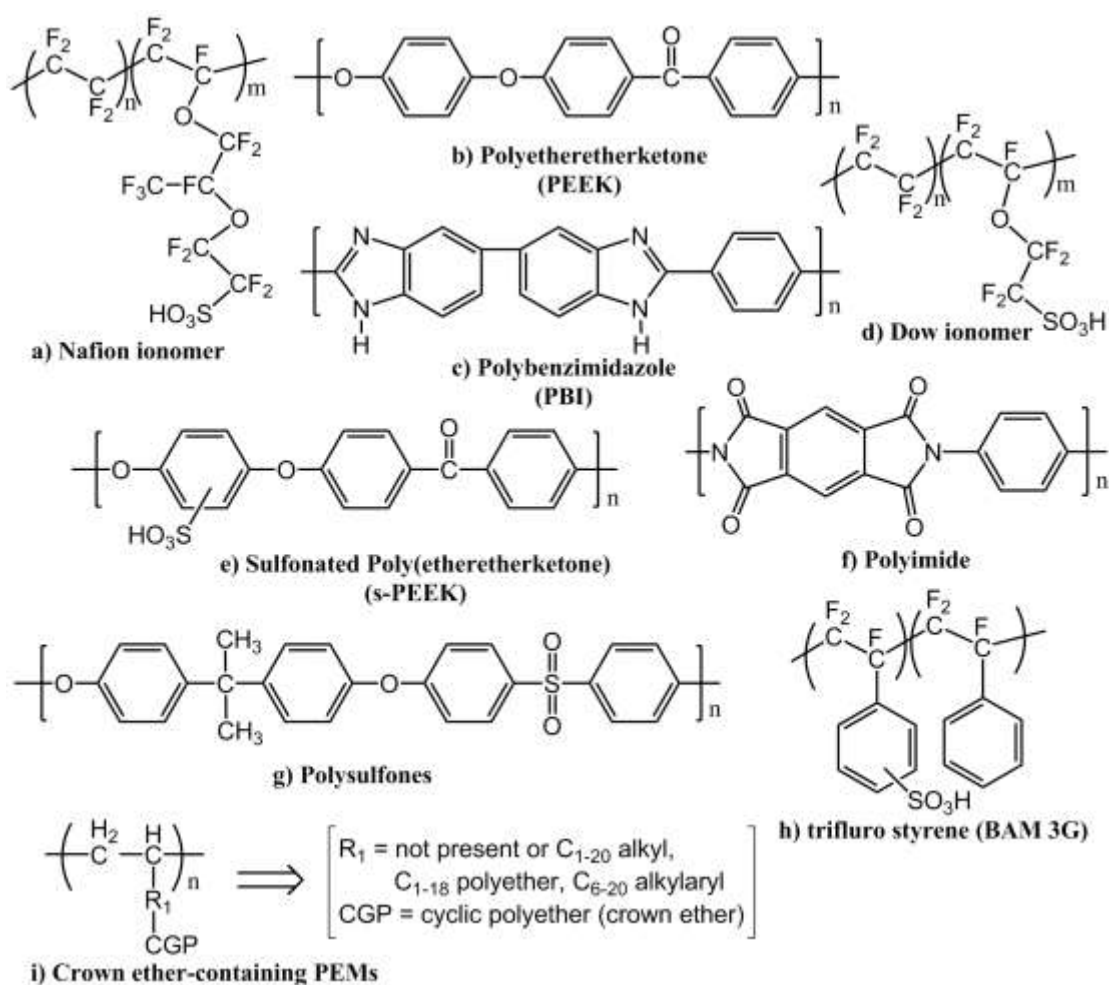


Figure 1.2 Chemical structures of PEMs used in fuel cells.

1.3 The Proton Transfer Mechanism

In PEMFCs, the proton conducting species are mainly responsible for transporting protons in short and long ranges. At the atomic level, only oxygen and nitrogen are suitable for carrying the proton in the PEMFCs, due to chemical stability and suitable binding constant of oxygen and nitrogen to protons. The possible proton conducting species with oxygen are water, the oxygen anion, the hydroxyl anion, alcohol, ether, ester, carboxylic acid, inorganic oxoacid, oxygen-containing heterocycles; and with nitrogen are ammonia, amino groups, and nitrogen-containing heterocycles. The study of proton transport has received considerable attention over a century because of its paramount importance in chemical, biological, and electrochemical systems. In PEM fuel cells (hydrogen-oxygen), the oxidation of molecular hydrogen takes place at the anode to form protons (H^+) and these resulting protons must be transported across to the cathode through the membrane to complete the conversion of chemical energy into electrical energy. The proton transfer mechanism through different processes can occur through the “vehicular mechanism”⁴⁴ or the “Grotthuss mechanism” (for anhydrous proton transfer).⁴⁵⁻⁵² The vehicular mechanism is the more preferred in the aqueous solution. Compounds containing a small amount of water are expected to conduct through the vehicular mechanism in which H_2O and/or NH_3 act as the proton carrier. Also, the proton conductivity obtained at high temperature, higher than $100\text{ }^\circ\text{C}$, is based on the heterocyclic molecules as the protic solvent. These conductivities, through the vehicular mechanism, are responsible for the mobility of solvated protons, resulting in the relatively high conductivity in oligomers.⁴⁴

Over two centuries ago, von Grotthuss proposed the collective shuttling of the hydrogen atom along with water wires.⁵³ Later, the Grotthuss mechanism has been developed by Huckel,⁵⁴ Bernal and Fowler,⁵⁵ Conway⁵⁶ and Agmon.⁵⁷ Recently, the in-depth proton transfer mechanism came from the combinations of *ab initio* molecular dynamics simulations (AIMD)^{51,52,58-61} and force-field approaches, which are based on the empirical valence bond formalism.⁶²⁻⁶⁴ In the Grotthuss mechanism models, the proton undergoes a hopping, by which it is transferred from an H_3O^+ ion to a neighbouring water molecule. The Grotthuss and vehicular mechanisms both contribute to proton conductivity in most of the polymer electrolyte systems.

Since the most widely used PEM – the perfluorosulfonic polymer Nafion - strongly depends upon water, operatibility becomes the limiting factor due to low temperature (less than 80 °C). Later on, the heterocyclic compounds have led to immense interest as potential proton carriers. The pioneering work of the Kreuer group^{46,65} on pyrrole and imidazole led to their extensive investigation as proton conductors. Recent reports on aromatic heterocyclic compounds such as imidazole^{45,65,66} as well as triazole,⁶⁷⁻⁷² tetrazole^{73,74} and benzimidazole^{34,35,75-77} show that they can effectively promote proton conduction in a polymer electrolyte membrane.

So far, various experimental^{45,46,65,78,79} and theoretical^{80,81} studies have been done to investigate the proton transfer process and proton conducting polymers have been made with dimers, oligomers or chains of imidazoles, in which the imidazole moieties were tethered to the polymer backbone. However, to the best of our knowledge, only a few computational studies have been done using triazoles and tetrazoles.⁸²⁻⁸⁴ The Bredas group⁸² and the Yan group⁸⁴ investigated the intermolecular proton-transfer barriers of triazole, which is about 1-2 kcal/mol and 2.6-4.1 kcal/mol respectively at the B3LYP/6-311+G level of theory. Once a proton is transferred from one imidazole or triazole moiety to an adjacent one, this moiety will rotate so as to reorient itself into the original position and this reorientation step was reported as the rate-limiting step. The important rate limiting step barriers are reported to be ranging from 8.0 kcal/mol to 39.2 kcal/mol.^{66,85-92}

1B: Frustrated Lewis Pairs (FLP)

In 1923, Gilbert N. Lewis formulated his theory of acids and bases,⁹³ by defining an “acid” as an electron pair acceptor (Lewis acids) and a “base” as an electron pair donor (Lewis bases). According to this concept, a Lewis acid is defined as having a low-lying “lowest unoccupied molecular orbital” (LUMO), which can interact with the lone electron pair in the high-lying “highest occupied molecular orbital” (HOMO) of a Lewis base. The chemical reactivity, from the combination of Lewis acids and bases, results in the formation of Lewis acid-base adducts. For

example, the Lewis acid borane (BH_3) combines with the Lewis base ammonia (NH_3) to generate the adduct ammonia-borane ($\text{NH}_3\text{-BH}_3$). This simple model extends well beyond main group chemistry and is now considered a principle that is fundamental to our understanding of many chemical reactions in the fields of inorganic, coordination and organic chemistry. Recent chemical explorations have encountered some systems that apparently diverge from this principle, because of steric hindrance. This is because steric hindrance precludes the formation of simple Lewis acid-base adducts. In 1942, H. C. Brown and co-workers examined the interaction of pyridines with simple boranes and found that lutidine formed a stable adduct with BF_3 , while it failed to form adducts with BMe_3 (see Figure 1.3). The steric clash of the methyl groups of lutidine and BMe_3 precluded adduct formation, but smaller bases were able to form the adducts with trimethyl borane due to the reduction in steric congestion.⁹⁴ Main group chemistry has seen numerous reports of adduct formation between a strong electrophilic acid, $\text{B}(\text{C}_6\text{F}_5)_3$ and a range of bases.⁹⁵⁻¹⁰⁴

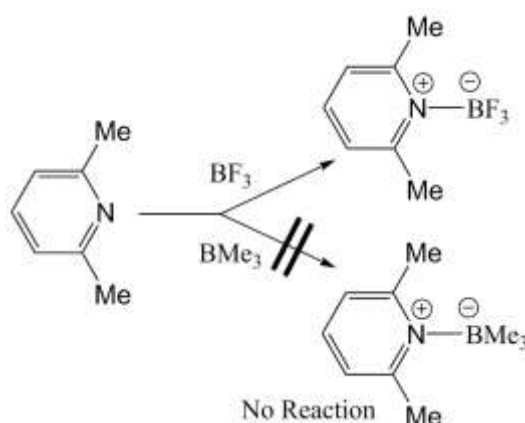


Figure 1.3 Example of steric blocked and open dative adducts formation.

In recent years, Stephan and coworkers have realized that reactivity could result from sterically encumbering both the Lewis acid and the Lewis base. Several sterically hindered Lewis acids and Lewis bases preclude the formation of a “quenched” adduct. Such complexes have been termed by Stephan and coworkers as Frustrated Lewis Pairs (FLPs), which present extraordinary reactivity due to steric reasons.^{105,106} Subsequent to this, there have been several ongoing investigations in the field of FLPs systems around the world, with major application centered on catalysis¹⁰⁷⁻¹¹⁴ and the activation of small molecules.^{6,105,106,115}

1.4 FLPs Activation of H₂

The major breakthrough in the field of “metal free” main group elements and Lewis acid-base pairs was contributed by Stephan and coworkers in 2006. They discovered that the sterically demanding secondary phosphine (C₆H₂Me₃)₂PH reacted with B(C₆F₅)₃ to form the zwitterionic compound [(C₆H₂Me₃)₂P(H)(C₆F₄)B(F)(C₆F₅)₂] **1**,⁶ which was subsequently treated with Me₂SiHCl to yield **2** (Figure 1.4). As the temperature reached up to 150 °C, the compound **2** underwent stoichiometric loss of H₂ in toluene solution to yield a phosphinoborane species (C₆H₂Me₃)₂P(C₆F₄)B(C₆F₅)₂ **3** (Figure 1.4). Most surprisingly, when **3** was reacted with hydrogen at room temperature, the zwitterionic phosphonium-borate **2** was regenerated. This proves that reversible small-molecule activation is achievable in the absence of a transition metal (Figure 1.4). Also, several other phosphine/borane¹¹⁶⁻¹²² and nitrogen/borane¹²³⁻¹²⁸ combinations have been investigated for the facile heterolytic activation of H₂.

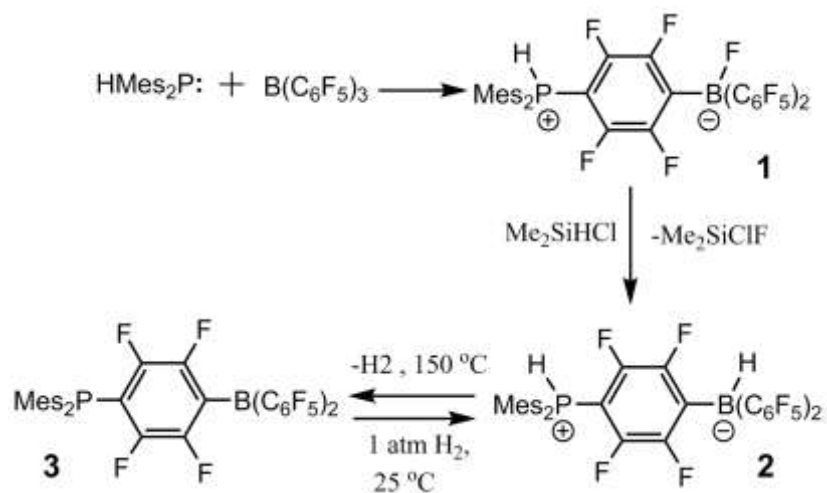


Figure 1.4 Synthesis and reactivity of a first metal free catalyst phosphonium hydridoborate capable of reversible H₂ activation.

Later, investigations by the Erker group in 2007 led to the development of an intramolecular zwitterionic alkyl-linked phosphonium–hydridoborate frustrated Lewis pair as a product of the anti-Markovnikov addition of *bis*(pentafluorophenyl)borane (HB(C₆F₅)₂), to a vinyl phosphine.¹¹⁷ Similarly, Rieger and Repo have reported the synthesis of intramolecular boron-nitrogen (B/N) FLPs derived from the reaction of 2-bromo benzylbromide, 2,2,6,6-tetramethyl piperidine and *bis*(pentafluorophenyl)

chloroborane ($\text{ClB}(\text{C}_6\text{F}_5)_2$)^{114,129} and showed that the (B/N) FLPs can efficiently activate the H_2 molecule under mild reaction conditions through an intramolecular reaction pathway. Later, intramolecular B-N FLPs were synthesized by the Repo group¹²³ and they exemplified a utility of new aminoboranes in the activation of hydrogen under near ambient conditions. Ashley's group, for the first time, discovered the synthesis of Tris[3,5-bis(trifluoromethyl)phenyl]borane on the practical scale, which formed FLPs with the 2,2,6,6-tetramethylpiperidine (TMP) that split H_2 heterolytically.¹³⁰ Similarly O'Hare group¹³¹ synthesized sterically hindered borane tris(2,2',2''-perfluorobiphenyl)borane (PBB) and combined the same with bulky nitrogen bases such as TMP, DABCO and 2,4-lutidine to forms FLPs. These FLPs showed facile heterolytic cleavage of H_2 , but the reverse reaction was not apparent upto a temperature of 120 °C.

After the discovery of the FLP concept, numerous inter- and intramolecular FLPs have been reported.^{105,106,115,132-135} These FLPs contain phosphorus, nitrogen, carbon donors and boron, aluminium acceptors, and have been successfully employed to activate molecular hydrogen (H_2)^{115,118,136-138} and other species such as CO_2 , CO , N_2O , NO and SO_2 .^{115,136-145} Recently, in 2013, the non-interacting, vicinal P/B FLPs (**4**) have been prepared by Erker and coworkers,¹⁴⁶ from the combination of dimesityl norbornenylphosphane with Piers' borane, $\text{HB}(\text{C}_6\text{F}_5)_2$. This structure was confirmed by X-ray crystallography and spectroscopic data. **4** rapidly cleaves the H-H bond heterolytically to form **5** and it also adds rapidly to CO_2 , to benzaldehyde, to SO_2 and even to NO at room temperature (see Figure 1.5).

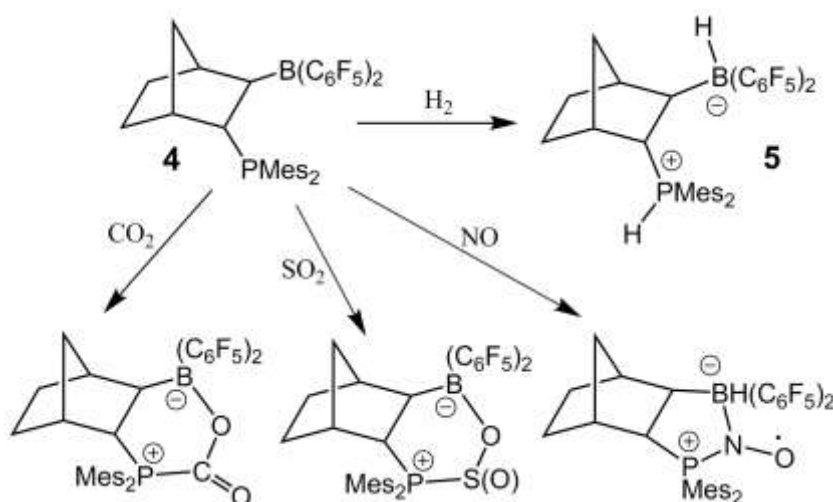


Figure 1.5 The FLPs **4** catalyst split H_2 and reactions with CO_2 , SO_2 and NO .

From the theoretical and computational point of view, the heterolytic splitting of H₂ using FLPs catalyst has been mainly studied by Papai's^{122,127,147} and Grimme's^{109,148} groups. For the encounter complex formed between the Lewis acid and Lewis base, Papai's group observed the electron transfer (ET) from (tBu)₃P to the σ* orbital of H₂ and from the σ* of H₂ to the p orbital of B(C₆F₅)₃, resulting in the cleavage of the H–H bond. Grimme's group examined the H₂ heterolytic split by FLPs, which was initially driven by the electric field (EF) generated by donor-acceptor atoms of the FLP.^{109,132,148} The Privalov group¹⁴⁹ demonstrated that the structure of the P-B species resembles a classical frustrated Lewis acid-base, increasing the frustration between phosphorus and boron, and thus decreasing the H₂ splitting barrier. On the basis of experimental and theoretical studies, the Tamm group¹⁵⁰ investigated and discussed the cleavage of molecular hydrogen heterolytically by employing bifunctional pyrazolylborane as the catalyst, with the formation of a mixture of hydrogenated *cis* and *trans* products. The Wang group designed a strategy to activate the metal free hydrogen sp³ carbon bridged FLPs for the activation of molecular hydrogen.

1.5 Reactions of Frustrated Lewis Pairs with Saturated-Unsaturated Compounds

i) Dehydrogenation of Alcohols

The catalytic hydrogenation-dehydrogenation of unsaturated-saturated compounds is undoubtedly one of the most important reactions in chemical industry and organic synthesis.^{151,152} To date, several theoretical^{122,153-160} studies have been carried out to determine the potential energy surface and the mechanisms of the molecular hydrogen activation in order to predict the properties of FLPs. For the first time, by theoretical calculations, Privalov address the likelihood of the dehydrogenation of primary and secondary alcohols by (tBu)₂PB(C₆F₅)₂. He also found that few hydrogenation-dehydrogenation reactions are nearly thermo-neutral. Therefore, this reaction is reversible under elevated temperatures in the case of formaldehyde-methanol. Also, the primary alcohols, such as ethanol and 2- phenyl-1-ethanol, are only moderately exothermic when suitably designed P/B catalysts are employed. Similarly, new FLPs catalysts have been designed with a weaker

interaction between the nitrogen and boron centers, which would be very effective for the alcohol dehydrogenation, as well as better than the transition-metal based systems.

ii) Hydrogenation of imines and oximes

In 2007, Stephan's¹⁶¹ and Klankermayer's¹⁶² groups have identified catalysts that could be employed for the H₂ activation and catalytic reduction of imines under mild conditions. The sterically encumbered nitrogen of imine is reduced at a temperature of 80-120 °C in high yield in the presence of H₂.¹⁶³ This catalyst has been successfully commercialized. Figure 1.6 shows the general proposed mechanism of catalytic reduction of imines or oximes by using the phosphor/borane catalyst. The imine substrate acts as an FLPs base, and thus effectively, the imine¹⁶¹ or oxime¹⁶⁴ reductions are possible in the presence of H₂, with the Lewis acid B(C₆F₅)₃ as the catalyst. These mechanisms proceed *via* the protonation of imine, followed by hydride transfer from the hydridoborate, as shown in Figure 1.6. By using this proposed mechanism, the electron rich imine ^tBuN=CPh(H) is reduced significantly faster than the electron-poor imine PhSO₂N=CPh(H). Recently, Stephan's group¹⁶⁵ hydrogenated a variety of imines at 100 °C with the combinations of H₂ and di-isobutylaluminum hydride (DIBAL) or tri-iso-butylaluminum (TIBAL) *via* hydroalumination followed by the hydrogenolysis/ σ -bond metathesis mechanism.

Despite the extremely rapid growth of FLP catalysis, the fields of asymmetric hydrogenation reactions have not been developed significantly. In 2008, the Klankermayer group¹⁶² reported the first FLP-catalyzed asymmetric hydrogenation of imines with 13% ee by using α -pinene-derived chiral borane. Shortly afterwards, the same group improved the ee by up to 83 % by using the combination of chiral borane and the phosphine generated by treating (+)-camphor-derived chiral borane and tri-tert-butylphosphine with H₂.^{166,167} The FLP approach is rapidly becoming more effective for the enantioselective hydrogenation of prochiral imines (ee up to 84 %).^{162,166,168} Depending on the initial mechanistic investigation, up to 87 % enantioselectivities have been obtained by using the dimethylphenyl silane for imines.¹⁶⁹

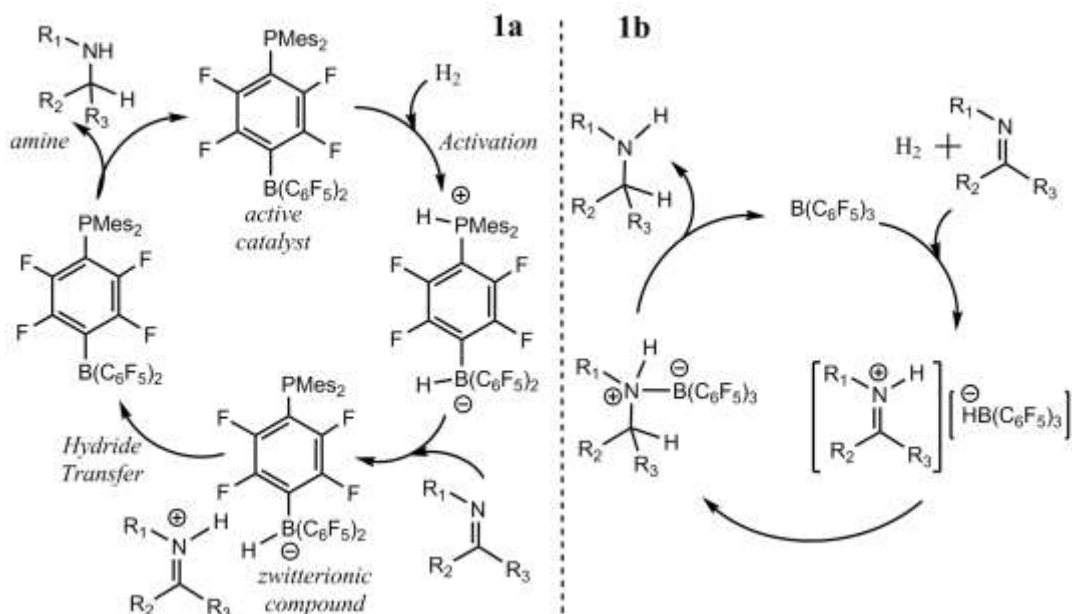


Figure 1.6 The general proposed mechanism of catalytic reduction of (a) imines by using phosphorus/borane; (b) imines or oximes using $B(C_6F_5)_3$ as catalysts.

iii) Hydrogenation of ketone and aldehyde

The $B(C_6F_5)_3$ -catalyzed reactions between hydrosilane and the aromatic aldehydes, ketones, and esters have been reported by the Piers group¹⁷⁰. In this report, a carbonyl group reaction was apparently an example of reactions catalyzed by FLP that became well known later.^{106,109,116,122,127,133,147,153,171-179} Figure 1.7 shows the three step mechanism for the hydrosilylation of carbonyl compounds, suggested by Piers and coworkers. The silane activation mechanism for the reduction of ketone and ester catalyzed by $B(C_6F_5)_3$ has been proposed by Yamamoto and coworkers.^{180,181} In recent years, the sterically hindered Lewis acid and Lewis base have been carefully chosen for the activation of small molecules, by greatly developing the concept of frustrated Lewis pairs (FLPs). There is no substituent bound to the carbonyl oxygen atom, and thus the donor-accepter interaction is even stronger between the carbonyl oxygen atom and the boron atom. This could be the reason why the FLPs have been rarely applied experimentally for aldehyde and ketone hydrogenations, in spite of computational studies suggesting this possibility, by the groups of Privalov^{182,183} and Wang.^{184,185} Privalov suggested that the hydrogenation of ketone would be likely to be analogous to that previously described for imine hydrogenations.^{161,162,170,186,187} Recently, Stephan reported¹¹¹ the atom-economic transformations for the aliphatic and aromatic ketone reduction by using metal free catalyst in the ether solvent. Similarly,

Ashley developed FLP based catalysts in the 1,4-dioxan solvent for the aliphatic and aromatic ketone and aldehyde hydrogenations.

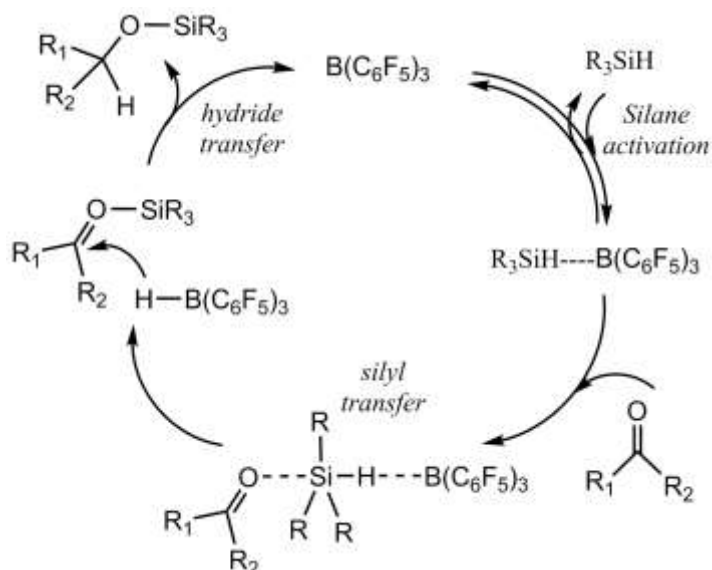


Figure 1.7 The proposed mechanism by the Piers group for borane-catalysed hydrosilylation.

1.6 Scope of the thesis

The present thesis discusses ways in which to improve proton transfer in fuel cell and hydrogenation-dehydrogenation reactions using frustrated Lewis pairs (FLPs). The studies towards this end have been conducted with density functional theory (DFT). For polymer electrolyte membrane (PEM) based fuel cells, a study of alternatives with reduced limitations is required, while for hydrogenation-dehydrogenation reactions, a detailed knowledge of the mechanism of these reactions is required. Both requirements have been fulfilled with computational studies with density functional theory (DFT). This thesis is divided into two parts: the first part is based on the study of proton transfer reactions in fuel cells (Chapter 3 and Chapter 4); while the second part is based on the study of hydrogenation-dehydrogenation reactions by using modifications to metal free systems such as frustrated Lewis pairs (Chapter 5 and Chapter 6).

The development of new proton conducting electrolytes that can function at high temperatures is the focus of Chapters 3 and 4. In chapter 3, to solve the difficulties existing in current high temperature PEM systems based on H_3PO_4 and imidazole, a new type of proton conducting species 1*H*-1,2,3-triazole has been

explored, and proved to have high proton conductivity and stability for fuel cell applications, when employed with hydrogenated zero-dimensional (0D) cage systems. In Chapter 4, to solve the problem of high reorientation barriers in PEMs having pendant groups, a new design of nitrogen containing pendant group PEMs has been considered that eliminates the need for the reorientation barrier during the proton transfer process.

The dihydrogen molecule is small but plays an important role in chemistry. Hydrogen production and hydrogen activation is not only an important chemical process, but also enriches our understanding of reactivity in saturated/unsaturated reactions. Transition metal-based systems are known to be effective catalysts for this reaction, but developing metal free catalytic (frustrated Lewis pair) systems would lead to highly desirable cheaper and greener alternatives. This chemistry has led to the design of new chemical systems that can do the important catalytic conversion of alcohols to the corresponding ketones based on a nitrogen/boron system described in Chapter 5. Then, in Chapter 6, important new insights have been provided into the mechanism of the heterolytic splitting of di-hydrogen and the catalytic hydrogenation of unsaturated compounds using modified FLP (MFLP) catalysts.

1.7. References

- (1) *National Hydrogen Energy Roadmap, USDOE: Washington, DC 2002.*
- (2) Steele, B. C. H.; Heinzel, A. *Nature* **2001**, *414*, 345-352.
- (3) Carla, H.-W. *Journal of Membrane Science* **1996**, *120*, 1-33.
- (4) Kubas, G. J. *Chemical Reviews* **2007**, *107*, 4152-4205.
- (5) Berke, H. *ChemPhysChem* **2010**, *11*, 1837-1849.
- (6) Welch, G. C.; Juan, R. R. S.; Masuda, J. D.; Stephan, D. W. *Science* **2006**, *314*, 1124-1126.
- (7) Bacon, F. T.; Fry, T. M. *Review Lecture: The Development and Practical Application of Fuel Cells*; Proceedings of the royal society of London. Series A, Mathematical and physical sciences, 1973; Vol. 334, 427-452.
- (8) Sørensen, B. *Hydrogen and Fuel Cells: Emerging Technologies and Applications, Elsevier Inc.: London* **2005**, P113-153.
- (9) Leo, B.; Michael, N. M. *Fuel Cell Systems. New York: Plenum Press; PLENUM Press: New York* **1993**, P73-115.

-
- (10) Alberti, G.; Casciola, M. *Annual Review of Materials Research* **2003**, *33*, 129-154.
- (11) Alberti, G.; Casciola, M. *Comprehensive Membrane Science and Engineering* **2010**, *2*, 431-465.
- (12) Li, Q.; He, R.; Jensen, J. O.; Bjerrum, N. J. *Chemistry of Materials* **2003**, *15*, 4896-4915.
- (13) Souzy, R.; Ameduri, B. *Progress in Polymer Science* **2005**, *30*, 644-687.
- (14) Souzy, R.; Ameduri, B.; Boutevin, B.; Capron, P.; Marsacq, D.; Gebel, G. *Fuel Cells* **2005**, *5*, 383-397.
- (15) Alberti, G.; Casciola, M.; Costantino, U.; Narducci, R.; Pica, M.; Sganappa, M. *Desalination* **2006**, *199*, 4-5.
- (16) Jannasch, P. *Current Opinion in Colloid & Interface Science* **2003**, *8*, 96-102.
- (17) Savadogo, O. *Journal of Power Sources* **2004**, *127*, 135-161.
- (18) Zhang, J.; Xie, Z.; Zhang, J.; Tang, Y.; Song, C.; Navessin, T.; Shi, Z.; Song, D.; Wang, H.; Wilkinson, D. P.; Liu, Z.-S.; Holdcroft, S. *Journal of Power Sources* **2006**, *160*, 872-891.
- (19) Roziere, J.; Jones, D. J. *Annual Review of Materials Research* **2003**, *33*, 503-555.
- (20) Hickner, M. A.; Ghassemi, H.; Kim, Y. S.; Einsla, B. R.; McGrath, J. E. *Chemical Reviews* **2004**, *104*, 4587-4612.
- (21) Alberti, G.; Casciola, M.; Massinelli, L.; Bauer, B. *Journal of Membrane Science* **2001**, *185*, 73-81.
- (22) Kerres, J. A. *Journal of Membrane Science* **2001**, *185*, 3-27.
- (23) Rusanov, A., L. ; Likhachev, D. Y.; Mullen, K. *Russian Chemical Reviews* **2002**, *71*, 761-774.
- (24) Zhou, H.; Miyatake, K.; Watanabe, M. *Fuel Cells* **2005**, *5*, 296-301.
- (25) Genies, C.; Mercier, R.; Sillion, B.; Petiaud, R.; Cornet, N.; Gebel, G.; Pineri, M. *Polymer* **2001**, *42*, 5097-5105.
- (26) Gao, Y.; Robertson, G. P.; Guiver, M. D.; Jian, X.; Mikhailenko, S. D.; Wang, K.; Kaliaguine, S. *Journal of Polymer Science Part A: Polymer Chemistry* **2003**, *41*, 2731-2742.
- (27) Gao, Y.; Robertson, G. P.; Guiver, M. D.; Mikhailenko, S. D.; Li, X.; Kaliaguine, S. *Macromolecules* **2004**, *37*, 6748-6754.

- (28) Gao, Y.; Robertson, G. P.; Guiver, M. D.; Wang, G.; Jian, X.; Mikhailenko, S. D.; Li, X.; Kaliaguine, S. *Journal of Membrane Science* **2006**, *278*, 26-34.
- (29) Cheng, H.; Xu, J.; Ma, L.; Xu, L.; Liu, B.; Wang, Z.; Zhang, H. *Journal of Power Sources* **2014**, *260*, 307-316.
- (30) Mohanty, A. K.; Mistri, E. A.; Banerjee, S.; Komber, H.; Voit, B. *Industrial & Engineering Chemistry Research* **2013**, *52*, 2772-2783.
- (31) Mukherjee, R.; Banerjee, S.; Komber, H.; Voit, B. *RSC Advances* **2014**, *4*, 46723-46736.
- (32) Pang, J.; Feng, S.; Zhang, H.; Jiang, Z.; Wang, G. *RSC Advances* **2015**, *5*, 38298-38307.
- (33) Gao, N.; Zhang, S. *Journal of Applied Polymer Science* **2013**, *128*, 1-12.
- (34) Glipa, X.; Bonnet, B.; Mula, B.; J. Jones, D.; Roziere, J. *Journal of Materials Chemistry* **1999**, *9*, 3045-3049.
- (35) Wainright, J. S.; Wang, J. T.; Weng, D.; Savinell, R. F.; Litt, M. *Journal of The Electrochemical Society* **1995**, *142*, L121-L123.
- (36) Deimede, V.; Voyiatzis, G. A.; Kallitsis, J. K.; Qingfeng, L.; Bjerrum, N. J. *Macromolecules* **2000**, *33*, 7609-7617.
- (37) Sannigrahi, A.; Arunbabu, D.; Sankar, R. M.; Jana, T. *Macromolecules* **2007**, *40*, 2844-2851.
- (38) Liu, Y.; Shi, Z.; Xu, H.; Fang, J.; Ma, X.; Yin, J. *Macromolecules* **2010**, *43*, 6731-6738.
- (39) Rikukawa, M.; Sanui, K. *Progress in Polymer Science* **2000**, *25*, 1463-1502.
- (40) Savadogo, O. *Journal of New Materials for Electrochemical Systems* **1998**, *1*, 47-66.
- (41) Kraytsberg, A.; Ein-Eli, Y. *Energy & Fuels* **2014**, *28*, 7303-7330.
- (42) Irvin, J. A.; Stasko, D.; Fallis, S.; Guenther, A. J.; Webber, C.; Blackwell, J.; Amer Chemical Soc 1155 16Th St, NW, Washington, DC 20036 USA: 2003; Vol. 225, p U875-U876.
- (43) Park, J.; Kim, D. *Journal of Membrane Science* **2014**, *469*, 238-244.
- (44) Kreuer, K.-D.; Rabenau, A.; Weppner, W. *Angewandte Chemie International Edition in English* **1982**, *21*, 208-209.
- (45) Kreuer, K.-D.; Paddison, S. J.; Spohr, E.; Schuster, M. *Chemical Reviews* **2004**, *104*, 4637-4678.
- (46) Kreuer, K.-D. *Chemistry of Materials* **1996**, *8*, 610-641.

- (47) Eikerling, M.; Kornyshev, A. A.; Kuznetsov, A. M.; Ulstrup, J.; Walbran, S. *The Journal of Physical Chemistry B* **2001**, *105*, 3646-3662.
- (48) Samuel, C. *Biochimica et Biophysica Acta (BBA) - Bioenergetics* **2006**, *1757*, 876-885.
- (49) Kreuer, K. D. *Journal of Membrane Science* **2001**, *185*, 29-39.
- (50) Noam, A. *Chemical Physics Letters* **1995**, *244*, 456-462.
- (51) Tuckerman, M. *J. Chem. Phys.* **1995**, *103*, 150.
- (52) Tuckerman, M.; Laasonen, K.; Sprik, M.; Parrinello, M. *The Journal of Physical Chemistry* **1995**, *99*, 5749-5752.
- (53) de Grotthuss, C. J. T. *Ann. Chim.* **1806**, *58*, 54-73.
- (54) Hückel, E. *Z. Elektrochem. Angew. Phys. Chem.*, **1928**, *34*, 546.
- (55) Bernal, J. D.; Fowler, R. H. *The Journal of Chemical Physics* **1933**, *1*, 515-548.
- (56) Conway, B. E.; Bockris, J. O.; apos; M; Linton, H. *The Journal of Chemical Physics* **1956**, *24*, 834-850.
- (57) Agmon, N. *Chemical Physics Letters* **1995**, *244*, 456-462.
- (58) Marx, D.; Chandra, A.; Tuckerman, M. E. *Chemical Reviews* **2010**, *110*, 2174-2216.
- (59) Marx, D. T., M. E.; Hutter, J.; Parrinello, M. *Nature* **1999**, *397*, 601-604.
- (60) Tuckerman, M. E.; Marx, D.; Parrinello, M. *Nature* **2002**, *417*, 925-929.
- (61) Geissler, P. L.; Dellago, C.; Chandler, D.; Hutter, J. r.; Parrinello, M. *Science* **2001**, *291*, 2121-2124.
- (62) Voth, G. A. *Accounts of Chemical Research* **2006**, *39*, 143-150.
- (63) Knight, C.; Maupin, C. M.; Izvekov, S.; Voth, G. A. *Journal of Chemical Theory and Computation* **2010**, *6*, 3223-3232.
- (64) Markovitch, O.; Chen, H.; Izvekov, S.; Paesani, F.; Voth, G. A.; Agmon, N. *The Journal of Physical Chemistry B* **2008**, *112*, 9456-9466.
- (65) Kreuer, K. D.; Fuchs, A.; Ise, M.; Spaeth, M.; Maier, J. *Electrochimica Acta* **1998**, *43*, 1281-1288.
- (66) Kawada, A.; McGhie, A. R.; Labes, M. M. *The Journal of Chemical Physics* **1970**, *52*, 3121-3125.
- (67) Zhou, Z.; Li, S.; Zhang, Y.; Liu, M.; Li, W. *Journal of the American Chemical Society* **2005**, *127*, 10824-10825.

- (68) Granados-Focil, S.; Woudenberg, R. C.; Yavuzcetin, O.; Tuominen, M. T.; Coughlin, E. B. *Macromolecules* **2007**, *40*, 8708-8713.
- (69) Çelik, S. Ü.; Akbey, Ü.; Bozkurt, A.; Graf, R.; Spiess, H. W. *Macromolecular Chemistry and Physics* **2008**, *209*, 593-603.
- (70) Günday, S. T.; Bozkurt, A.; Meyer, W. H.; Wegner, G. *Journal of Polymer Science Part B: Polymer Physics* **2006**, *44*, 3315-3322.
- (71) Özden, Ş.; Çelik, S. Ü.; Bozkurt, A. *Journal of Polymer Science Part A: Polymer Chemistry* **2010**, *48*, 4974-4980.
- (72) Hazarika, M.; Jana, T. *ACS Applied Materials & Interfaces* **2012**, *4*, 5256-5265.
- (73) Li, S.; Zhou, Z.; Zhang, Y.; Liu, M.; Li, W. *Chemistry of Materials* **2005**, *17*, 5884-5886.
- (74) Casalini, R.; Chaloux, B. L.; Roland, C. M.; Ricks-Laskoski, H. L. *The Journal of Physical Chemistry C* **2014**, *118*, 6661-6667.
- (75) Zhuang, Y.; Seong, J. G.; Lee, W. H.; Do, Y. S.; Lee, M. J.; Wang, G.; Guiver, M. D.; Lee, Y. M. *Macromolecules* **2015**, *48*, 5286-5299.
- (76) Nakamoto, H.; Noda, A.; Hayamizu, K.; Hayashi, S.; Hamaguchi, H.-o.; Watanabe, M. *The Journal of Physical Chemistry C* **2007**, *111*, 1541-1548.
- (77) Xiao, L.; Zhang, H.; Scanlon, E.; Ramanathan, L. S.; Choe, E.-W.; Rogers, D.; Apple, T.; Benicewicz, B. C. *Chemistry of Materials* **2005**, *17*, 5328-5333.
- (78) Steininger, H.; Schuster, M.; Kreuer, K. D.; Kaltbeitzel, A.; Bingol, B.; Meyer, W. H.; Schauff, S.; Brunklaus, G.; Maier, J.; Spiess, H. W. *Physical Chemistry Chemical Physics* **2007**, *9*, 1764-1773.
- (79) Schuster, M. F. H.; Meyer, W. H.; Schuster, M.; Kreuer, K. D. *Chemistry of Materials* **2004**, *16*, 329-337.
- (80) Tataru, W.; Wojcik, M. J.; Lindgren, J.; Probst, M. *The Journal of Physical Chemistry A* **2003**, *107*, 7827-7831.
- (81) Iannuzzi, M. *The Journal of Chemical Physics* **2006**, *124*, 204710.
- (82) Zhou, Z.; Liu, R.; Wang, J.; Li, S.; Liu, M.; Bredas, J.-L. *The Journal of Physical Chemistry A* **2006**, *110*, 2322-2324.
- (83) Subbaraman, R.; Ghassemi, H.; Zawodzinski Jr, T. *Solid State Ionics* **2009**, *180*, 1143-1150.
- (84) Li, A.; Yan, T.; Shen, P. *Journal of Power Sources* **2011**, *196*, 905-910.

- (85) Basch, H.; Krauss, M.; Stevens, W. J. *Journal of the American Chemical Society* **1985**, *107*, 7267-7271.
- (86) Goward, G. R.; Saalwachter, K.; Fischbach, I.; Spiess, H. W. *Solid State Nuclear Magnetic Resonance* **2003**, *24*, 150-162.
- (87) Goward, G. R.; Schuster, M. F. H.; Sebastiani, D.; Schnell, I.; Spiess, H. W. *The Journal of Physical Chemistry B* **2002**, *106*, 9322-9334.
- (88) Fischbach, I.; Spiess, H. W.; Saalwachter, K.; Goward, G. R. *The Journal of Physical Chemistry B* **2004**, *108*, 18500-18508.
- (89) Mangiatordi, G. F.; Butera, V.; Russo, N.; Laage, D.; Adamo, C. *Physical Chemistry Chemical Physics* **2012**, *14*, 10910-10918.
- (90) Benhabbour, S. R.; Chapman, R. P.; Scharfenberger, G.; Meyer, W. H.; Goward, G. R. *Chemistry of Materials* **2005**, *17*, 1605-1612.
- (91) Yamada, M.; Honma, I. *The Journal of Physical Chemistry B* **2004**, *108*, 5522-5526.
- (92) Mangiatordi, G. F.; Laage, D.; Adamo, C. *Journal of Materials Chemistry A* **2013**, *1*, 7751-7759.
- (93) Lewis, G. N. *Valence and the Nature of the Chemical Bond*. Chemical Catalog Company, New York **1923**.
- (94) Brown, H. C.; Schlesinger, H. I.; Cardon, S. Z. *Journal of the American Chemical Society* **1942**, *64*, 325-329.
- (95) Massey, A. G.; Park, A. J. *Journal of Organometallic Chemistry* **1964**, *2*, 245-250.
- (96) Piers, W. E. In *Advances in Organometallic Chemistry*; Academic Press: 2004; Vol. Volume 52, p 1-76.
- (97) Bradley, D. C.; Harding, I. S.; Keefe, A. D.; Motevalli, M.; Zheng, D. H. *Journal of the Chemical Society, Dalton Transactions* **1996**, 3931-3936.
- (98) Denis, J.-M.; Forintos, H.; Szelke, H.; Toupet, L.; Pham, T.-N.; Madec, P.-J.; Gaumont, A.-C. *Chemical Communications* **2003**, 54-55.
- (99) Lucarini, M.; Pedulli, G. F. *Journal of Organometallic Chemistry* **1995**, *494*, 123-131.
- (100) Su, Z. M.; Wang, X. J.; Huang, Z. H.; Wang, R. S.; Feng, J. K.; Sun, J. Z. *Synthetic Metals* **2001**, *119*, 583-584.
- (101) Yamaguchi, S.; Akiyama, S.; Tamao, K. *Journal of Organometallic Chemistry* **2002**, *652*, 3-9.

- (102) Blackwell, J. M.; Piers, W. E.; Parvez, M.; McDonald, R. *Organometallics* **2002**, *21*, 1400-1407.
- (103) Guidotti, S.; Camurati, I.; Focante, F.; Angellini, L.; Moscardi, G.; Resconi, L.; Leardini, R.; Nanni, D.; Mercandelli, P.; Sironi, A.; Beringhelli, T.; Maggioni, D. *The Journal of Organic Chemistry* **2003**, *68*, 5445-5465.
- (104) Lesley, M. J. G.; Woodward, A.; Taylor, N. J.; Marder, T. B.; Cazenobe, I. n.; Ledoux, I.; Zyss, J.; Thornton, A.; Bruce, D. W.; Kakkar, A. K. *Chemistry of Materials* **1998**, *10*, 1355-1365.
- (105) Stephan, D. W. *Dalton Transactions* **2009**, 3129-3136.
- (106) Stephan, D. W. *Organic & Biomolecular Chemistry* **2008**, *6*, 1535-1539.
- (107) Takeuchi, K.; Hounjet, L. J.; Stephan, D. W. *Organometallics* **2013**, *32*, 4469-4472.
- (108) Stephan, D. W. *Organic & Biomolecular Chemistry* **2012**, *10*, 5740-5746.
- (109) Grimme, S.; Kruse, H.; Goerigk, L.; Erker, G. *Angewandte Chemie International Edition* **2010**, *49*, 1402-1405.
- (110) Paradies, J. *Angewandte Chemie International Edition* **2014**, *53*, 3552-3557.
- (111) Mahdi, T.; Stephan, D. W. *Journal of the American Chemical Society* **2014**, *136*, 15809-15812.
- (112) Stephan, D. W. *Journal of the American Chemical Society* **2015**, *137*, 10018-10032.
- (113) Greb, L.; Daniliuc, C.-G.; Bergander, K.; Paradies, J. *Angewandte Chemie International Edition* **2013**, *52*, 5876-5879.
- (114) Sumerin, V.; Schulz, F.; Atsumi, M.; Wang, C.; Nieger, M.; Leskelä, M.; Repo, T.; Pyykko, P.; Rieger, B. *Journal of the American Chemical Society* **2008**, *130*, 14117-14119.
- (115) Stephan, D. W.; Erker, G. *Angewandte Chemie International Edition* **2010**, *49*, 46-76.
- (116) Welch, G. C.; Stephan, D. W. *Journal of the American Chemical Society* **2007**, *129*, 1880-1881.
- (117) Spies, P.; Erker, G.; Kehr, G.; Bergander, K.; Frohlich, R.; Grimme, S.; Stephan, D. W. *Chemical Communications* **2007**, 5072-5074.
- (118) Jiang, C.; Blacque, O.; Fox, T.; Berke, H. *Dalton Transactions* **2011**, *40*, 1091-1097.

- (119) Welch, G. C.; Masuda, J. D.; Stephan, D. W. *Inorganic Chemistry* **2006**, *45*, 478-480.
- (120) Zeonjuk, L. L.; Vankova, N.; Mavrandonakis, A.; Heine, T.; Röschenthaler, G.-V.; Eicher, J. *Chemistry – A European Journal* **2013**, *19*, 17413-17424.
- (121) Liu Zeonjuk, L.; St. Petkov, P.; Heine, T.; Roschenthaler, G.-V.; Eicher, J.; Vankova, N. *Physical Chemistry Chemical Physics* **2015**, *17*, 10687-10698.
- (122) Rokob, T. A.; Hamza, A.; Stirling, A.; Soós, T.; Pápai, I. *Angewandte Chemie International Edition* **2008**, *47*, 2435-2438.
- (123) Chernichenko, K.; Nieger, M.; Leskela, M.; Repo, T. *Dalton Transactions* **2012**, *41*, 9029-9032.
- (124) Zaher, H.; Ashley, A. E.; Irwin, M.; Thompson, A. L.; Gutmann, M. J.; Kramer, T.; O'Hare, D. *Chemical Communications* **2013**, *49*, 9755-9757.
- (125) Pyykko, P.; Wang, C. *Physical Chemistry Chemical Physics* **2010**, *12*, 149-155.
- (126) Xu, B.-H.; Bussmann, K.; Fröhlich, R.; Daniliuc, C. G.; Brandenburg, J. G.; Grimme, S.; Kehr, G.; Erker, G. *Organometallics* **2013**, *32*, 6745-6752.
- (127) Rokob, T. A.; Hamza, A.; Papai, I. *Journal of the American Chemical Society* **2009**, *131*, 10701-10710.
- (128) Lindqvist, M.; Borre, K.; Axenov, K.; Kotai, B.; Nieger, M.; Leskela, M.; Papai, I.; Repo, T. *Journal of the American Chemical Society* **2015**, *137*, 4038-4041.
- (129) Sumerin, V.; Schulz, F.; Nieger, M.; Atsumi, M.; Wang, C.; Leskela, M.; Pyykko, P.; Repo, T.; Rieger, B. *Journal of Organometallic Chemistry* **2009**, *694*, 2654-2660.
- (130) Herrington, T. J.; Thom, A. J. W.; White, A. J. P.; Ashley, A. E. *Dalton Transactions* **2012**, *41*, 9019-9022.
- (131) Binding, S. C.; Zaher, H.; Mark Chadwick, F.; O'Hare, D. *Dalton Transactions* **2012**, *41*, 9061-9066.
- (132) Schirmer, B.; Grimme, S. *Frustrated Lewis Pairs I: Uncovering and Understanding* **2013**, *332*, 213 - 230.
- (133) Erker, G.; Stephan, D. W. *Frustrated Lewis Pairs II, Top. Curr. Chem., Springer-Verlag, Berlin, Germany* **2013**.
- (134) Stephan, D. W. *Chemical Communications* **2010**, *46*, 8526-8533.
- (135) Kenward, A. L.; Piers, W. E. *Angewandte Chemie International Edition* **2008**, *47*, 38-41.

- (136) Whittemore, S. M.; Edverson, G.; Camaioni, D. M.; Karkamkar, A.; Neiner, D.; Parab, K.; Autrey, T. *Catalysis Today* **2015**, *251*, 28-33.
- (137) Jiang, C.; Blacque, O.; Berke, H. *Organometallics* **2009**, *28*, 5233-5239.
- (138) Spies, P.; Kehr, G.; Bergander, K.; Wibbeling, B.; Frohlich, R.; Erker, G. *Dalton Transactions* **2009**, 1534-1541.
- (139) Stephan, D. W.; Erker, G. *Chemical Science* **2014**, *5*, 2625-2641.
- (140) Wang, Y.; Chen, W.; Lu, Z.; Li, Z. H.; Wang, H. *Angewandte Chemie International Edition* **2013**, *52*, 7496-7499.
- (141) Dureen, M. A.; Stephan, D. W. *Journal of the American Chemical Society* **2010**, *132*, 13559-13568.
- (142) Sajid, M.; Kehr, G.; Daniliuc, C. G.; Erker, G. *Angewandte Chemie International Edition* **2014**, *53*, 1118-1121.
- (143) Tran, S. D.; Tronic, T. A.; Kaminsky, W.; Michael Heinekey, D.; Mayer, J. M. *Inorganica Chimica Acta* **2011**, *369*, 126-132.
- (144) Kolychev, E. L.; Bannenberg, T.; Freytag, M.; Daniliuc, C. G.; Jones, P. G.; Tamm, M. *Chemistry – A European Journal* **2012**, *18*, 16938-16946.
- (145) Liu, Y.; Hu, L.; Chen, H.; Du, H. *Chemistry – A European Journal* **2015**, *21*, 3495-3501.
- (146) Sajid, M.; Kehr, G.; Wiegand, T.; Eckert, H.; Schwickert, C.; Pottgen, R.; Cardenas, A. J. P.; Warren, T. H.; Frohlich, R.; Daniliuc, C. G.; Erker, G. *Journal of the American Chemical Society* **2013**, *135*, 8882-8895.
- (147) Hamza, A.; Stirling, A.; András Rokob, T.; Pápai, I. *International Journal of Quantum Chemistry* **2009**, *109*, 2416-2425.
- (148) Schirmer, B.; Grimme, S. *Chemical Communications* **2010**, *46*, 7942-7944.
- (149) Nyhlén, J.; Privalov, T. *European Journal of Inorganic Chemistry* **2009**, *2009*, 2759-2764.
- (150) Theuergarten, E.; Schluns, D.; Grunenber, J.; Daniliuc, C. G.; Jones, P. G.; Tamm, M. *Chemical Communications* **2010**, *46*, 8561-8563.
- (151) *Acc. Chem. Res.* **2007**, *40*, special issue 12 on hydrogenation and transfer hydrogenation.
- (152) *Adv. Synth. Catal.* **2003**, *345*, special issue 1-2 on catalytic hydrogenation.
- (153) Muck-Lichtenfeld, C.; Grimme, S. *Dalton Transactions* **2012**, *41*, 9111-9118.
- (154) Gilbert, T. M. *Dalton Transactions* **2012**, *41*, 9046-9055.
- (155) Guo, Y.; He, X.; Li, Z.; Zou, Z. *Inorganic Chemistry* **2010**, *49*, 3419-3423.

- (156) Schulz, F.; Sumerin, V.; Heikkinen, S.; Pedersen, B.; Wang, C.; Atsumi, M.; Leskela, M.; Repo, T.; Pyykko, P.; Petry, W.; Rieger, B. *Journal of the American Chemical Society* **2011**, *133*, 20245-20257.
- (157) Lu, G.; Li, H.; Zhao, L.; Huang, F.; Wang, Z.-X. *Inorganic Chemistry* **2010**, *49*, 295-301.
- (158) Kathmann, S. M.; Cho, H.; Chang, T.-M.; Schenter, G. K.; Parab, K.; Autrey, T. *The Journal of Physical Chemistry B* **2014**, *118*, 4883-4888.
- (159) Bako, I.; Stirling, A.; Balint, S.; Papai, I. *Dalton Transactions* **2012**, *41*, 9023-9025.
- (160) Dang, L. X.; Schenter, G. K.; Chang, T.-M.; Kathmann, S. M.; Autrey, T. *The Journal of Physical Chemistry Letters* **2012**, *3*, 3312-3319.
- (161) Chase, P. A.; Jurca, T.; Stephan, D. W. *Chemical Communications* **2008**, 1701-1703.
- (162) Chen, D.; Klankermayer, J. *Chemical Communications* **2008**, 2130-2131.
- (163) Chase, P. A.; Welch, G. C.; Jurca, T.; Stephan, D. W. *Angewandte Chemie International Edition* **2007**, *46*, 8050-8053.
- (164) Mohr, J.; Oestreich, M. *Angewandte Chemie International Edition* **2014**, *53*, 13278-13281.
- (165) Hatnean, J. A.; Thomson, J. W.; Chase, P. A.; Stephan, D. W. *Chemical Communications* **2014**, *50*, 301-303.
- (166) Chen, D.; Wang, Y.; Klankermayer, J. *Angewandte Chemie International Edition* **2010**, *49*, 9475-9478.
- (167) Ghattas, G.; Chen, D.; Pan, F.; Klankermayer, J. *Dalton Transactions* **2012**, *41*, 9026-9028.
- (168) Sumerin, V.; Chernichenko, K.; Nieger, M.; Leskelä, M.; Rieger, B.; Repo, T. *Advanced Synthesis & Catalysis* **2011**, *353*, 2093-2110.
- (169) Chen, D.; Leich, V.; Pan, F.; Klankermayer, J. *Chemistry – A European Journal* **2012**, *18*, 5184-5187.
- (170) Parks, D. J.; Piers, W. E. *Journal of the American Chemical Society* **1996**, *118*, 9440-9441.
- (171) Welch, G. C.; Cabrera, L.; Chase, P. A.; Hollink, E.; Masuda, J. D.; Wei, P.; Stephan, D. W. *Dalton Transactions* **2007**, 3407-3414.
- (172) Erker, G.; Stephan, D. W. *Frustrated Lewis Pairs I: Uncovering and Understanding, Top. Curr. Chem., Springer-Verlag, Berlin, Germany* **2013**.

- (173) Stirling, A.; Hamza, A.; Rokob, T. A.; Papai, I. *Chemical Communications* **2008**, 3148-3150.
- (174) Kronig, S.; Theuergarten, E.; Holschumacher, D.; Bannenberg, T.; Daniliuc, C. G.; Jones, P. G.; Tamm, M. *Inorganic Chemistry* **2011**, *50*, 7344-7359.
- (175) Timoshkin, A. Y.; Morokuma, K. *Physical Chemistry Chemical Physics* **2012**, *14*, 14911-14916.
- (176) Wu, D.; Jia, D.; Liu, A.; Liu, L.; Guo, J. *Chemical Physics Letters* **2012**, *541*, 1-6.
- (177) Rokob, T. A.; Bako, I.; Stirling, A.; Hamza, A.; Papai, I. *Journal of the American Chemical Society* **2013**, *135*, 4425-4437.
- (178) Pu, M.; Privalov, T. *The Journal of Chemical Physics* **2013**, *138*, 154305.
- (179) Rendler, S.; Oestreich, M. *Angewandte Chemie International Edition* **2008**, *47*, 5997-6000.
- (180) Gevorgyan, V.; Liu, J.-X.; Rubin, M.; Benson, S.; Yamamoto, Y. *Tetrahedron Letters* **1999**, *40*, 8919-8922.
- (181) Gevorgyan, V.; Rubin, M.; Benson, S.; Liu, J.-X.; Yamamoto, Y. *The Journal of Organic Chemistry* **2000**, *65*, 6179-6186.
- (182) Privalov, T. *Chemistry – A European Journal* **2009**, *15*, 1825-1829.
- (183) Nyhlen, J.; Privalov, T. *Dalton Transactions* **2009**, 5780-5786.
- (184) Li, H.; Zhao, L.; Lu, G.; Huang, F.; Wang, Z.-X. *Dalton Transactions* **2010**, *39*, 5519-5526.
- (185) Zhao, L.; Lu, G.; Huang, F.; Wang, Z.-X. *Dalton Transactions* **2012**, *41*, 4674-4684.
- (186) Parks, D. J.; Blackwell, J. M.; Piers, W. E. *The Journal of Organic Chemistry* **2000**, *65*, 3090-3098.
- (187) Piers, W. E.; Marwitz, A. J. V.; Mercier, L. G. *Inorganic Chemistry* **2011**, *50*, 12252-12262.

Chapter 2

Theoretical Methods and Computational Details

ABSTRACT

The aim of the thesis is (i) to develop efficient polymer electrolyte membranes (PEMs) for fuel cells, membranes that can be effective in the absence of water and other solvating media at elevated temperatures and (ii) substitute the highly effective transition metal-based catalyst systems with cheaper and greener metal free catalysts for hydrogenation-dehydrogenation reactions. This chapter is focused on the elaboration on some of the theoretical approaches that have been employed in this thesis.

In the past few decades, various quantum mechanical methods have been implemented for treating the electronic structure of molecules, clusters and solids. This chapter begins with a brief introduction to the non-relativistic Schrödinger equation and the many-body problem by discussing the Born-Oppenheimer approximation in section 2.1. In section 2.2 is provided a brief summary of density functional theory (DFT) along with the Thomas-Fermi model, the Hohenberg-Kohn theorems, the Kohn-Sham equations and the different exchange-correlation functionals. Section 2.3 describes the RI-J and MARI-J approximations implemented in the Turbomole software to improve the computational efficiency. In section 2.4 and 2.5 is briefly described the methods taken into account for the solvent corrections and the energetic span model (ESM) which is employed to calculate the turn over frequency (TOF) from the theoretically obtained energy profile.

2.1 The many-body problem or (Basic Quantum Mechanics)

A major goal of electronic structure calculations is to solve the Schrodinger equation. For a given system composed of N-electrons and M nuclei, the energy can be determined by solving the Schrodinger equation. The *time-independent Schrödinger equation*^{1,2} is given by:

$$\hat{H}\Psi = E\Psi \quad \dots (2.1)$$

where E is the electronic energy, $\Psi = \Psi(x_1, x_2 \dots x_N)$ is the wave-function which describes the state of the N-electron quantum-mechanical system and is a function of the space-spin coordinates, x_i , of all the electrons of the system, and H is the Hamiltonian operator. H is the sum of the kinetic energy T and potential energy V operators. The molecular Hamiltonian for a time-independent multi-electron system is written as:

$$\hat{H} = -\frac{1}{2} \sum_{i=1}^N \frac{1}{m} \nabla_i^2 - \frac{1}{2} \sum_{A=1}^M \frac{1}{M_A} \nabla_A^2 - \sum_{i=1}^N \sum_{A=1}^M \frac{Z_A}{r_{iA}} + \sum_{i=1}^N \sum_{j>i}^N \frac{1}{r_{ij}} + \sum_{A>1}^M \sum_{B>A}^M \frac{Z_A Z_B}{R_{AB}} \quad \dots (2.2)$$

In this equation, the nuclei and i and j are related to the electrons of the system defined by A and B . The first two terms depict the kinetic energy of electrons (with mass m) and nuclei (with mass M_A), respectively. The third term corresponds to the electrostatic interaction between the nuclei and the electrons separated by distance r_{iA} , the fourth terms is the electron-electron repulsion separated by r_{ij} and the last term is the nucleus-nucleus repulsive interaction, where R_{AB} is the distance between the A^{th} and the B^{th} nucleus.

The Hamiltonian operator leads to complexity in the Schrodinger Equation, thereby making it difficult to solve exactly for systems of more than two mutually interacting particles. In 1927, the first step for overcoming this difficulty was taken with the help of the *Born-Oppenheimer approximation* (BO).³ Since the nuclei are much heavier than the electrons, the nuclei motion is much slower than that of the electrons. Therefore, we can separate the movement of nuclei and electrons. When we consider the movement of electrons, it is reasonable to consider that the positions of nuclei are fixed. Under the Born-Oppenheimer approximation Eq. (2.2), the second term is neglected and the final term - the repulsion between the nuclei - can be

considered as a constant for a fixed configuration of the nuclei. The remaining terms in Eq. (2.2) are called as the electronic Hamiltonian (\hat{H}_{elec}),

$$\hat{H}_{elec} = -\frac{1}{2} \sum_{i=1}^N \nabla_i^2 - \sum_{i=1}^N \sum_{A=1}^M \frac{Z_A}{r_{iA}} + \sum_{i=1}^N \sum_{j>i}^N \frac{1}{r_{ij}} \quad \dots \quad (2.3)$$

The solution of the electronic Hamiltonian is an electronic wavefunction. The energy obtained therefore depends only on the electronic coordinates and the total energy is obtained as a sum of the electronic energy and the constant nuclear repulsion. There are many theoretical methods which can be used to solve the Schrodinger equation such as the Hartree-Fock (HF) approximation and beyond HF approaches such as Møller-Plesset (MP)⁴ perturbation theory, configuration interaction (CI)⁵ and coupled cluster (CC) methods.⁶ However, density functional theory (DFT)⁷, which uses the electron density [$\rho(\mathbf{r})$] as the central quantity instead of the wavefunction, has become the method of choice for handling chemical systems that are larger than 15-20 atoms. The DFT method allows for accurate results to be obtained while being computationally cheaper than other methods.⁸⁻¹⁰

2.2 Density Functional Theory (DFT)

In quantum chemistry, density functional theory (DFT)⁷ has been used as an extremely useful method for the electronic structure calculations. In DFT, the complicated N-electron wavefunction and the associated Schrodinger equation is replaced by the treatment of the electronic density from a single electron equation which is simpler to solve. This is based on the independent work of Thomas and Fermi using electron density as a basic variable for the study of the N-electron quantum-chemical system.

2.2.1 Thomas-Fermi Theorem

In 1927, Thomas¹¹ and Fermi¹² used electron density as the basic variable instead of the wavefunction. In this method, the electrons are treated as independent particles forming a uniform electron gas and the electron-electron repulsion energy arises solely due to electrostatic interactions. The *Thomas-Fermi* (TF) total energy of an atom with a nuclear charge Z in terms of electron density is given by,

$$E_{TF}[\rho(r)] = C_F \int \rho^{5/3}(r) dr - Z \int \frac{\rho(r)}{r} dr + \frac{1}{2} \iint \frac{\rho(r_1)\rho(r_2)}{|r_1 - r_2|} dr_1 dr_2 \quad \dots (2.4)$$

The Thomas-Fermi coefficient C_F is equal to 2.871.

Where the first term is the kinetic energy of the electron, the second and third terms are the electron-nucleus and electron-electron interactions respectively. The energy functional $E_{TF} = [E_{TF}[\rho(r)]]$ is then minimized under the constraint that the electron densities should integrate to the total number of electrons in the system, in order to obtain the ground state electron density of the systems.

$$N = \int \rho(r) dr \quad \dots (2.5)$$

Applying the method of Lagrange multipliers to incorporate the constraint, the ground-state electron density must satisfy the variational principle

$$\delta \{ E_{TF}[\rho] - \mu_{TF} (\int \rho(r) dr - N) \} = 0 \quad \dots (2.6)$$

This yields the Euler-Lagrange equation,

$$\mu_{TF} = \frac{\delta E_{TF}[\rho]}{\delta \rho(r)} = \frac{5}{3} C_F \rho^{2/3}(r) - \left[\frac{Z}{r} - \int \frac{\rho(r_2)}{|r - r_2|} dr_2 \right] \quad \dots (2.7)$$

Hence, the Thomas-Fermi theory involves solving Equation (2.7) under the constraint (2.5) and inserting the resulting electron density in Equation (2.4) to yield the total energy.

This simple Thomas-Fermi method is not so important in computing the ground state energy and density but more as an illustration that the energy can be determined purely using the electron density. In the past, the TF method has been used for the calculation of atoms and molecules, and quite a few literature citations are available.^{11,12}

2.2.2 Hohenberg-Kohn Theorem

In 1964, modern density-functional theory was born with the landmark paper of Hohenberg and Kohn.¹³ The concepts of their theory originate from two theorems. The first Hohenberg-Kohn theorem stated that “the external potential $v(r)$ (second

term in the Eq. 2.6) is determined, within a trivial additive constant, by the electron density $\rho(r)$. Since $[\rho(r)]$ determines the number of electrons, it follows that $[\rho(r)]$ also determines the ground-state wavefunction Ψ and all other properties such as kinetic energy $T[\rho(r)]$, potential energy $V[\rho(r)]$ and total energy $E[\rho(r)]$ of the system. The energy of the system as a functional of electron density is written as

$$E[\rho] = T[\rho] + V_{ne}[\rho] + V_{ee}[\rho] = \int \rho(r)v(r)dr + F_{HK}[\rho] \quad \dots (2.8)$$

where

$$F_{HK}[\rho] = T[\rho] + V_{ee}[\rho] \quad \dots (2.9)$$

Thus, F_{HK} is a Hohenberg-Kohn universal functional. Note that $F_{HK}[\rho]$ is only dependent on ρ and independent from any external potential $v(r)$.

The second Hohenberg-Kohn theorem establishes the energy variational principle, stating that “*the exact ground state electron density minimizes the exact energy functional*”. Which means, for any given trial density, that $\tilde{\rho}(r)$ is such that $\tilde{\rho}(r) \geq 0$, $\int \tilde{\rho}(r)dr = N$, and $\rho(r)$ is non-negative. The energy functional is always greater than or equal to the exact ground state energy, E_0 ,

$$E_0 \leq E_v[\tilde{\rho}] \quad \dots (2.10)$$

E_0 is the energy which corresponds to the ground state electron density. It can be seen that the determination of the form of the $F_{HK}[\rho]$ is the crucial part in construction of the energy functional for obtaining the exact ground state energy.

The classical part of the electron-electron interaction in Eq. (2.9) is the Columbic potential energy,

$$J[\rho] = \frac{1}{2} \iint \frac{\rho(r_1)\rho(r_2)}{|r_2 - r_1|} dr_1 dr_2 \quad \dots (2.11)$$

In the Thomas-Fermi theory, $V_{ee}[\rho(r)]$ is replaced by $J[\rho(r)]$ and the kinetic energy $T[\rho(r)]$ is taken from the theory of a non-interacting uniform electron gas. Kohn and Sham proposed introducing orbitals into the problem allowing for more accurate computation of $T[\rho(r)]$ with a small residual correction that is handled separately.

2.2.3 Kohn-Sham Equations

Kohn and Sham¹⁴ in 1965 have proposed to solve the problem for any interacting system by introducing a corresponding fictitious non-interacting reference system, in which there are no electron-electron repulsion terms and for which the ground-state electron density is exactly the same as the density of the interacting system. The exact kinetic energy $T_s[\rho]$ of the non-interacting reference system is,

$$T_s[\rho] = -\frac{1}{2} \sum_i^N \langle \psi_i | \nabla^2 | \psi_i \rangle \quad \dots (2.12)$$

and $T_s[\rho] \neq T[\rho]$. The electron density is,

$$\rho(r) = \sum_i^N \sum_s |\psi_i(r, s)|^2 \quad \dots (2.13)$$

with r, s including the space and spin coordinates respectively. Here ψ_i are the natural spin orbitals. The universal functional F_{KH} , Eq. (2.9), can be rewritten for the Kohn-Sham DFT as,

$$F[\rho] = T_s[\rho] + J[\rho] + E_{xc}[\rho] = F_{HK}[\rho] \quad \dots (2.14)$$

which contains the kinetic correlation energy as well as the non-classical part of the energy. The explicit form of this functional is not known, but various approximate density functionals for it have been proposed.

The total energy functional is then expressed in atomic units as

$$E[\rho] = T_s[\rho] + J[\rho] + E_{xc}[\rho] + \int v(r) \rho(r) dr \quad \dots (2.15)$$

$$= \sum_i^N \sum_s \int \psi_i^*(x) \left(-\frac{1}{2} \nabla^2\right) \psi_i(x) dr + J[\rho] + E_{xc}[\rho] + \int v(r) \rho(r) dr \quad \dots (2.16)$$

In the above equation (2.16), the first term is the kinetic energy functional of the system of non-interacting electrons with the same density, the second term is the classical Coulomb energy for the electron-electron interaction, the third term is the energy functional incorporating all the many-body effects of exchange and correlation and the last term is the attractive Coulomb potential provided by the fixed nuclei.

The minimum of the Kohn-Sham functional is obtained by varying the energy functional (Eq. 2.16) with respect to the electron density. This leads to the KS orbital equations,

$$\left[-\frac{1}{2}\nabla^2 + v_{\text{eff}}\right]\psi_i = \varepsilon_i\psi_i \quad \dots (2.17)$$

$$\rho(r) = \sum_i^N \sum_s |\psi_i(r, s)|^2 \quad \dots (2.18)$$

$$v_{\text{eff}}(r) = v(r) + \frac{\delta J[\rho]}{\delta \rho(r)} + \frac{\delta E_{\text{xc}}[\rho]}{\delta \rho(r)} = v(r) + \int \frac{\rho(r')}{|r-r'|} dr' + v_{\text{xc}}(r) \quad \dots (2.19)$$

Here ε_i are eigenvalues, ψ_i are KS orbitals, v_{eff} is the Kohn-Sham effective potential and v_{xc} is the exchange-correlation potential. Finally, the total energy can be determined from the resulting density through

$$E = \sum_i^N \varepsilon_i - \frac{1}{2} \int \frac{\rho(r)\rho(r')}{|r-r'|} dr dr' + E_{\text{xc}}[\rho] + \int v_{\text{xc}}(r)\rho(r) dr \quad \dots (2.20)$$

The exchange-correlation functional as defined by KS remains unknown. E_{xc} includes the non-classical aspects of the electron-electron interaction along with the component of the kinetic energy of the real system that is different from the fictitious non-interacting system. Since E_{xc} is not known exactly, it is necessary to approximate it.

2.2.4 Exchange-Correlation Functionals

“Density functional theory is in principle exact! But, in practice approximations have to be made” --- Walter Kohn

The challenging task in DFT is the development of an accurate functional for expressing the exchange-correlation energy, E_{xc} in terms of the density ρ . The accuracy of the DFT calculations decides the exchange-correlation term in the energy expression. By now, there is an almost endless list of approximations with varying levels of complexity. Recently, a useful way for categorizing the many and varied E_{xc} functionals that exist has been proposed by Perdew.¹⁵ The most common types of exchange-correlation functionals are a) the local-density approximation (LDA), b) the

generalized-gradient approximation (GGA), c) the meta-GGA and d) the hybrid functionals.

a) The local-density approximation (LDA)

The simplest approximation proposed by Kohn and Sham is the local density approximation (LDA) for the exchange and correlation energy, and can be written as,

$$E_{xc}^{LDA}[\rho] = \int \rho(r) \varepsilon_{xc}(\rho(r)) dr \quad \dots (2.21)$$

Where $\varepsilon_{xc}(\rho)$ is the exchange-correlation energy per particle of the homogeneous electron gas of density $[\rho(r)]$. It is well known that the LDA suits best for cases with slowly varying density, there are hundreds of application of the LDA to the atoms and molecules.¹⁶ Though the binding energies from the LDA are overestimated by about 10%, the quantities that involve differences of energies tend to come out quite good. In modern LDA, the functionals differ only in how their correlation contributions have been fitted to the many-body free electron gas data. The Perdew-Zunger (PZ)¹⁷ Perdew-Wang (PW)¹⁸, and Vosko-Wilk-Nusair (VWN)¹⁹ functionals are all common LDA functionals.

b) The generalized-gradient approximation (GGA)

In a molecular system, the electron density is typically rather far from spatially uniform, so there is good reason to believe that the LDA approach will have limitations. One obvious way to improve the correlation functional is to make it depend not only on the local value of the density, but on the extent to which the density is locally changing (the gradient of the density). Mathematically, the first derivative of a function at a single position is a local property, so the more common term in modern nomenclature for functionals that depend on both the density and the gradient of the density is ‘gradient corrected’. Including a gradient correction defines the ‘generalized gradient approximation’ (GGA).^{20,21} In the GGA approximation, the unknown functional is approximated by an integral over a function that depends only on the density and its gradient at a given point in space.²²

$$E_{xc}^{GGA}[\rho(r)] = \int d(r) \rho(r) \varepsilon_{xc}^{GGA}[\rho(r); \nabla \rho(r)] \quad \dots (2.22)$$

Among the earlier developed functionals, the PW91¹⁸ derived from the LDA contains no empirical input. Its close relative PBE²⁰ and the Becke²³ exchange and the Lee-Yand-Parr²⁴ correlation functional (BLYP) constructed from the Colle-Salvetti correlation energy formula²⁵ belong to the category of semi-empirical functionals,²⁶⁻³² and are still popular. It has general applicability and gives rather accurate results for a wide range of systems.

c) The meta-GGA

Since, the improvement from the inclusion of the first derivative, an obvious avenue for improvement would be to also try and include the second derivative of the electron density. Such functionals are termed as meta-GGA functionals.^{33,34} There are the class of meta-GGAs, which have a dependence on the higher order derivatives of the electron density and/or the kinetic energy density in addition to the electron density and its gradient. An alternative meta-GGA formalism that is more numerically stable is to include in the exchange-correlation potential as dependent on the kinetic-energy density τ , defined as:

$$\tau(r) = \sum_i^{occ.} \frac{1}{2} |\nabla \psi_i(r)|^2 \quad \dots (2.23)$$

where, ψ_i are the self-consistently determined Kohn–Sham orbitals. Various such MGGGA functionals for exchange, correlation, or both have been developed including B95, B98, TPSS, and VSXC. The cost of a meta-GGA calculation is entirely comparable to that for a GGA calculation, and the former is typically more accurate than the latter for a pure density functional.

d) The hybrid functionals

The fourth generations of well known exchange correlation functionals are the hybrid functionals that are mixtures of the Hartree-Fock exchange with DFT exchange-correlation. This is the basic idea of the hybrid exchange-correlation functionals and B3LYP^{24,29} is an example of one such commonly used hybrid functional. The E_{xc} term for the B3LYP functional is written as

$$E_{xc}^{B3LYP} = E_{xc}^{LDA} + a_0(E_{xc}^{HF} - E_{xc}^{LDA}) + a_x(E_x^{GGA} - E_x^{LDA}) + a_c(E_c^{GGA} - E_c^{LDA}) \quad \dots (2.24),$$

where the parameters are $a_0=0.20$, $a_x=0.72$ and $a_c=0.81$. E_{xc}^{LDA} is the VWN, E_x^{GGA} is the Becke88 exchange and E_c^{GGA} is the LYP (Lee-Yang-Parr) correlation. Other popular hybrid functionals are PBE0³⁵, M06-2X³⁶ and BH & HLYP³², which has 50% Hartree-Fock exchange.

2.3 RI-J and MARI-J approximations

The Resolution of the Identity (RI-J)³⁷⁻⁴² and multipole accelerated resolution of identity (MARI-J)⁴³ approximations help to evaluate the electronic Coulomb integral for both molecular and periodic systems with computational efficiency. These approximations improve the computational efficiency of large-scale calculations but require the use of a second or “auxiliary” basis set. The MARI-J method implemented in the Turbomole software partitions the Coulomb interaction into two parts. By using multipole expansions, the majority of interactions are evaluated in a far field part and a computationally dominant near field part takes care of near field interactions through direct integration of the four-center electron repulsion integrals.

$$\iint \frac{\mu(r)v(r)\kappa(r')\lambda(r')}{|r-r'|} dr dr' = \mu\nu|\kappa\lambda \quad \dots (2.25)$$

where μ , ν , κ , λ are the basis functions. Application of the RI-J (density fitting) approximation to the near field part helps to reduce the four-center electron repulsion integrals to a three center integral. In RI approximation, the electron density ρ is approximated as a linear combination \tilde{q} of auxiliary basis functions α .

$$\rho(r) \approx \tilde{\rho}(r) = \sum_{\alpha} c_{\alpha} \alpha(r) \quad \dots (2.26)$$

where c_{α} is the expansion coefficient and can be evaluated using a positive definite two electron operator ‘ g ’

2.4 Solvent Correction

The Conductor-like Screening Model (COSMO)⁴⁴ is a continuum solvation model (CSM), where the solute molecule forms a cavity within the dielectric continuum of permittivity ϵ that represents the solvent. The charge distribution of the solute polarizes the dielectric medium. The response of the medium is described by

the generation of screening charges on the cavity surface. The polarization charges of the continuum, caused by the polarity of the solute, are obtained from a scaled-conductor approximation derived by COSMO. The charge q^* on the surface segments can be calculated if distribution of the electric charge in the molecule is known. The charge q is lower by approximately a factor $f(\epsilon)$, for solvents with a finite dielectric constant.

$$q^* = f(\epsilon)q \quad \dots (2.27)$$

The factor $f(\epsilon)$ is approximately,

$$f(\epsilon) = \frac{\epsilon - 1}{\epsilon + x} \quad \dots (2.28)$$

where the value of x is set to be $\frac{1}{2}$ based on theoretical arguments.

The interaction energy between the solvent and the solute molecule has been calculated from the solvent screening charges and the known charge distribution of the molecule. The half of the solute-solvent interaction energy gives the dielectric energy. The total free energy of the solvated molecule is obtained from the sum of the energy of the isolated system calculated with the solvated wave function and dielectric energy.

$$E = E(\psi^{solv}) + E_{diel} \quad \dots (2.29)$$

The COSMO method can be used for all methods in theoretical chemistry where the charge distribution of a molecule can be determined; for example, for semi-empirical calculations, HF calculations or density functional theory (DFT) calculations.

2.5 Energetic Span Model

Traditionally, the efficiency of a catalyst system can be expressed as the number of cycles performed per unit time and the catalyst efficiency can be obtained from the turnover frequency (TOF). Nevertheless, until recently, there was no simple method to calculate the TOF from the energy profile obtained from theoretical calculations. In this regard, the concept of the Energetic Span Model (ESM) introduced by Kozuch and Shaik,⁴⁵⁻⁵² provides a way to calculate the TOF from a

theoretically obtained energy profile (the E-representation). The TOF for the catalytic cycle is

$$TOF = \frac{k_B T}{h} \cdot \frac{e^{-\Delta G_r / RT} - 1}{\sum_{i,j}^N e^{T_i - I_j - \delta G'_{i,j} / RT}} = \frac{\Delta}{M} \quad \dots (2.30)$$

$$\delta G'_{i,j} = \begin{cases} \Delta G'_{i,j} & \text{if } i \geq j \\ 0 & \text{if } j < j \end{cases} \quad \dots (2.31)$$

Here ΔG_r is the energy of the global reaction, T_i and I_j are the calculated free energies of each transition state (TS) and intermediate, respectively and the units of TOF are in s^{-1} . This represents the net forward rate constant of the entire cycle. $\Delta G'_{i,j}$ is either ΔG_r or zero, according to the position of T_i vs. I_j in the specific term of the summation, as specified in eq. (2.31). Thus, by analogy to Ohm's law, eq. (2.30) represents the *catalytic-flux* law. The TOF is the "net molecular flux" that generates products and is given by the driving force Δ (catalytic potential) divided by M (the kinetic resistance to catalysis). Christiansen⁵³ introduced the term Δ and M to define the TOF as a function of kinetic rate constants (the k-representation)⁴⁷ in a steady state system. From Christiansen's formulation, by applying Eyring's transition state theory⁴⁵, one can derive the Δ and M terms in the E-representation. Equation 2.30 can be simplified as such that the "-1" term can be neglected from numerator for the exothermic reaction ($\Delta G_r < 0$) and the denominator term is usually dominated by a single term of summation.

$$TOF \approx \frac{k_B T}{h} e^{-\delta E / RT} \quad \dots (2.32)$$

where δE is the energetic span of the cycle, as

$$\delta E = T_{TDTS} - I_{TDI} \quad \text{if the TDTS comes after the TDI} \quad \dots (2.33)$$

$$\delta E = T_{TDTS} - I_{TDI} + \Delta G_r \quad \text{if the TDTS comes before the TDI} \quad \dots (2.34)$$

The fundamental two terms appear in eq (2.32): the TDTS (TOF-determining transition state) and the TDI (TOF-determining intermediate). The ΔG_r term in Eq. (2.34), the TDTS and TDI are not necessarily the highest and lowest energy states of

the cycle – these consider all the possible pairs of transition states and intermediates. The ESM offers a quantification of the influence of each determining states (intermediate and transition state) on the TOF: the so called “degree of TOF control” (X_{TOF}). The degree of TOF control explicitly in the E-representation is,

$$X_{\text{TOF}, T_i} = \frac{\sum_j^N e^{(T_i - I_j - \delta G'_{i,j})/RT}}{\sum_{ij}^N e^{(T_i - I_j - \delta G'_{i,j})/RT}} \quad \dots (2.35)$$

$$X_{\text{TOF}, I_j} = \frac{\sum_i^N e^{(T_i - I_j - \delta G'_{i,j})/RT}}{\sum_{ij}^N e^{(T_i - I_j - \delta G'_{i,j})/RT}} \quad \dots (2.36)$$

where equation (2.35) and (2.36) corresponds to the degree of TOF of TS and intermediate respectively. The concentration will affect the degree of TOF control significantly, when either several intermediates or transition states are important, or when extreme concentrations are involved.

The calculated energy profile of a catalytic reaction therefore can be used to estimate the turnover frequency (TOF) by ESM. According to ESM, neither one transition state nor one reaction step possesses all the kinetic information that determines the efficiency of a catalyst. The TDI and TDTS are not necessarily the ones with the highest and lowest energy value states along the reaction pathway, nor do they have to be adjoined as a single step. As such, in catalysis, there are rate-determining states, not rate-determining steps. From this model, one can conclude that the smaller the energetic span, the faster the reaction would be.⁵⁴⁻⁵⁸

2.6. References

- (1) Schrödinger, E. *Ann. Phys* **1926**, 79, 361.
- (2) Schrödinger, E. *Ann. Phys.* **1926**, 79, 489.
- (3) Born, M.; Oppenheimer, J. R. *Ann Phys* **1927**, 84, 457.
- (4) Møller, C.; Plesset, M. S. *Physical Review* **1934**, 46, 618-622.
- (5) David Sherrill, C.; Schaefer, H. F. In *Advances in Quantum Chemistry*; Academic Press: 1999; Vol. Volume 34, p 143-269.

- (6) Bartlett, R. J. *The Journal of Physical Chemistry* **1989**, 93, 1697-1708.
- (7) Parr, R. G.; Yang, W. *Clarendon Press, New York* **1989**.
- (8) Alonso, J. A.; Girifalco, L. A. *Journal of Physics and Chemistry of Solids* **1977**, 38, 869-876.
- (9) Jacob, B.; Gross, E. K. U.; Dreizler, R. M. *Journal of Physics B: Atomic and Molecular Physics* **1978**, 11, 3795.
- (10) Gross, E. K. U.; Dreizler, R. M. *Physical Review A* **1979**, 20, 1798-1807.
- (11) Thomas, L. H. *Mathematical Proceedings of the Cambridge Philosophical Society* **1927**, 23, 542-548.
- (12) Fermi, E. *Z. phys.* **1928**, 48, 73-79.
- (13) Hohenberg, P.; Kohn, W. *Physical Review* **1964**, 136, B864-B871.
- (14) Kohn, W.; Sham, L. J. *Physical Review* **1965**, 140, A1133-A1138.
- (15) Perdew, J. P.; Schmidt, K. *edited by edited by Doren V. Van, Alsenoy C. Van, and Geerlings, P., (AIP Press, Melville, New York)* **2001**.
- (16) Dahl, J. P.; Avery, J., Eds. *Local Density Approximations in Quantum Chemistry and Solid State Physics, (Plenum, New York)* **1984**.
- (17) Perdew, J. P.; Zunger, A. *Physical Review B* **1981**, 23, 5048-5079.
- (18) Perdew, J. P.; Wang, Y. *Physical Review B* **1992**, 45, 13244-13249.
- (19) Vosko, S. H.; Wilk, L.; Nusair, M. *Canadian Journal of Physics* **1980**, 58, 1200-1211.
- (20) Perdew, J. P.; Burke, K.; Ernzerhof, M. *Physical Review Letters* **1996**, 77, 3865.
- (21) Perdew, J. P.; Burke, K.; Ernzerhof, M. *Physical Review Letters* **1997**, 78, 1396-1396.
- (22) Perdew, J. P.; Burke, K.; Wang, Y. *Physical Review B* **1996**, 54, 16533-16539.
- (23) Becke, A. D. *Physical Review A* **1988**, 38, 3098.
- (24) Lee, C.; Yang, W.; Parr, R. G. *Physical Review B* **1988**, 37, 785-789.
- (25) Colle, R.; Salvetti, O. *Theoretica chimica acta* **1975**, 37, 329-334.
- (26) Becke, A. D. *The Journal of Chemical Physics* **1986**, 84, 4524-4529.
- (27) Becke, A. D. *The Journal of Chemical Physics* **1992**, 96, 2155-2160.
- (28) Becke, A. D. *The Journal of Chemical Physics* **1992**, 97, 9173-9177.
- (29) Becke, A. D. *The Journal of Chemical Physics* **1993**, 98, 5648-5652.
- (30) Becke, A. D. *The Journal of Chemical Physics* **1996**, 104, 1040-1046.
- (31) Becke, A. D. *The Journal of Chemical Physics* **1997**, 107, 8554-8560.

- (32) Becke, A. D. *The Journal of Chemical Physics* **1993**, *98*, 1372-1377.
- (33) Tao, J.; Perdew, J. P.; Staroverov, V. N.; Scuseria, G. E. *Physical Review Letters* **2003**, *91*, 146401.
- (34) Perdew, J. P.; Ruzsinszky, A.; Csonka, G. b. I.; Constantin, L. A.; Sun, J. *Physical Review Letters* **2009**, *103*, 026403.
- (35) Adamo, C.; Barone, V. *The Journal of Chemical Physics* **1999**, *110*, 6158-6170.
- (36) Zhao, Y.; Truhlar, D. *Theoretical Chemistry Accounts* **2008**, *120*, 215-241.
- (37) Eichkorn, K.; Treutler, O.; O`hm, H.; Ha`ser, M.; Ahlrichs, R. *Chemical Physics Letters* **1995**, *240*, 283-289.
- (38) Burow, A. r. M.; Sierka, M.; Mohamed, F. *The Journal of Chemical Physics* **2009**, *131*, 214101.
- (39) Whitten, J. L. *The Journal of Chemical Physics* **1973**, *58*, 4496-4501.
- (40) Dunlap, B. I.; Connolly, J. W. D.; Sabin, J. R. *The Journal of Chemical Physics* **1979**, *71*, 3396-3402.
- (41) Vahtras, O.; Almlöf, J.; Feyereisen, M. W. *Chemical Physics Letters* **1993**, *213*, 514-518.
- (42) Eichkorn, K.; Weigend, F.; Treutler, O.; Ahlrichs, R. *Theoretical Chemistry Accounts* **1997**, *97*, 119-124.
- (43) Sierka, M.; Hogekamp, A.; Ahlrichs, R. *J. Chem. Phys.* **2003**, *118*, 9136.
- (44) Klamt, A.; Schuurmann, G. *Journal of the Chemical Society, Perkin Transactions 2* **1993**, 799-805.
- (45) Kozuch, S.; Shaik, S. *Journal of the American Chemical Society* **2006**, *128*, 3355-3365.
- (46) Kozuch, S.; Shaik, S. *The Journal of Physical Chemistry A* **2008**, *112*, 6032-6041.
- (47) Kozuch, S.; Lee, S. E.; Shaik, S. *Organometallics* **2009**, *28*, 1303-1308.
- (48) Kozuch, S.; Shaik, S. *Accounts of Chemical Research* **2011**, *44*, 101-110.
- (49) Kozuch, S.; Shaik, S. *Journal of Molecular Catalysis A: Chemical* **2010**, *324*, 120-126.
- (50) Kozuch, S.; Martin, J. M. L. *ACS Catalysis* **2011**, *1*, 246-253.
- (51) Uhe, A.; Kozuch, S.; Shaik, S. *Journal of Computational Chemistry* **2011**, *32*, 978-985.

- (52) Kozuch, S. In *Understanding Organometallic Reaction Mechanisms and Catalysis*; Wiley-VCH Verlag GmbH & Co. KGaA: 2015, p 217-248.
- (53) Christiansen, J. A. *Advances in Catalysis* **1953**, 5, 311.
- (54) Normand, A. T.; Hawkes, K. J.; Clement, N. D.; Cavell, K. J.; Yates, B. F. *Organometallics* **2007**, 26, 5352-5363.
- (55) Tobisch, S. *Chemistry – A European Journal* **2008**, 14, 8590-8602.
- (56) Hawkes, K. J.; Cavell, K. J.; Yates, B. F. *Organometallics* **2008**, 27, 4758-4771.
- (57) Liu, P.; Cheong, P. H.-Y.; Yu, Z.-X.; Wender, P. A.; Houk, K. N. *Angewandte Chemie International Edition* **2008**, 47, 3939-3941.
- (58) Guiducci, A. E.; Boyd, C. L.; Clot, E.; Mountford, P. *Dalton Transactions* **2009**, 5960-5979.

Chapter 3

Exploring the Potential of Doped Zero-Dimensional Cages for Proton Transfer in Fuel Cells

ABSTRACT

Calculations with density functional theory (DFT) and MP2 have been done to investigate the potential of recently synthesized durable zero-dimensional (0D) nitrogen based cage structures to perform as efficient proton exchange membranes (PEMs) in fuel cells. Our calculations suggest that the hydrogenated 0D cages, in combination with hydrogen bonding 1,2,3 and 1,2,4 triazole molecules, would perform as highly efficient PEMs. The results are important in the context of the need for efficient PEMs for fuel cells, especially at higher temperatures (greater than 120 °C) where conventional water based PEMs such as Nafion have been found to be ineffective.

3.1 Introduction

Fuel cells are considered a promising alternative energy conversion device. Their promise lies in their essential “green-ness” - they generate water, heat and electricity without emitting pollutants, with hydrogen as the fuel and the oxygen in the air as the oxidant.¹⁻³ The most important component of the fuel cell is the electrolyte that lies at the “heart of the fuel cell”.⁴ The electrolyte separates the anode and cathode and conducts a specific ion at very high rates during the operation of the fuel cell.

Among the various fuel cell types, proton exchange membrane fuel cells (PEMFCs) are a type of fuel cell where protons conducting membranes, or proton exchange membranes (PEMs), are used as the electrolyte. The PEMFC that is most well known is Nafion⁵ - a sulfonated tetrafluoroethylene based fluoropolymer-copolymer, whose chemical structure is shown in Figure 3.1. This PEM operates best at temperatures below 80 °C, because Nafion functions in conjunction with water molecules, with the proton transport taking place through different processes - the Vehicular Mechanism⁶ or the Grotthuss mechanism^{4,7-13} - that require the use of the water as a medium for aiding the transport of the proton. Since, at temperatures above 80 °C, the chances of water evaporating increase, this reduces the efficiency of Nafion.

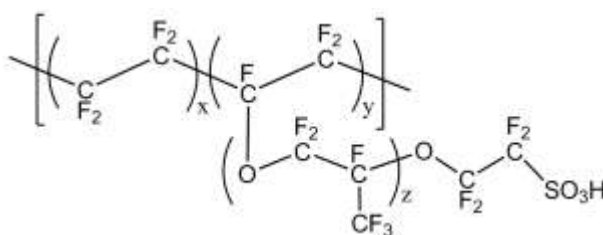


Figure 3.1 Chemical structure of Nafion.

The inability of Nafion to function at temperatures above 80 °C has resulted in a search for new PEMs that can function at higher temperatures: specifically those that can function at temperatures greater than 120 °C. This is because there are several applications where it might become necessary to operate the fuel cell at elevated temperatures. Moreover, under high-temperature conditions, catalyst poisoning from carbon monoxide (CO) impurities in fuels becomes less serious because the catalyst

activity is improved at elevated temperatures. This enables the use of fuels with less stringent purity requirements. Therefore, several attempts have been made to operate fuel cells at higher temperatures using PEMs that are durable and efficient at higher temperatures. Different proton conducting media and alternative polymer membranes have been proposed, developed and tested. These include the use of alternative proton conduction media such as phosphoric acid and phosphonic acid¹⁴ and membranes such as polybenzimidazole.^{15,16} However, despite such progress, a PEM that can exhibit both high durability as well as high proton conductivity rates has not yet been found. Hence, there is still considerable interest in the development of novel, improved membranes for PEMFCs.

The objective of the current chapter is to propose a new material for use as a PEM and investigate its potential for efficient proton transfer, using computational methods. The material in question is a porous cage network that has been recently synthesized by Tozawa *et al.*¹⁷ This zero-dimensional (0-D) cage structure (shown in Figure 3.2) contains four phenyl rings separated by amine groups, and will henceforth be referred to as “*N-cage*”. The *N-cage* structure has been found to exhibit good thermal stability, with the onset of decomposition having experimentally been observed only at temperatures above 300 °C.¹⁷ Each cage molecule contains twelve N=C imine double bonds. Calculations, which are discussed below in the section 3.3, indicate that these imine bonds can be easily hydrogenated to yield a saturated structure that will henceforth be referred to as *N-cage-H₂*. It is postulated that the saturated *N-cage-H₂* structure, when combined with a dopant base that has the ability to exchange protons, can become an excellent candidate for PEMFCs. This is because of the possibility of forming hydrogen bonded networks between the hydrogenated zero dimensional cage structure and the dopant molecules that can reside inside the porous cages. Recent studies¹⁸ indicate that the formation of dynamic hydrogen bond networks within the membrane is an important pre-requisite to high proton conductivity. Hence it is likely that porous, doped *N-cage-H₂* like zero dimensional structures, which can accommodate many dopant molecules and which have twelve nitrogens in each cage that can be protonated, can become excellent candidates for the role of proton exchange membranes in fuel cells.

The focus of the current work is to investigate this possibility through (DFT)/MP2 calculations. The favorability of making the *N-cage-H₂* structure has first

been investigated by studying the thermodynamic ease of the reaction between H_2 and the *N-cage* molecule. The potential of *N-cage-H₂* to function as a PEM has then been studied by calculations on a system having *N-cage-H₂* along with (i) phosphoric acid, (ii) imidazole and (iii) triazole molecules in the porous cage structure. Investigations have been done to determine the feasibility of each of these dopants acting as an effective counterpart to *N-cage-H₂* for proton transfer. Finally, the most promising of the three has then been considered for further calculations determining the barrier to intermolecular proton transfer from the cage to the dopant and back to the cage.

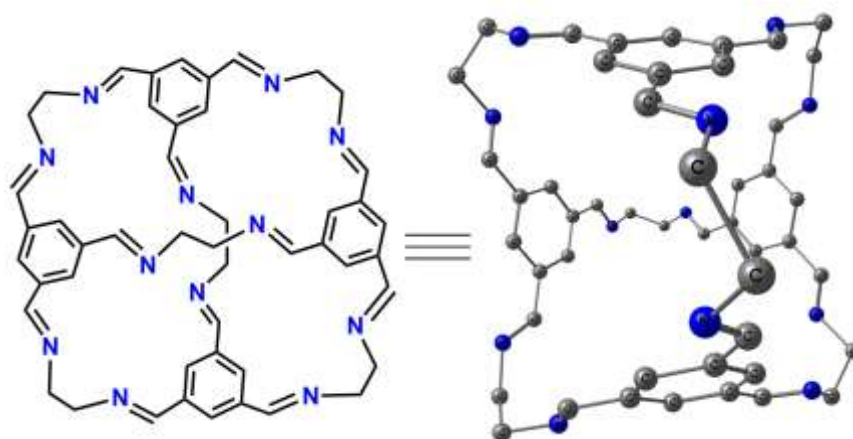


Figure 3.2 The recently synthesized zero-dimensional *N-cage* structure; the color scheme is as follows: carbon-brown and nitrogen-blue; the hydrogen atoms are not shown for the purpose of clarity.

3.2 Computational Details

All DFT calculations were performed using the Turbomole 6.0s programs.¹⁹ Geometry optimizations were performed using the Perdew, Burke, and Erzenhof density functional (PBE).²⁰ The electronic configuration of the atoms was described by a triple-zeta basis set augmented by a polarization function (Turbomole basis set TZVP). The resolutions of identity (RI)²¹ along with the multipole accelerated resolution of identity (marij)²² approximations were employed for an accurate and efficient treatment of the electronic Coulomb term in the density functional calculations. In order to improve the calculation of the energy values, a further correction was made through single point MP2 calculations,²³ along with the RI approximation, for the DFT (PBE) optimized structures. . With regard to the transition states obtained during the investigations of the proton transfer process, care was taken

to ensure that the obtained transition state structures possessed only one imaginary frequency corresponding to the correct normal mode.

That this approach, described above, provides reliable results has been further validated through benchmarking calculations done by comparison to previously published proton transfer barriers. As Figure 3.4 indicates, the potential energy (ΔE) surface published by Li *et al.*²⁴ reporting calculations done at the B3LYP/6-311+G(d)/MP2/ccpVTZ level of theory for the proton transfer reaction in the 1,2,3-triazole-triazolium dimer matches almost exactly with the calculations that we have done at our aforementioned RIPBE/RIMP2 level of theory (see Figure 3.4).

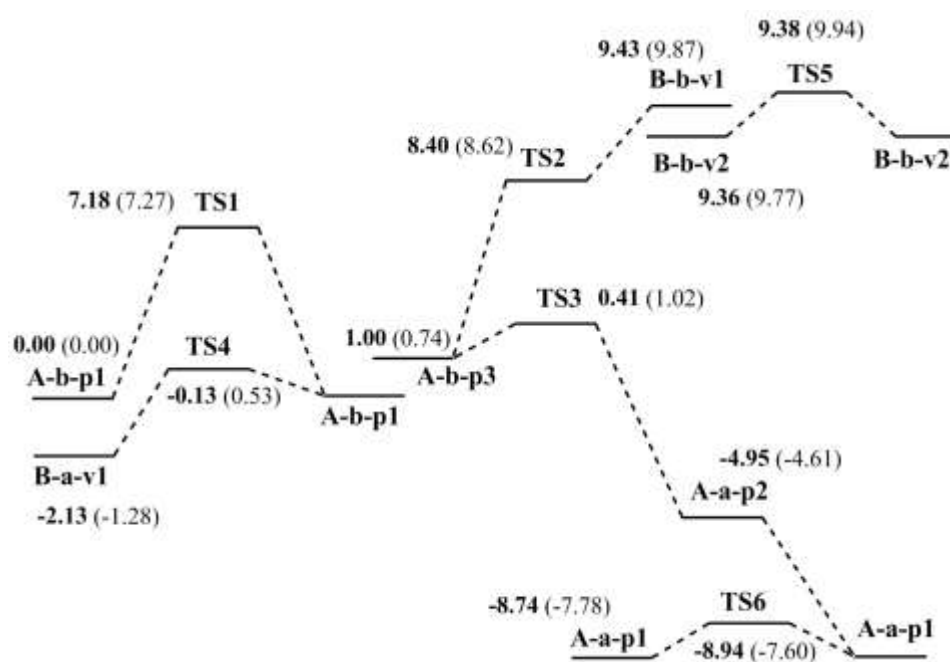


Figure 3.4 The potential energy surface for proton transfer in triazole-triazolium dimers; all the symbols for the different minimum energy structures and transition states as well as all the values (converted to kcal/mol) inside the parenthesis are those obtained from Figure 4 of the paper,²⁴ their values having been obtained from a B3LYP/6-311 + G(d)/ MP2/ccpVTZ level of theory; the values outside of the parenthesis are the values that have been obtained from our computational approach.

Furthermore, using our RIPBE/RIMP2 computational approach, we have redone the calculations for determining the proton transfer barriers (ΔE) for the imidazolium-imidazole (ImH^+ -Im), 1,2,3-Triazolium-1,2,3-Triazole (TrH^+ -Tr), and Tetrazolium-Tetrazole (TeH^+ -Te) complexes, that have been published by Mangiatordi *et al.*²⁵ using a full MP2 approach. The results are shown in Table 3.1;

indicate practically no difference between the values obtained through the two different approaches. Thus, these validating benchmarking calculations indicate the reliability of the computational approach employed in our work.

The contributions of internal energy and entropy were further obtained from frequency calculations done on the optimized structures at 298.15 K in order to obtain the ΔG values that are discussed in Section 3.3 (see the Figures 3.11 and 3.13 below).

Table 3.1 The barriers to proton transfer obtained from full MP2 calculations done for imidazolium-imidazole ($\text{ImH}^+\text{-Im}$), 1,2,3-Triazolium-1,2,3-Triazole ($\text{TrH}^+\text{-Tr}$), and Tetrazolium-Tetrazole ($\text{TeH}^+\text{-Te}$) Complexes²⁵ compared with the values obtained from our computational approach.

	$\text{ImH}^+\text{-Im}$	$\text{TrH}^+\text{-Tr}$	$\text{TeH}^+\text{-Te}$		
			c	d	e
MP2 from reference	0.5	0.4	1.4	0.0	0.4
Our MP2 calculations	0.5	0.4	1.5	0.0	0.6

3.3. Results and Discussion

3.3.1 Proton Transfer through *N*-cage in Tandem with H_3PO_4

The *N*-cage structure was optimized using the input obtained from a crystal structure¹⁷. The addition of twelve molecules of H_2 to this structure would lead to the hydrogenated “*N*-cage- H_2 ” structure, through the hydrogenation of the twelve imine moieties in the cage. The optimized structure of the *N*-cage- H_2 is shown in Figure 3.5. The ΔG for the formation of the *N*-cage- H_2 is -72.8 kcal/mol, which indicates the favourability of the reaction. Further calculations were done to explore the addition of molecules of the dopant X (where X = phosphoric acid, imidazole and triazole) to *N*-cage- H_2 . The addition of two molecules of X was found to lead to the formation of a hydrogen bonded network between the two dopant molecules and *N*-cage- H_2 (see Figures 3.6, 3.7 and 3.8 below). This system: “[*N*-cage- H_2][2X]”, will be considered as the model for studying the possibility of proton transfer through the cage. It is noted here that larger models can also be considered by the addition of more dopant molecules into the porous cage, and, therefore alternative proton conducting routes can also be investigated connecting other amine nitrogens in the cage. However, the

purpose of the current investigation is to illustrate the efficiency of the proton transfer process for a given, representative hydrogen bonded network formed between the cage and the dopant molecules, and the “[*N-cage-H₂*][2X]” model adopted here is adequate for this purpose.

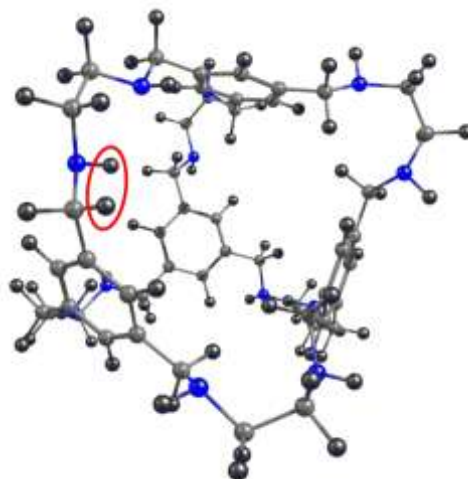


Figure 3.5 The zero-dimensional cage structure where all the imine groups in the cage have been hydrogenated: “[*N-cage-H₂*]”; hydrogens in the N-C bond is circled in red to indicate one of the twelve imine groups that have been hydrogenated; the color scheme is as follows: carbon – brown, nitrogen – blue, hydrogen – yellow.

In order to investigate the energetics of proton transfer through this [*N-cage-H₂*] network, the first study conducted is as follows: the structures of [*N-cage-H₂*][2X] were optimized with the addition of a proton: that is, the structures optimized were [*N-cage-H₂*][2X][H]⁺. During the optimization procedure, two structures were considered – one where the proton was placed on the amine nitrogen on the cage, and the other where the proton was placed on the adjacent, hydrogen bonding dopant molecule, X. This procedure yielded the following interesting results for the three cases considered:

(i) For the case where the dopant employed was phosphoric acid, only one final optimized structure was obtained, even though two different structures had been considered, as mentioned above. In this final, optimized structure, the proton was found to be on the amine nitrogen of *N-cage-H₂*. This optimized structure is shown in Figure 3.6 below – the proton is circled in red in the structure. All attempts to start with different input conformations in order to obtain geometry where the proton was stable on the phosphoric acid proved unsuccessful. This result indicates that if

phosphoric acid is employed as the dopant in the *N-cage-H₂* structure, it will fail to remove the proton from the cage. It is pertinent to note in this regard that if the hydrogenation of the cage was done in an alternate fashion: if one of the carbons of the phenyl ring and a nitrogen of an adjoining imine group,²⁶ which can act as a Frustrated Lewis Pair, were to be hydrogenated in preference to the N=C bond, then calculations indicate that such a hydrogenated cage would be able to transfer a proton to the hydrogen bonded network formed by the two phosphoric acid molecules. However, such an alternative hydrogenation pathway may only exist for certain hydrogenating agents such as ammonia borane. For the remaining cases, it is likely that the twelve N=C bonds in *N-cage* would be preferentially hydrogenated. Hence, the calculations indicate that for such structures, the phosphoric acid would not be a good dopant: even though it would be able to form a hydrogen bonded network, it would fail to be an effective counterpart to the cage in doing a proton transfer.

(ii) For the case where the dopant employed was imidazole, the situation was found to be exactly reversed. For this case, it was seen that the proton remained only on the imidazole molecule in all the optimized structures. This is shown in Figure 3.7 below: the proton is circled in red and is seen to remain only on the nitrogen of the imidazole moiety. All attempts made to obtain optimized structures where the proton was transferred on to the nitrogen of the cage proved unsuccessful: the proton was found to be only stable on the imidazole in all the cases. Hence, this result indicates that imidazole would also fail to be an effective counterpart to *N-cage-H₂* for proton transfer.

(iii) For [*N-cage-H₂*][2X][H]⁺, the final case discussed is X = triazole. For triazole, two possible isomers exist: 1,2,3 triazole and 1,2,4 triazole and the formation of a protonated hydrogen bonded network, [*N-cage-H₂*][2X][H]⁺, is possible for both isomers. Both 1,2,3 triazole²⁷ and 1,2,4 triazole²⁸ have been experimentally employed as dopants in proton conducting studies with proton exchange membranes. What is discussed in this section 3.3.2 are the results for X = 1,2,3 triazole, with the results with 1,2,4 triazole being discussed in a later section. Figure 3.8 shows the structures obtained for this dopant: it was found that two structures could indeed be obtained for this case, one where the proton was stable on the cage and the other where the proton (circled in red in the figure) was stable on the nitrogen of the 1,2,3 triazole. Hence, the calculations suggest that, of the three dopants, it is triazole that would be most

effective in participating in proton exchange with [*N*-cage-*H*₂] to make an effective proton exchange membrane.

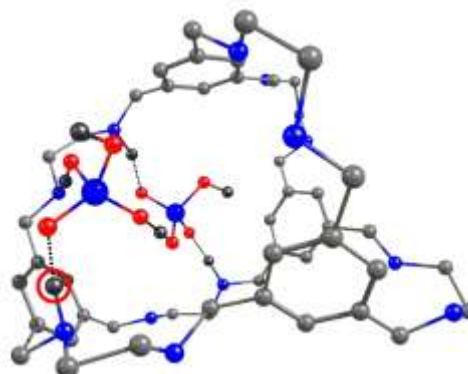


Figure 3.6 The optimized structure where the proton, circled in red, is always found to be situated on the amine nitrogen of the cage; the color scheme is as follows: carbon – brown, nitrogen - blue; hydrogen – yellow; only a few hydrogen atoms that take part in the hydrogen bonding network have been shown, for the purpose of clarity.

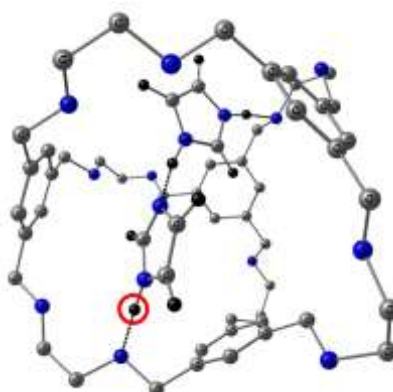


Figure 3.7 The optimized structure where the proton, circled in red, is always found to be situated on the nitrogen of the dopant imidazole; the color scheme is as follows: carbon – brown, nitrogen – blue, hydrogen – yellow; only a few hydrogen atoms that take part in the hydrogen bonding network have been shown, for the purpose of clarity.

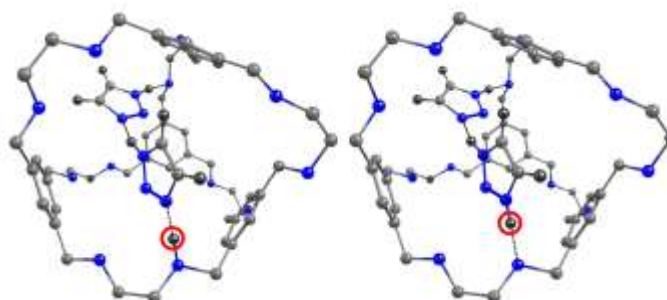


Figure 3.8 The two optimized structures that have been obtained for the cage doped with 1,2,3 triazole, with the proton, circled in red, present on both the cage and on the dopant; the color scheme is as follows: carbon – brown, nitrogen – blue, hydrogen – yellow; only a few hydrogen atoms that take part in the hydrogen bonding network have been shown, for the purpose of clarity.

The reason for the difference in the proton abstraction behaviour of the three dopants in the $[N\text{-cage-H}_2][2X][H]^+$ model lies in the difference in the ability of the dopant molecule to stabilize the positive charge of the proton. The following calculation makes this point more clear: the structures X and $[XH]^+$ were optimized for X = phosphoric acid, imidazole and 1,2,3 triazole, and the difference in the stability between the protonated and neutral species is shown in Figure 3.9 below. As the figure indicates, the protonated structure is more stable in all the three cases. However, the dopant that is most effective in stabilizing the proton is imidazole, followed by 1,2,3 triazole, with phosphoric acid predicted to be the least effective. The reason for this trend is because of the difference in the basicities of the three moieties. As has been experimentally determined by Meotner *et al.*,²⁹ triazoles have lower proton affinity as compared to imidazole. This difference in the proton affinity, and therefore the basicity between imidazole and triazole explains why the proton is too stabilized with imidazole as the base and cannot be “recaptured” by the nitrogen of the cage, while the lower basicity of triazole allows the proton to be stabilized by both the cage and the triazole moiety. It is noted here that there are several other bases whose proton affinities (ΔH values) have also been experimentally determined.²⁹ As Table 3.2 indicates, the current calculations provide values close to the experimentally obtained ΔH values, in addition to faithfully reproducing the observed experimental trend in the proton affinities.

Table 3.2 A comparison of the experimentally obtained ΔH values for different bases, taken from the reference: Meotner *et al.*²⁹ (*the second column of the table below*) with the calculated values for ΔH from the same paper (*the third column of the table below*) and the values, that we have calculated (*fourth column in the table below*); all values are in kcal/mol.

Base	ΔH_{expt} (values from the reference paper) ²⁹	ΔH_{cal} (values from the reference paper) ²⁹	ΔH_{cal} (our calculations)
Imidazole	-222.1	-230.0	-224.6
1methylimidazole	-228.0	-234.7	-229.2
4methylimidazole	-224.8	-233.7	-229.0
Pyrazole	-212.8	-216.0	-210.4
1, 2, 4 triazole H ⁺ at N ₄	-212.4	-214.5	-208.9
Oxazole H ⁺ at N ₄	-207.8	-212.0	-207.2

Hence, the above discussion indicates that bases with intermediate basicities such as 1,2,3 triazole, would be the best choice as a dopant for $[N\text{-cage-H}_2]$: they can abstract the proton from the nitrogen of the cage, while not binding too strongly to it so as to allow the cage to abstract it back, thereby making for a good proton exchange pair with the cage. This intermediate value obtained for 1,2,3 triazole also suggests a guide for choosing other dopants in the future: if a base is to be considered as the counterpart to hydrogenated zero dimensional cage structures such as $[N\text{-cage-H}_2]$, then the difference in the stability between the protonated and neutral species for such a molecule should fall in the range indicated by 1,2,3 triazole: $\Delta G = -213.8$ kcal/mol for the reaction: $X + H^+ \rightarrow [XH]^+$. Since our calculations indicate that the ΔG and the ΔH values for the reaction $X + H^+ \rightarrow [XH]^+$ are quite similar, as the entropic change in adding a proton is very small, ΔH values, that is the proton affinity, of bases in the vicinity of -213.8 kcal/mol would be a good guide as to which bases would act as good dopants for the zero-dimensional cages such as $[N\text{-cage-H}_2]$ for the purposes of proton transfer in fuel cell membranes. A perusal of the proton affinity values determined experimentally²⁹ therefore indicates that 4-methylimidazole (-224.8 kcal/mol), 1-methylimidazole (-228.0 kcal/mol), pyrazole (-212.8 kcal/mol) and others with similar proton affinities would also be good dopants for $[N\text{-cage-H}_2]$.

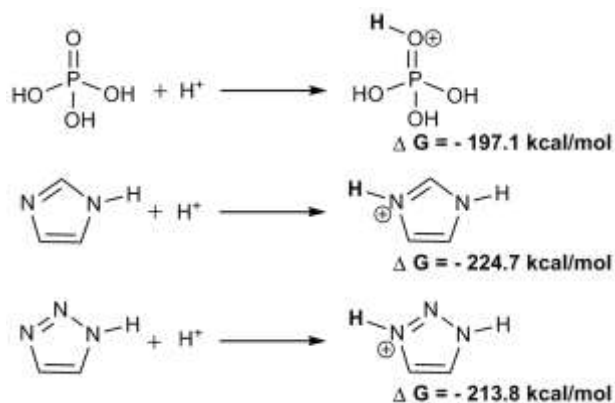


Figure 3.9 The free energies for the protonated phosphoric acid, imidazole and 1,2,3 triazole dopants.

Having identified the triazoles as good dopants for the zero-dimensional cages, it was also necessary to determine the ease with which the proton could move between the cage and the base, since that would determine the efficiency of the proton conduction process if such doped cages were to be employed as fuel cells. Discussed in the next section is the potential energy surface obtained for the proton transfer process from the cage to the hydrogen bonded triazole network and back to the cage.

3.3.2 Proton Conduction Studies

Figure 3.10 below shows the energy profile (ΔE values) for the transfer of a proton from a nitrogen of [*N-cage-H*₂] to the hydrogen bonded 1,2,3 triazole, from that triazole molecule to the adjoining hydrogen bonded triazole moiety and then from the second triazole back to another nitrogen atom of [*N-cage-H*₂]. The barriers for these three proton transfer processes have been calculated using Transition State Theory. Frequency calculations were done in order to ensure that the obtained transition state structures contained only one negative frequency corresponding to the correct normal mode.

As Figure 3.10 indicates, all the three transition states obtained corresponded to very low barrier reactions. **TS_{1a}**, which corresponds to the first transfer of the proton from the nitrogen of [*N-cage-H*₂] (structure **1a**, see Figure 3.10) to the nitrogen of 1,2,3 triazole (leading to the structure **2a**, see Figure 3.10), has the highest barrier for the entire proton transfer cycle. This barrier is found to be only 1.7 kcal/mol (ΔE value), which indicates that the proton transfer would be facile, with the efficiency for

the process likely to be high at higher temperatures. The other two barriers, **TS_{2a}** and **TS_{3a}**, corresponding to the transfer of the proton from one 1,2,3 triazole molecule to the other (forming **3a**, see Figure 3.10), and then back to another nitrogen of the cage (structure **4a**, see Figure 3.10 below) are found to be even lower: 0.3 kcal/mol and 0.5 kcal/mol respectively, thereby indicating the facility of the proton transfer for the [*N-cage-H₂*][X] [H⁺] case where X = 1,2,3 triazole. Figure 3.11 shows the corresponding ΔG values for the same proton transfer cycle. The reason the ΔE and the ΔG values have been shown in separate figures is to highlight the fact that the incorporation of entropic effects renders the proton transfer process even more facile, with the rate determining barrier for the process (corresponding to the transition state **TS_{1a}**) reduced to only 0.2 kcal/mol. It is noted that the other two transition states are actually found to lie slightly *lower* in energy than the corresponding reactants (see Figure 3.11) because the original positive difference in the ΔE terms is so small that the favourable addition of entropic and other terms leaves the free energy of the transition state structures lower than the free energy of the corresponding reactant structures. The net result of the ΔG calculations is therefore to indicate that the proton transfer process for the [*N-cage-H₂*][2X] [H⁺] system, where X = 1,2,3 triazole, is likely to be a highly facile one. Since many such proton transfer pathways will be likely to exist in the doped system due to the possibility of more dopant molecules being housed in the porous cages and thus being able to transfer protons through other routes between different nitrogens of [*N-cage-H₂*], the results indicate that the [*N-cage-H₂*] system doped with 1,2,3 triazole would be likely to perform in a highly efficient manner as a proton exchange membrane.

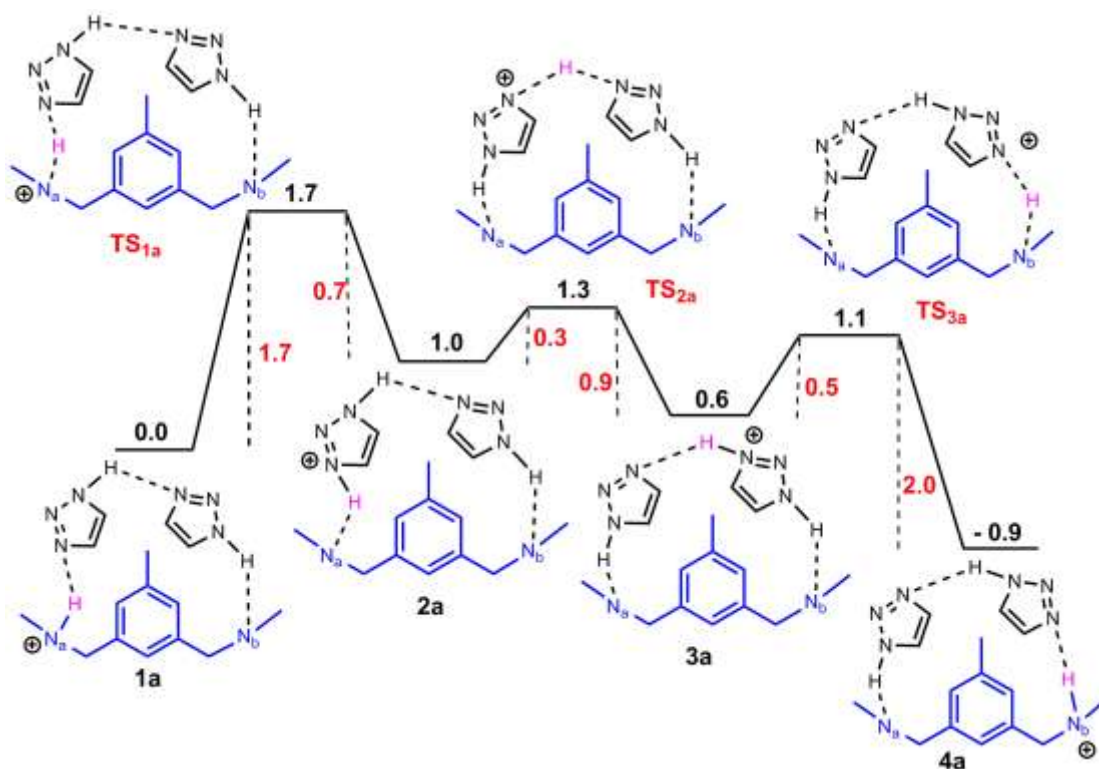


Figure 3.10 The potential energy for the transfer of the proton through the hydrogen bonded network from one end of the cage to the other; the dopant employed in 1,2,3 triazole; all values (ΔE) are in kcal/mol.

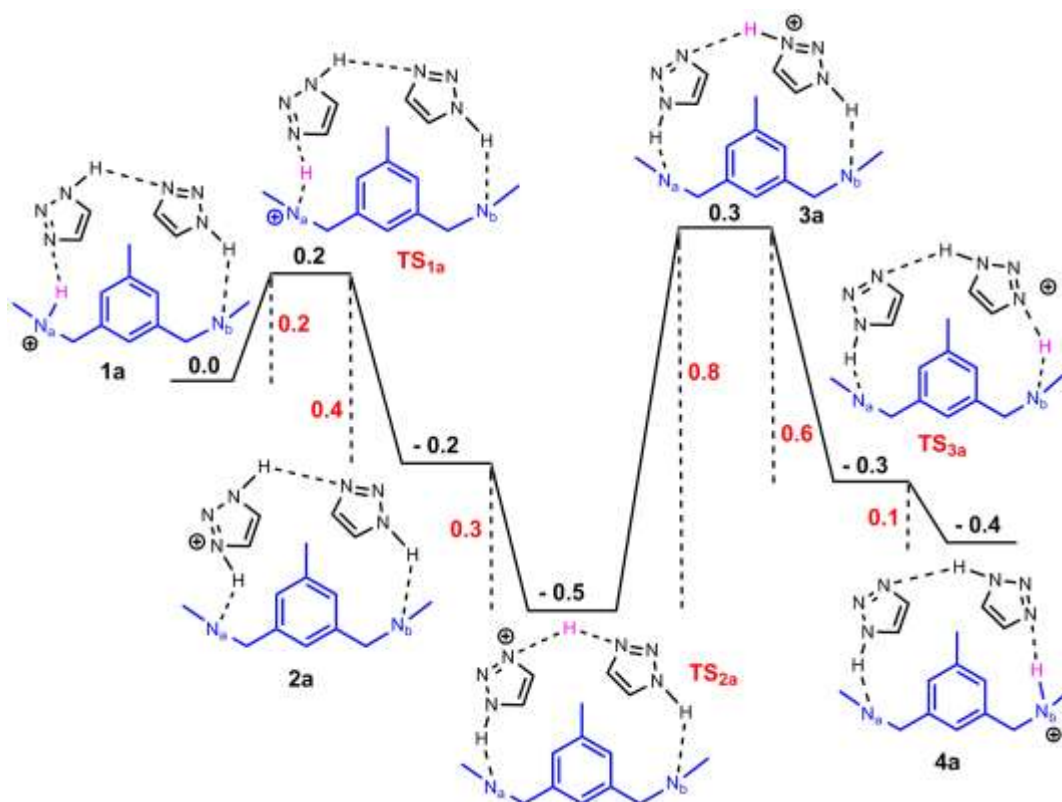


Figure 3.11 The free energy surface for the transfer of the proton through the hydrogen bonded network from one end of the cage to the other; the dopant employed in 1,2,3 triazole; all values (ΔG) are in kcal/mol.

3.3.3 Proton Transfer with 1,2,4 triazole

Discussed in the previous section is the proton transfer pathway for [*N*-cage- H_2][2X] [H^+], where X is 1,2,3 triazole. The corresponding potential energy surface has also been determined for X = 1,2,4 triazole, the other triazole isomer. Figure 3.12 below shows the potential energy surface calculated as the difference in the ΔE values between the different reactants, intermediates and transition states along the proton transfer route. Only two transition states were obtained: after the first proton transfer from the cage (structure **1b**, see Figure 3.12) to the hydrogen bonded dopant, going through the transition state **TS_{1b}**, (see Figure 3.12), the intermediate obtained has the proton already transferred to the second 1,2,4 triazole molecule (structure **2b**, see Figure 3.12), that is, the transfer of the proton from the first 1,2,4 triazole molecule to the second is a barrierless process. The second transition state, **TS_{2b}**, connects this intermediate to the final structure, **3b**, along the potential energy surface (see Figure 3.12). The barrier heights are found to be higher for this case in comparison to [*N*-cage- H_2][2X] [H^+], where X = 1,2,3 triazole. These values are reduced, as in the earlier case, when ΔG values are considered: the slowest step of the proton transfer pathway considered is 0.6 kcal/mol (corresponding to the transition state **TS_{1b}**, see Figure 3.13), 0.4 kcal/mol higher than the slowest step for X = 1,2,3 triazole case. However, the smallness of the barrier heights indicates that 1,2,4 triazole can also be a good dopant for [*N*-cage- H_2] in order to make the zero dimensional cage an effective proton exchange membrane.

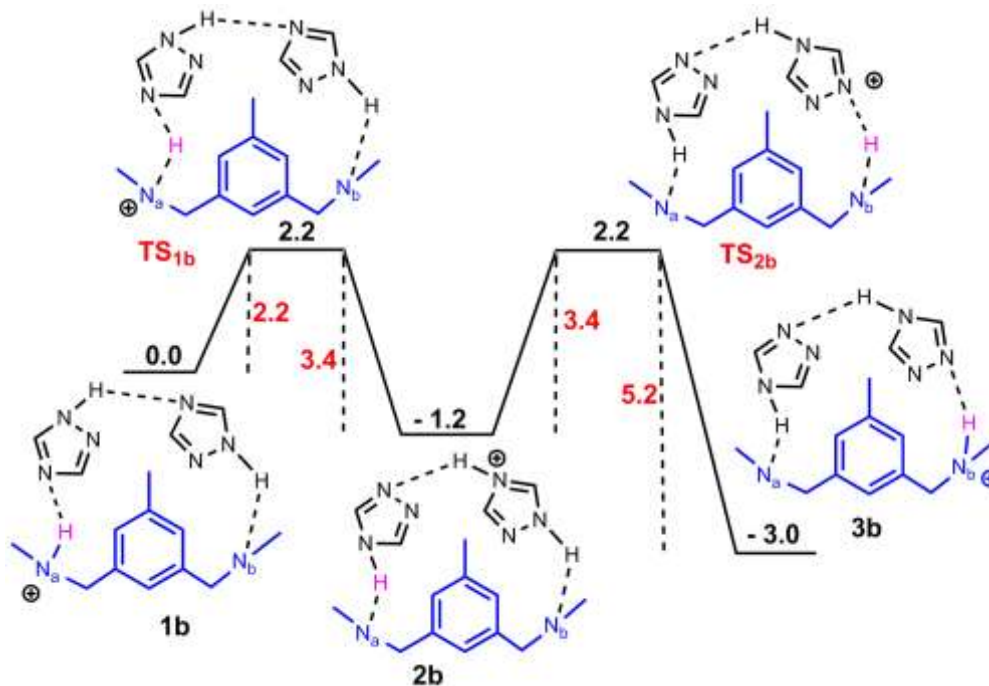


Figure 3.12 The potential energy for the transfer of the proton through the hydrogen bonded network from one end of the cage to the other; the dopant employed in 1,2,4 triazole; all values (ΔE) are in kcal/mol.

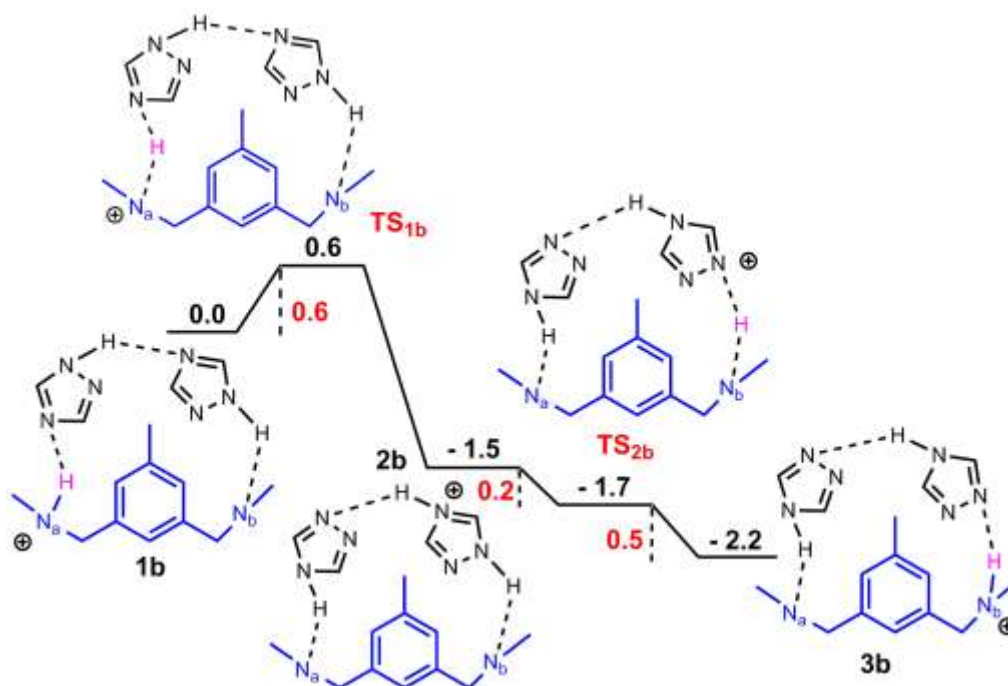


Figure 3.13 The free energy for the transfer of the proton through the hydrogen bonded network from one end of the cage to the other; the dopant employed in 1,2,4 triazole; all values (ΔG) are in kcal/mol.

It is to be noted that all the calculations discussed in the previous sections have focused on *static* quantum chemical calculations on zero dimensional cage structures, and it is also important to note that the calculations have been done with a *model system* consisting of a single zero dimensional cage doped with imidazole, triazole or phosphoric acid molecules. Were this system to be employed as a membrane in a fuel cell, it would consist of a stacking of several doped 0D cage molecules, and its performance as a fuel cell membrane could therefore be influenced by other factors such as local concentration effects wherein dopant molecules might cluster more around certain regions of the porous membrane and less in other regions. Such effects are not captured by the current computational model employed and might require further investigations in the future.

Furthermore, it is also possible that thermal fluctuations, which cannot be captured by the static nature of the quantum chemical calculations described here, can have effects such as the distortion of the cage due to elongation/fluctuation of the C-C and N-C bonds in the cage. Zhang *et al.*,³⁰ for instance, have observed that *ab initio* molecular dynamics simulations done on the zero dimensional C₆₀ cage structure resulted in distortion of the cage at high temperatures (up to 1800 K), though the cage structure was still preserved. Sun *et al.*³¹ observed, through *ab initio* molecular dynamics simulations done at 300 K, that the presence of H₂ molecules in B-N cage structures led to distortion of B-N bonds in the cage due to the asymmetric distribution of the H₂ molecules in the cage. Joshi *et al.*³² have observed an increase in bond length fluctuations in small gallium clusters, Ga₃₀ and Ga₃₁, upon conducting *ab initio* molecular dynamics simulations and increasing the temperature from 0 K to 900 K in such systems. Chandrachud *et al.*³³ have investigated the behaviour of small sized gold cages (Au₁₆ and Au₁₇) through *ab initio* molecular dynamics simulations and found that the increase in temperature from 0 K to 600 K led to distortions in the cage structure, as well as to a degree of isomerization for both the gold cages considered. While it is clear that the behaviour of different cage structures, in the presence and absence of dopants, is likely to be dependent on its chemical constitution, the examples of the different cage structures cited here indicate that regardless of the chemical nature of the cage, thermal effects, captured by *ab initio* molecular dynamics simulations, would lead to the distortion of the cage, though the cage structure would remain intact up to high temperatures. The static calculations

discussed in the work presented here cannot account for the thermal distortions that are likely in the doped *N-cage* structures at the temperatures under which the fuel cell would operate, and this is a limitation of the current work. It is, however, also clear that the *N-cage* structure should remain intact even at high temperatures, and the ease of proton transfer from the cage to the dopant base and back to the cage should be even more facilitated at higher temperatures, due to the greater ease with which the barrier to proton transfer can be surmounted. Therefore, it is likely that (a) the doped *N-cage* structure would persist at fuel-cell operating temperatures, even though distortions in the cage structure would be likely and (b) the efficiency of the proton transfer, and therefore the effectiveness of the proposed fuel cell membrane, would also be high at the higher temperatures.

3.4 Conclusions

The recently synthesized and characterized zero dimensional nitrogen based (“*N-cage*”) structures have been experimentally found to be stable up to temperatures well above 300 °C.¹⁷ Such cages structures are also porous and can thus be easily doped with hydrogen bonding bases such as phosphoric acid, imidazole and 1,2,3 and 1,2,4 triazoles. Since it has been demonstrated¹⁸ that formation of dynamic hydrogen bond networks within the membrane is an important pre-requisite to high proton conductivity,¹⁸ such zero dimensional doped *N-cage* structures have the potential to be excellent proton exchange membranes in fuel cells. This potential has been explored through full quantum mechanical calculations with DFT and MP2 methods. The results indicate that the hydrogenated zero dimensional cages (“*N-cage-H₂*”) would perform very efficiently as PEMs in combination with two hydrogen bonding 1,2,3 and 1,2,4 triazole molecules (“[*N-cage-H₂*][2X]”, where X = 1,2,3 and 1,2,4 triazole). The process of transferring a proton from one nitrogen in the cage to another through the network of triazole molecules was found to be nearly barrierless - the slowest step in the proton transfer process studied had a barrier of 0.2 kcal/mol (ΔG value) for X = 1,2,3 triazole. The corresponding barrier in 1,2,3 triazole was 0.6 kcal/mol. The results thus highlight the possibility of the existence of highly efficient proton conducting channels in the proposed [*N-cage-H₂*][2X] PEMs. The results are significant due to the need for developing new, efficient PEMs that can perform in the absence of water at high temperatures.

3.5 References

- (1) Appleby, A. J.; Foulkes, F. R. *Fuel cell handbook / A.J. Appleby, F.R. Foulkes*; Van Nostrand Reinhold: New York :, **1989**.
- (2) Savadogo, O. *Journal of New Materials for Electrochemical Systems* **1998**, *1*, 47-66.
- (3) Steele, B. C. H.; Heinzl, A. *Nature* **2001**, *414*, 345-352.
- (4) Kreuer, K.-D.; Paddison, S. J.; Spohr, E.; Schuster, M. *Chemical Reviews* **2004**, *104*, 4637-4678.
- (5) Carla, H.-W. *Journal of Membrane Science* **1996**, *120*, 1-33.
- (6) Kreuer, K.-D.; Rabenau, A.; Weppner, W. *Angewandte Chemie International Edition in English* **1982**, *21*, 208-209.
- (7) Kreuer, K.-D. *Chemistry of Materials* **1996**, *8*, 610-641.
- (8) Eikerling, M.; Kornyshev, A. A.; Kuznetsov, A. M.; Ulstrup, J.; Walbran, S. *The Journal of Physical Chemistry B* **2001**, *105*, 3646-3662.
- (9) Samuel, C. *Biochimica et Biophysica Acta (BBA) - Bioenergetics* **2006**, *1757*, 876-885.
- (10) Kreuer, K. D. *Journal of Membrane Science* **2001**, *185*, 29-39.
- (11) Noam, A. *Chemical Physics Letters* **1995**, *244*, 456-462.
- (12) Tuckerman, M. *J. Chem. Phys.* **1995**, *103*, 150.
- (13) Tuckerman, M.; Laasonen, K.; Sprik, M.; Parrinello, M. *The Journal of Physical Chemistry* **1995**, *99*, 5749-5752.
- (14) Allcock, H. R.; Hofmann, M. A.; Ambler, C. M.; Lvov, S. N.; Zhou, X. Y.; Chalkova, E.; Weston, J. *Journal of Membrane Science* **2002**, *201*, 47-54.
- (15) Wainright, J. S.; Wang, J. T.; Weng, D.; Savinell, R. F.; Litt, M. *Journal of The Electrochemical Society* **1995**, *142*, L121-L123.
- (16) Glipa, X.; Bonnet, B.; Mula, B.; J. Jones, D.; Roziere, J. *Journal of Materials Chemistry* **1999**, *9*, 3045-3049.
- (17) Tozawa, T.; Jones, J. T. A.; Swamy, S. I.; Jiang, S.; Adams, D. J.; Shakespeare, S.; Clowes, R.; Bradshaw, D.; Hasell, T.; Chong, S. Y.; Tang, C.; Thompson, S.; Parker, J.; Trewin, A.; Bacsa, J.; Slawin, A. M. Z.; Steiner, A.; Cooper, A. I. *Nature Materials* **2009**, *8*, 973-978.

-
- (18) Nagamani, C.; Viswanathan, U.; Versek, C.; Tuominen, M. T.; Auerbach, S. M.; Thayumanavan, S. *Chemical Communications* **2011**, *47*, 6638-6640.
- (19) Ahlrichs, R.; Bär, M.; Häser, M.; Horn, H.; Kölmel, C. *Chemical Physics Letters* **1989**, *162*, 165-169.
- (20) Perdew, J. P.; Burke, K.; Ernzerhof, M. *Physical Review Letters* **1996**, *77*, 3865.
- (21) Eichkorn, K.; Treutler, O.; O'hm, H.; Häser, M.; Ahlrichs, R. *Chemical Physics Letters* **1995**, *240*, 283-289.
- (22) Sierka, M.; Hogekamp, A.; Ahlrichs, R. *J. Chem. Phys.* **2003**, *118*, 9136.
- (23) Hattig, C.; Weigend, F. *The Journal of Chemical Physics* **2000**, *113*, 5154-5161.
- (24) Li, A.; Yan, T.; Shen, P. *Journal of Power Sources* **2011**, *196*, 905-910.
- (25) Mangiatordi, G. F.; Hermet, J.; Adamo, C. *The Journal of Physical Chemistry A* **2011**, *115*, 2627-2634.
- (26) Pal, A.; Vanka, K. *Chemical Communications* **2011**, *47*, 11417-11419.
- (27) Zhou, Z.; Li, S.; Zhang, Y.; Liu, M.; Li, W. *Journal of the American Chemical Society* **2005**, *127*, 10824-10825.
- (28) Li, S.; Zhou, Z.; Zhang, Y.; Liu, M.; Li, W. *Chemistry of Materials* **2005**, *17*, 5884-5886.
- (29) Meot-Ner, M.; Liebman, J. F.; Del Bene, J. E. *The Journal of Organic Chemistry* **1986**, *51*, 1105-1110.
- (30) Zhang, Q. M.; Yi, J.-Y.; Bernholc, J. *Physical Review Letters* **1991**, *66*, 2633-2636.
- (31) Sun, Q.; Wang, Q.; Jena, P. *Nano Letters* **2005**, *5*, 1273-1277.
- (32) Joshi, K.; Krishnamurty, S.; Kanhere, D. G. *Physical Review Letters* **2006**, *96*, 135703.
- (33) Chandrachud, P.; Joshi, K.; Krishnamurty, S.; Kanhere, D. *Pramana* **2009**, *72*, 845-855.

CHAPTER 4

Proposing Efficient New Pendant Group Polymer Electrolyte Membranes for Fuel Cells



ABSTRACT

There is a need to develop new membranes for fuel cells that can conduct protons with high efficiency and at high temperatures. This chapter reports a theoretical study of proton transfer barriers in newly proposed polymer electrolyte membranes (PEMs), having pendant nitrogen containing crown ether groups on an alkyl backbone. The proton transfer in the proposed pendant group PEMs would occur without the need of an external agent such as water or phosphoric acid, and without the need for the pendant groups to rotate and reorient themselves after each proton transfer. The current study shows that this would make the proposed PEMs very efficient, with low proton transfer barriers. This has been seen to be true for a range of different PEM cases considered, differing in the number of linker atoms in the alkyl backbone, and in the number of nitrogens contained in each pendant group, thus indicating the potential of the proposed pendant crown ether group structures as PEMs for fuel cells.

4.1 Introduction

The need to develop new avenues for clean energy is paramount in the modern age. Polymer electrolyte membrane fuel cells (PEMFCs) that combine dihydrogen and dioxygen to generate electrical energy, producing no greenhouse gases during the process, hold great promise in this regard. There has, therefore, been considerable interest shown in developing new PEMFCs, with special attention being focused on developing new membranes that can separate the anode and the cathode in the fuel cell, and help transport the proton efficiently from the anode to the cathode. Indeed, the membrane has been described as the “heart” of the fuel cell.¹

Investigations have revealed that proton transport in the polymer electrolyte membranes (PEMs) occurs primarily through two processes: 1) the vehicular mechanism² and 2) the Grotthuss mechanism^{1,3-9} (or structure diffusion). In PEMs that employ water, such as Nafion,¹⁰ the proton is transported through water channels in complex forms associated with water molecules, such as H_3O^+ and H_5O_2^+ , by the vehicular mechanism. Alternatively, protons are transferred by the forming and breaking of bonds in the water network, with the cooperation of pendant sulphonate groups in the Nafion membrane. These mechanisms of proton transport have led to Nafion being employed as a successful PEM in PEMFCs, but it has also been noted that the use of water in Nafion results in a disadvantage: the PEMFC shows poor conductivities at temperatures above the boiling point of water. High proton conductivities are, however, desirable at higher temperatures ($> 100\text{ }^\circ\text{C}$), because operating the PEMFC at high temperatures can make heat management easier, increase fuel cell efficiency, reduce cost, and prevent catalyst poisoning.¹¹

This limitation of the use of water in PEMs has provided the impetus for the development of a particular type of proton transfer known as “anhydrous proton transfer”. This is when a proton can be transferred from the cathode to the anode without the aid of a solvent-type medium such as water. One possible means of achieving this is by having pendant groups on a polymer backbone. Such a membrane can transport a proton through two steps: (i) by transferring the proton from one pendant group to the next, followed by (ii) the reorientation of the pendant group back to the original position, thus being ready for the next proton transfer. Steps (i) and (ii) are illustrated in Figure 4.1 below for a membrane with phenol as the pendant group.

Such membranes have the advantage of increased proton conductivity with increase in temperature, even at higher temperatures. This is in contrast to the proton transport that occurs with the assistance of the solvent (usually water) where the proton conductivity is seen to decrease with the increase in temperature.

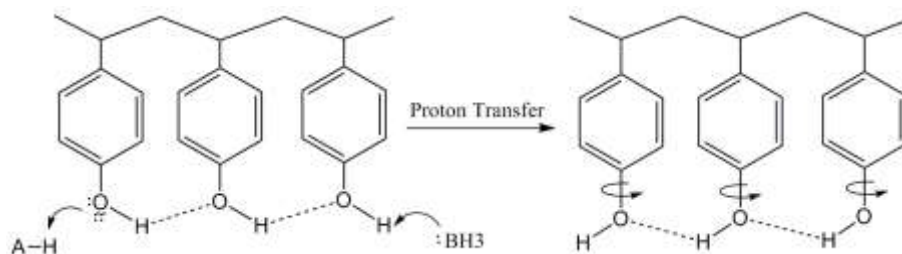


Figure 4.1 Anhydrous proton transfer through polymer electrolyte membranes (PEMs) with pendant groups usually proceeds through two steps: (i) proton transfer and (ii) reorientation of the pendant group.

However, despite their attractiveness, such PEMs, having pendant groups on a polymer backbone, have a disadvantage in that the reorientation step (ii) is the slow step,¹² with a significant barrier,¹²⁻²⁰ ranging from 8.0 kcal/mol²⁰ to 39.2 kcal/mol.¹² The reason a rotation or reorientation barrier is required in such membranes can be understood when one considers an example, such as the case of the proton transfer reaction between two nitrogen containing moieties, which has been studied and reported²¹⁻²⁵ for model systems such as imidazole^{1,12,26} and triazole.²⁷ The transfer process in such systems involves one nitrogen accepting a proton while another nitrogen in the same molecule donates a proton to the neighboring molecule. This is illustrated in Figure 4.2 below for the case of imidazole. What this “sharing” of the proton transfer process leads to be the requirement of the imidazole moiety having to rotate so as to reorient itself into the original position, ready to accept the next proton.

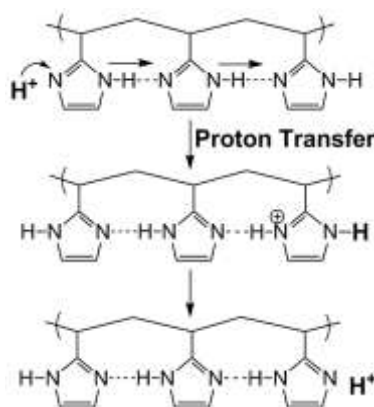


Figure 4.2 Schematic representation of proton transfer through imidazole pendant groups on a polymer backbone: the proton transfer is shared between two nitrogens.

The above discussion makes it clear that one approach for increasing the efficiency of anhydrous proton transfer PEMs would be to employ a pendant ligand that *does not have to be reoriented during the process of proton transfer*. Such a PEM containing PEMFC can combine the twin advantages of anhydrous proton transfer at high temperatures with high efficiency. The focus of the current computational investigation is to investigate potential PEMs that can do just that. What has been proposed are PEMs having crown ethers as the pendant groups. An illustrative example of a pendant groups crown ether is shown in Figure 4.3 below, having $-\text{CH}_2-\text{CH}_2-$ groups connecting five oxygens and a nitrogen atom: the aza18-crown 6-ether. The proposed PEM structure shown in Figure 4.3 has the pendant groups connected with a single CH_2 linker along the alkyl backbone. Figure 4.3 shows a proton transfer process starting from the aza crown ether pendant group on the left (A) to the adjacent nitrogen moiety on the middle pendant group (B). This leads to a new intermediate that can transfer a proton to the next pendant group on the right (D). The end result of the proton transfer from A to D is that, in the final structure, the pendant group A is now in a position to receive the next proton without having had to undergo the reorientation step. This is because, as shown in Figure 4.3, the *same* nitrogen atom acts as both hydrogen bond donor as well as acceptor as it accepts and also releases the proton to the nitrogen of the neighboring pendant group. It is this “single-site” behavior from the nitrogen that eliminates the need for the reorientation barrier.

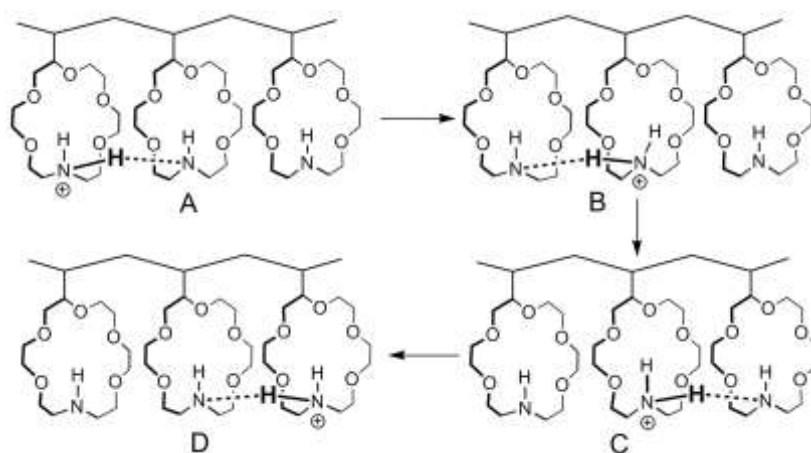


Figure 4.3 Schematic representation of proton transfer through crown ether pendant groups on a polymer backbone; the proton being transferred is shown in a larger font than the other hydrogen atoms.

Hence, the choice of nitrogen containing crown ethers as the pendant groups can lead to new PEMs that can display high proton conducting efficiency. It is to be noted that crown ethers have been employed as effective complexing agents for cations and also to form complexes with H_3O^+ or H_5O_2^+ , depending on the ring size.²⁸ The proposed PEM structures in the current work are crown ethers with one, two and three nitrogen atoms in each group: the mono-aza, di-aza and tri-aza crown ethers respectively (see Figure 4.4 for the schematic structures and Figure 4.5 for the computationally optimized geometries). The computational studies with the proposed structures will indicate their potential to act as PEMs in fuel cells.



Figure 4.4 Chemical structures of the aza-18-crown-6 ether pendant groups that have been investigated in the current study.

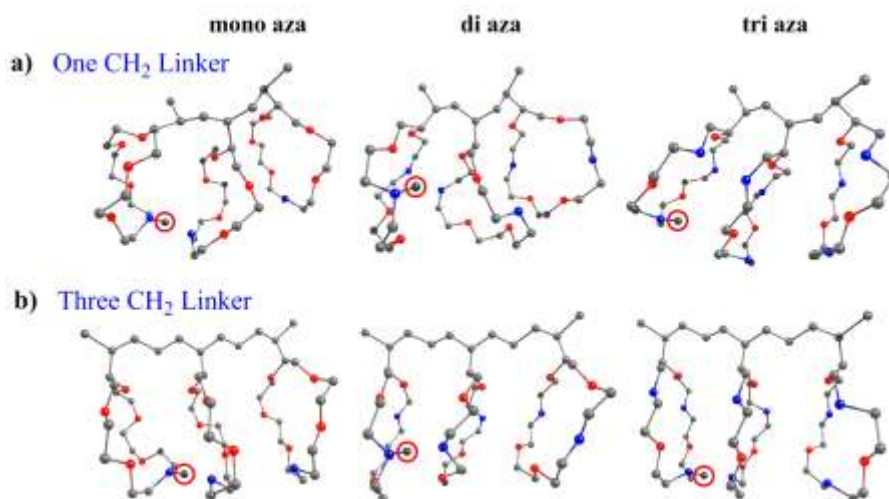


Figure 4.5 The optimized structures of the mono, di and tri aza-crown ether groups that are pendant to the polymer backbone with (a) one and (b) three methylene (CH_2) group linkers; the color scheme is as follows: carbon-gray; nitrogen-blue; oxygen-red; hydrogen-black;

hydrogen atoms, other than the proton being transferred, have not been shown for the purpose of clarity.

4.2 Computational Details

The geometry optimizations were carried out employing density functional theory (DFT) with the Turbomole 6.4 suite of programs.²⁹ The Perdew, Burke, and Ernzerhof (PBE)³⁰ functional was used for the geometry optimization calculations. The triple- ζ basis set augmented by a polarization function (Turbomole basis set TZVP) was used for all the atoms. The resolution of identity (RI)³¹ along with the multipole accelerated resolution of identity (marij)³² approximations were employed for an accurate and efficient treatment of the electronic Coulomb term. In order to improve the calculation of the energy values, a further correction was made through single point PBE0 calculations^{30,33} for the DFT (PBE)-optimized structures. The PBE0 functional has been used in previous computational studies on polymer electrolyte fuel cell membranes,³⁴ as well as in studying N-to-N proton transfer reactions,³⁵ which is pertinent in the current calculations. Moreover, the PBE and the PBE0 functionals have been shown to provide the best results in describing hydrogen bond interactions and hydrogen bonding strengths.³⁶ Furthermore, the PBE0 functional has been shown to give the best results in the calculation of pKa values, involving proton transfer reactions, in phenolic derivatives.³⁷ In addition to these studies which are pertinent to the current work, there are several other investigations in other areas of research where the PBE0 functional has been shown to provide excellent results.³⁸⁻⁴³

Frequency calculations have been done at the DFT level in order to obtain the zero point energy, the internal energy and entropic contributions (calculated at 298.15 K). Hence, in addition to the ΔE values, ΔG values have also been reported. With regard to the transition states obtained during the investigations of the proton-transfer process, care was taken to ensure that the obtained transition-state structures possessed only one imaginary frequency corresponding to the correct normal mode.

4.3 Results and Discussion

Discussed in the following sub-sections is the energetics of the proton transfer process calculated for the different proposed PEMs. Two parameters will be varied in the PEM models considered: (i) the number of nitrogen atoms in each pendant crown ether group: the mono, di- and tri-aza cases shall be considered and (ii) the number of linker atoms between each pendant group: cases with one CH₂ linker and three CH₂ linkers shall be considered.

4.3.1 The Mono-aza Crown Ether Case

The first case considered is the “mono-aza” crown ether: an 18-crown 6-ether suspended from an alkyl backbone. The lone nitrogen in the 18-crown 6-ether is placed at the bottom of the cyclic pendant group, away from the polymer backbone. As mentioned above, there are two possibilities that have been considered for this case: a system (i) with a single CH₂ linker between the carbons containing the pendant groups and (ii) with three CH₂ linkers.

(i) Mono-aza Crown Ether Pendant Groups with a Single CH₂ Linker

Figure 4.6 below shows the energy profile for the proton transfer process for the system with a single CH₂ linker in the alkyl backbone for the 18-crown mono-aza crown ether pendant groups. Three pendant groups have been considered in the model employed, because studying the proton transfer process with three pendant groups makes it more clear why the reorientation step is not required for these systems. As Figure 4.6 indicates, the proton is first placed on the nitrogen of the crown ether on the left. This leads to stable minima, where the other hydrogen of the crown ether makes a hydrogen bond with the nitrogen of the adjacent pendant group. This is a favorable reactant structure for the proton transfer process. A proton transfer from this reactant requires a transition state that is only 1.1 kcal/mol (ΔE value) higher in energy, which suggests a very facile reaction. This low value compares very favorably with the proton transfer barriers that have been calculated in the past for other PEM systems.^{16-18,20,44} Following this first proton transfer step, an intermediate complex is formed, referred to as “**int.1**” in Figure 4.6, which is a structure stabilized by hydrogen bonding between the two nitrogen atoms, with the difference that it is now the middle nitrogen that has the proton. The hydrogen-bond stabilized intermediate

int.1 is more stable than the reactant structure by 2.6 kcal/mol (see Figure 4.6). What is also clear from the optimized structures for **int.1** and **int.2**, is that this loss in hydrogen bonding leads to the approach of the crown ether pendant group on the right towards the middle crown ether. This is shown by the decrease in the N-N bond distance between the two crown ether groups: from 3.14 Å in **int.1** to 2.76 Å in **int.2**. This approach of the crown ether on the right leads to the formation of the next intermediate structure denoted as **int.2** in Figure 4.6, lying -2.2 kcal/mol along the energy surface. The hydrogen bond in **int.2** is between the nitrogens of the middle and right crown ethers. This intermediate is the precursor to the next proton transfer step, where the proton is taken by the nitrogen of the crown ether on the right. This step is, again, very facile, having a barrier of only 0.9 kcal/mol. Taken from the lowest intermediate in the entire cycle: **int.1**, the barrier height is 1.3 kcal/mol, which is still indicative of a favorable reaction. It is to be noted that the corresponding free energy (ΔG) values have been shown in parenthesis, and the barrier heights are comparable or reduced even further when the ΔG values are considered, indicating that the inclusion of internal energy and entropic effects has a further salutary effect in reducing the proton transfer barrier. Indeed, as is clear from the Figures 4.6, 4.8, 4.11, 4.13, 4.16 and 4.17 below, for some of the systems studied and discussed later, the original positive difference in the ΔE terms is so small that the favorable addition of entropic and other terms leaves the free energy of the transition-state structures *lower* than the free energy of the corresponding reactant structures.

Care was taken to obtain several possible conformations of **1a** and **2a**, and the lowest conformations have been considered for the energy calculations. However, it is to be noted that, while the trimer structures **1a** and **2a** appear symmetric, there is a difference of 1.3 kcal/mol (ΔG value) between the structures, with **2a** being more stable. The reason for this is an extra, weak bonding interaction between the proton of the nitrogen and a crown ether oxygen in the middle ring of **2a**, which provides extra stabilization to the structure. This weak bonding interaction is indicated in Figure 4.7 below, and was not found in **1a**. The difference in the structures and the energies of **1a** and **2a** is therefore due to the fact that the presence of the extra proton in the structures “breaks” the symmetry between the three rings, and so, structure **2a** is not a mirror image of **1a**: the bonding in the coordination nitrogen of the central ring having a hydrogen bond with the nitrogen of the ring on the left in **1a** is different from the

bonding in the coordination nitrogen of the central ring having a hydrogen bond with the nitrogen of the ring on the right in **2a**. A similar difference in energy between the initial and final structures is also observed in the other structures that have been discussed in the succeeding sections.

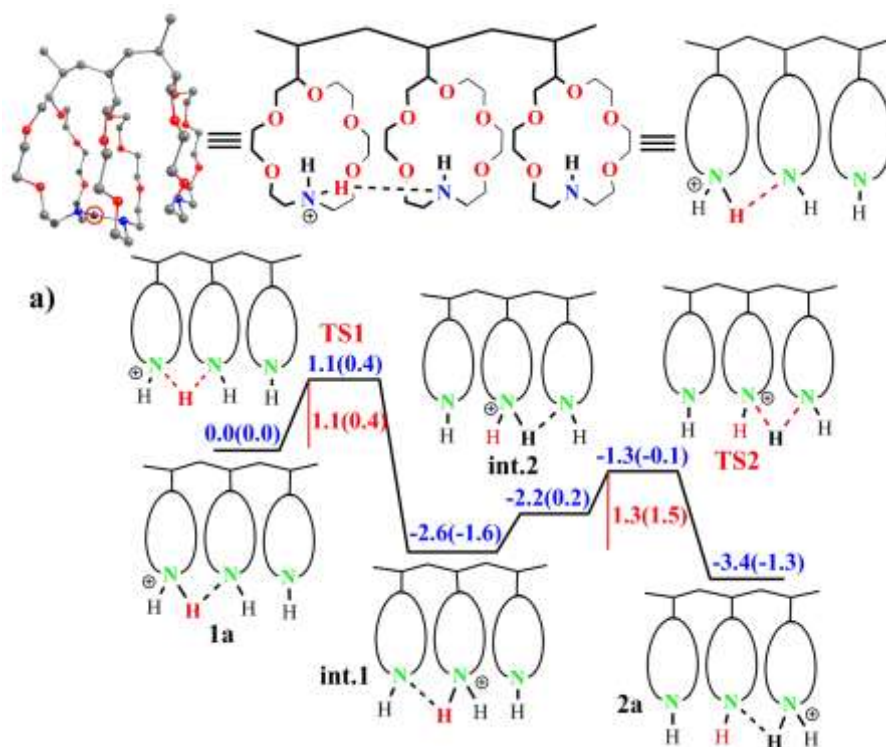


Figure 4.6 The potential energy surface for proton transfer through the mono-aza-18-crown-6-ether from the crown ether on the left to the crown ether on the right, with one CH₂ linker in the alkyl backbone; the proton being transferred is shown in a larger font than the other hydrogen atoms; all values are in kcal/mol.

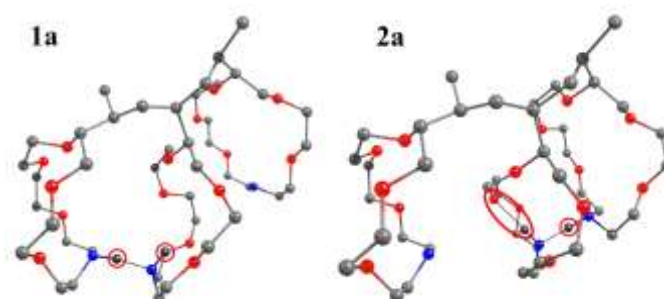


Figure 4.7 Optimized structures for **1a** and **2a**; the color scheme is the same as for Figure 4.5 above; there is an extra weak bonding interaction in the middle ring **2a** between the proton on the central nitrogen and a crown ether oxygen (circled in the structure), which stabilizes **2a** by 1.3 kcal/mol over **1a**.

(ii) Mono-aza Crown Ether Pendant Groups with Three CH₂ Linkers

As mentioned earlier, we decided to investigate how changing the number of CH₂ linkers between the pendant crown ether groups would affect the energetics of the proton transfer process. The current subsection therefore discusses the proton transfer process when the pendant groups are separated by three CH₂ linkers, as opposed to one CH₂ linker. As shown in Figure 4.8 below, the proton transfer process in such a system would again involve two steps: (i) proton transfer from the first pendant group to the one in the middle, and then (ii) proton transfer to the final nitrogen atom on the pendant group on the right. The ΔE value for the barrier for the slowest step is quite comparable for the two cases (1.3 kcal/mol for the 1-CH₂ linker case, 2.0 kcal/mol for the 3-CH₂ linker case, see Figures 4.6 and 4.8), while a comparison of the corresponding ΔG values shows only a slightly larger difference, with the 3-CH₂ linker case preferred by about 0.9 kcal/mol (1.5 kcal/mol for the 1-CH₂ linker case, 0.6 kcal/mol for the 3-CH₂ linker case, see Figures 4.6 and 4.8).

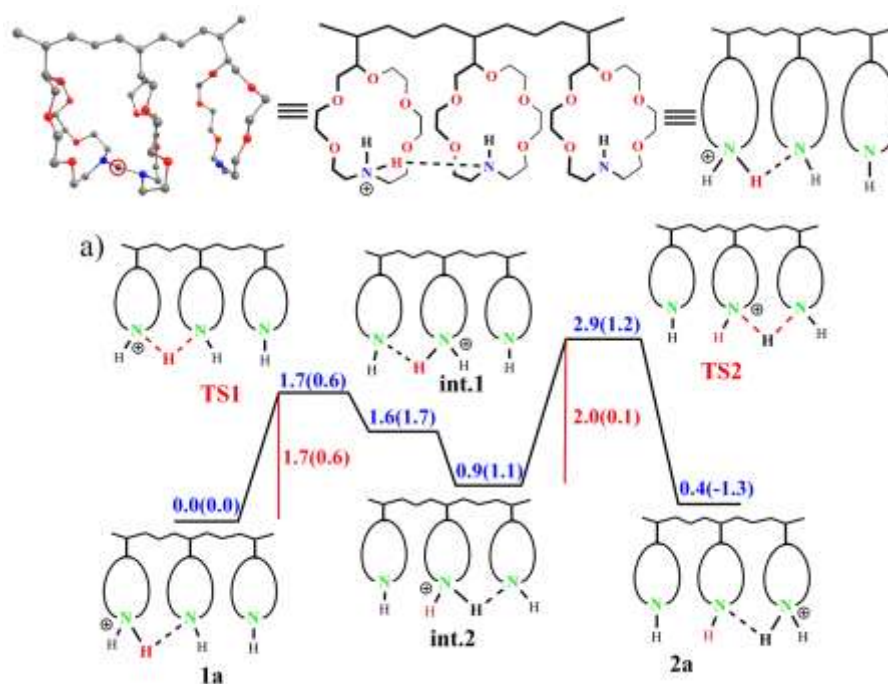


Figure 4.8 Potential energy for proton transfer through the mono-aza-18-crown-6-ether from the crown ether on the left to the third crown ether, with three CH₂ linkers in the alkyl backbone; the proton being transferred is shown in a larger font than the other hydrogen atoms; all values are in kcal/mol.

Overall, the results for the proton transfer considered for the one and three CH₂ linker group cases shows that the barriers for the slowest step of the transfer process: 1.3 kcal/mol for the 1-CH₂linker case and 1.7 kcal/mol for the 3-CH₂linker case, are smaller than the slowest step barriers that have been obtained for other pendant group PEM that have been investigated,^{16-18,20,44} thus demonstrating the importance of proton transfer without a orientation barrier in pendant group PEMs.

4.3.2 The Di-aza Crown Ether Case

We have also considered the possibility of having more than one nitrogen in the 18-crown 6-ether structures. Discussed in the current subsection is the case where two nitrogen atoms have been placed in the pendant groups. Figure 4.9 below shows the structure of the di-aza pendant crown ether considered, with the nitrogens placed in the middle of the 18-crown ether. It is to be noted that in such a structure, the proton transfer can take place from either of the two nitrogen atoms of the pendant group to the correspondingly placed nitrogen atoms in the next 18-crown ether pendant group. Hence, there are two pathways possible for the transfer of the proton in this type of PEM. Moreover, since there are two CH₂ linker cases that are being considered: the one and three linker cases, as in the mono-aza crown ether case discussed above, this means that there are four proton transfer pathways that will have to be investigated for the di-aza crown ether case. These are discussed below.

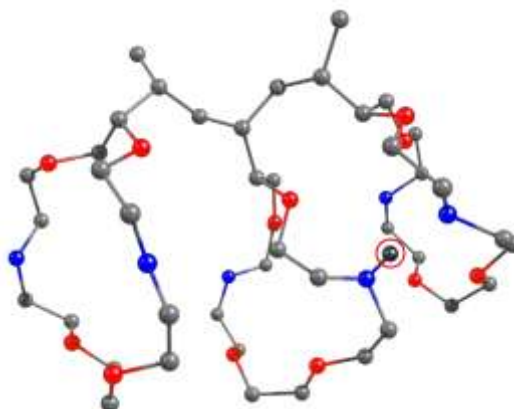


Figure 4.9 The optimized structure of the di-aza pendant crown ether; the color scheme is as follows: carbon-gray; nitrogen-blue; oxygen-red; hydrogen-black; all hydrogen atoms have not been shown for the purpose of clarity.

(i) Di-aza Crown Ether Pendant Groups with Single CH₂ Linkers

The proton transfer for the di-aza case has been studied in the same way as discussed above: with the proton being transferred *via* the nitrogen atoms in the pendant groups from the left to the middle to the right. As shown in Figure 4.11 below, this leads to two energy profiles, because of the possibility of two pathways, each involving one set of corresponding nitrogen atoms on the three pendant groups. As the energy profiles indicate, there are differences observed in the value for the slowest step in the proton transfer processes. For the **2_1** case shown below, the slowest step is the first proton transfer step, while for the case denoted as **2_2** in Figure 4.11, the slowest step is the second proton transfer step from the pendant group in the middle to the pendant group on the right. The optimized structures of the four transition states for the proton transfer steps for have been shown in Figure 4.10.

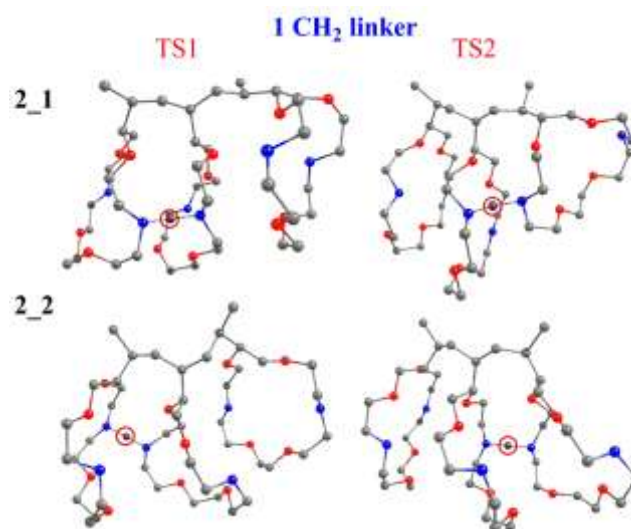


Figure 4.10 The optimized structures of the transition states during the proton transfer process for the mono aza 18-crown 6-ether pendant group PEM, with one CH₂ linker in the alkyl backbone; the color scheme is as in the Figures 4.5, 4.7, 4.9.

In terms of the transition state structures, there are distinct differences observed between the four transition states, with regard to the orientation of the crown ether rings and of the alkyl backbone. The chief reason for the difference in the barrier heights between the **2_1** and the **2_2** cases is due to the stability of the intermediate, **int_1**, structure in each case. While both the **2_1_int_1** and the **2_2_int_1** structures were found to be stable, the **2_2_int_1** structure was found to be more stable, thereby leading to the greater barrier height for the proton transfer calculated from this

reactant structure. The reason for the greater stability of **2_2_int_1** is the nature of the hydrogen bonding in the intermediate. As shown in Figure 4.12 below, showing the optimized structures of **2_1_int_1** and the **2_2_int_1** cases, there are two hydrogen bonds, featuring separate N-H groups in **2_2_int_1**, while the two hydrogen bonds feature the same N-H group in the **2_1_int_1** case. This leads to greater compactness between the left ring and middle rings in **2_2_int_1**, thereby leading to more steric crowding between the two pendant groups in comparison to the **2_2_int_1** and thus explaining the difference in their relative stabilities.

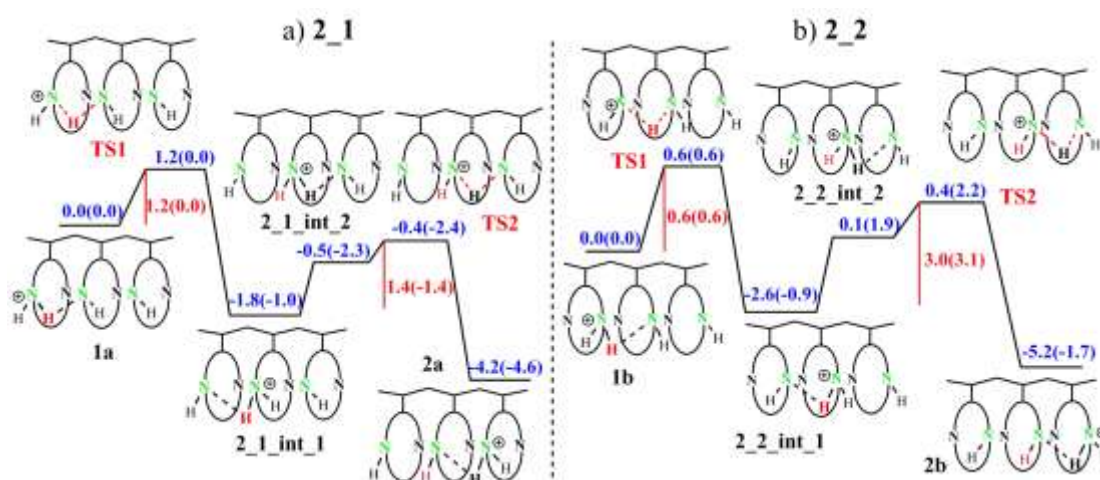


Figure 4.11 The potential energy for proton transfer through the di-aza18-crown-6-ether pendant groups; there is a single CH_2 linker in the alkyl backbone; the proton being transferred is shown in a slightly bigger font than the other hydrogen atoms; all values are in kcal/mol.

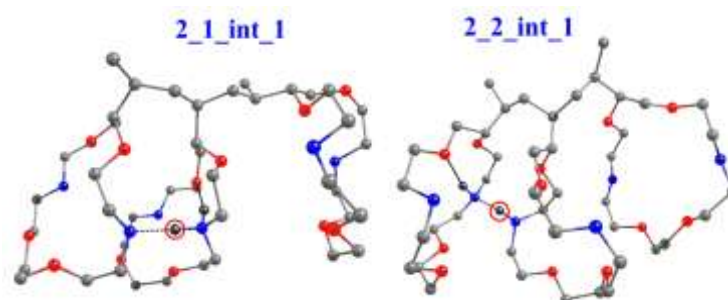


Figure 4.12 The optimized structures of **int_1** for the **2_1** and the **2_2** cases; the color scheme is as follows: carbon-gray; nitrogen-blue; oxygen-red; hydrogen-black; only a few hydrogen atoms that take part in the hydrogen-bonding network have been shown; the rest have not been shown for the purpose of clarity.

(ii) Di-aza Crown Ether Pendant Groups with Three CH₂ Linkers

Shown in Figure 4.13 below are the energy profiles for the transfer of proton from the left to the right for the PEMs designed with three CH₂ linkers between the di-aza 18 crown pendant groups. Here, too, a significant difference is observed in the energy profiles, principally depending on the difference in the relative stabilities of the intermediate complexes. In the **2_1** case, the first intermediate is stable while for the **2_2** case, the second intermediate is stable. As in the one linker case, the difference in the stabilities of the intermediates in the **2_1** and the **2_2** cases is again due to the relative orientations of the pendant groups. The optimized structures for the two intermediates for the **2_1** case are shown in Figure 4.14 below. Two different perspectives: the front and side views are shown for the two structures. These perspectives reveal that the **int_1** structure is more staggered than the **int_2** structure for the **2_1** case, thus leading to the observed greater stability for **int_1** compared to the **int_2** structure. Likewise, for the **2_2** case, **int_2** was found to be more stable. A perusal of the intermediate **int_1** and **int_2** structures for **2_2** showed that the difference in this case was due to an extra hydrogen bond present in **int_2**. Therefore, the analysis of the intermediate and transition state structures discussed so far, for the mono and di-aza cases, indicates that the relative stabilities of the different species along the potential energy surface depends on (i) the steric interactions between the pendant groups, which is an unfavorable interaction and (ii) the number of hydrogen bonds between the pendant groups, which is a favorable interaction. It is this interplay between the favorable and unfavorable factors that determines the nature of the potential energy surfaces. What is also of note is that the highest barrier calculated among all the four possibilities considered for the di-aza 18 crown ether case, (3.8 kcal/mol, ΔG value) is still significantly lower than the barriers that have been determined and reported for other pendant group PEMs (ranging from 8.0 kcal/mol to 10.7 kcal/mol)¹⁷⁻²⁰, thus showing the potential of the newly proposed PEMs, due to the elimination of the reorientation barrier.

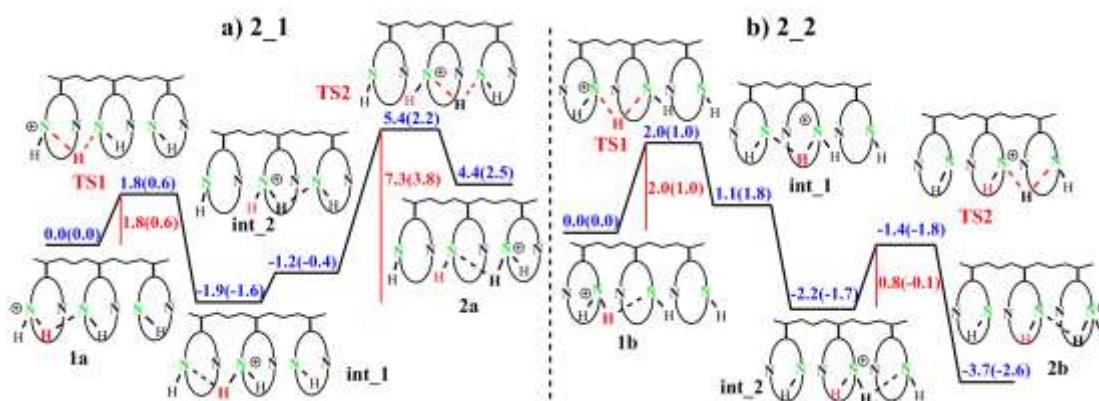


Figure 4.13 The potential energy surface for proton transfer through di-aza18-crown-6-ether pendant groups; with three CH₂ linkers in the alkyl backbone; the proton being transferred is shown with a slightly larger font than the other hydrogens; all values are in kcal/mol.

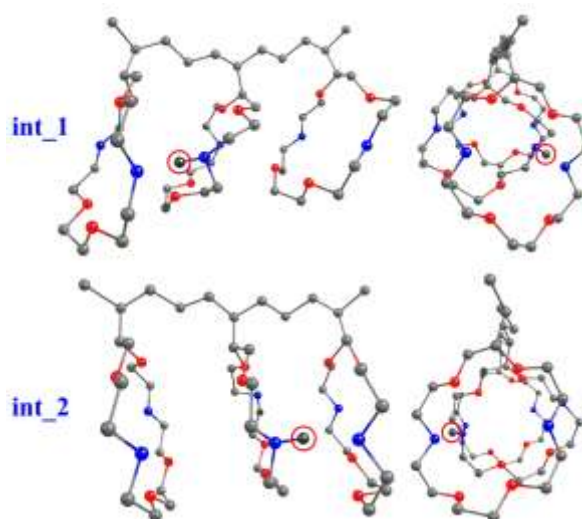


Figure 4.14 The optimized structures of **int_1** and **int_2** for the **2_1** case; the color scheme is as follows: carbon-gray; nitrogen-blue; oxygen-red; hydrogen atoms have not been shown for the purpose of clarity.

4.3.3 The Tri aza-crown Ether Case

The final type of pendant PEM that has been considered is one with three nitrogens present in each pendant group, each nitrogen separated from the other two by CH₂-CH₂-O-CH₂-CH₂ groups (see the optimized structure of the pendant groups for the one CH₂ linker case, shown in Figure 4.15 above). For this case, there are three

separate routes that can be investigated for the transfer of the proton between the adjacent nitrogens in the three pendant groups. Moreover, as before, cases with one and three CH₂ linkers have been considered, thus giving rise to six different proton transfer pathways, the ΔE and ΔG for which have been calculated. As for the earlier cases, the difference in the stability of the intermediates and the subsequent effect on the barrier heights is again found to be due to the two factors that have been discussed above for the di-aza case: the unfavorable steric interactions between the pendant crown ether groups and the number of favorable N-H-O hydrogen bonding interactions possible in each structure. The potential energy surfaces, both ΔE and ΔG , are shown in Figure 4.16 below for the 1-CH₂ linker case and in Figure 4.17 below for the 3-CH₂ linker case. The calculations show that the proton transfer process, like for the mono-aza and the di-aza cases, is again seen to be quite facile in all the six possible cases considered, with the highest barrier among all the barriers considered found to be only 4.9 kcal/mol (ΔG value), once again indicating the high efficiency that can be expected for the proton transfer through the proposed PEMs, where the need for the reorientation of the pendant group has been eliminated.



Figure 4.15 The optimized structure for the tri-aza pendant group case; there is one CH₂ pendant group in the alkyl backbone in the example shown above; the color scheme is the same as in Figures 4.5, 4.9 and 4.14.

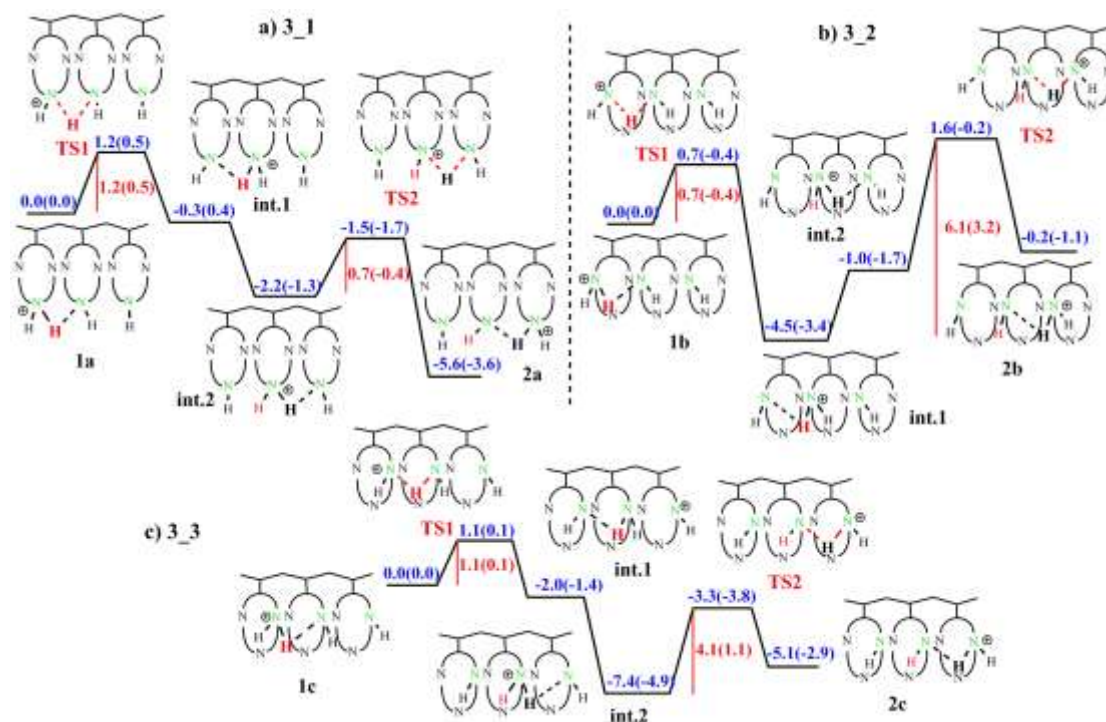


Figure 4.16 The potential energy surface for proton transfer through tri-aza 18-crown 6-ether pendant groups, with one CH₂ linker in the alkyl backbone; the proton being transferred is shown with a slightly larger font than the other hydrogens; all values are in kcal/mol.

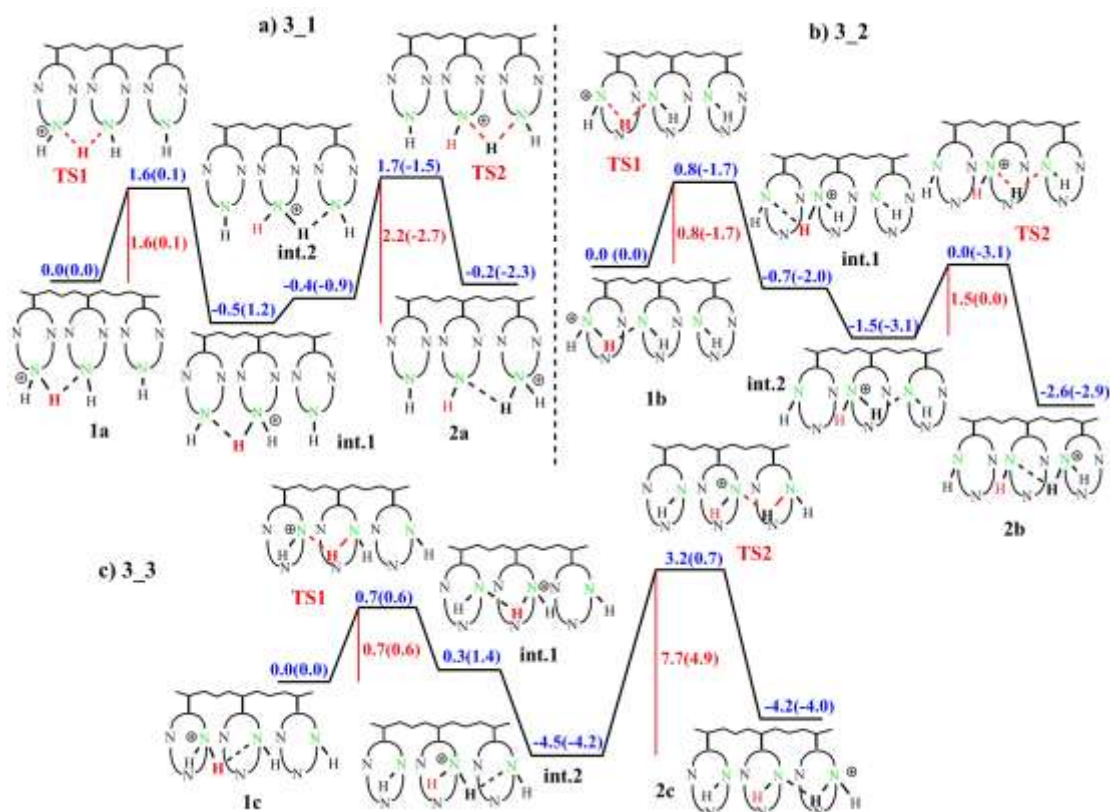


Figure 4.17 The potential energy surface for proton transfer through tri-aza 18-crown 6-ether pendant groups, with three CH₂ linkers in the alkyl backbone; the proton being transferred is shown with a slightly larger font than the other hydrogens; all values are in kcal/mol.

4.4 The Relative Efficiencies of the Different PEMs Considered: Overall Picture

What has been discussed in the previous sections is the potential of structures, having 18-crown ethers with nitrogens as pendant groups on an alkyl backbone with one or three CH₂ linkers, to perform as PEMs in fuel cells. Added to the advantage of, such proposed PEMs not employing water as a solvent/proton transferring medium, is the elimination of the reorientation step during the proton transfer. 18-crown ether structures having one, two or three nitrogens in each pendant group have been considered, and all the possible pathways for the proton transfer between the groups has been studied. The results from the calculations are summarized in the bar graphs shown in Figure 4.18 below. Specifically, the calculated barrier (ΔG) for the slowest, rate determining step has been shown for the proton transfer process in the proposed mono, di- and tri-aza PEMs, for both the one and the three CH₂ linker possibilities for each case. It is to be noted that since there are two different pathways in each di-aza linker PEM and three separate pathways in the each tri-aza linker case, only the most efficient pathway has been shown in Figure 4.18 for each case.

A comparison of the different barrier heights shows that all the different pendant group cases that have been considered are likely to be very good candidates for PEMs. The barrier for the rate determining step for proton transfer has been seen to range from about 0.5 kcal/mol to 5.0 kcal/mol over all the cases studied. Therefore, even the least efficient PEM case obtained is indicated to be more efficient than other pendant group cases (having barriers ranging from 8.0 kcal/mol to 10.7 kcal/mol)¹⁷⁻²⁰ that have been proposed and studied to date. This shows that the concept of eliminating the rotational barrier in the reorientation step, by having the same nitrogen atom accept and release protons, is a promising one that can lead to very efficient PEMs.

A further point that can be made is that there are more pathways for proton transfer in the tri-aza case than in the di-aza, and more pathways for proton transfer in

the di-aza case in comparison to the mono-aza. Since the highest barrier height for any proton transfer pathway is only around 5.0 kcal/mol, all the proton transfer pathways would be operational in the PEMs, especially since the PEMs proposed are for high temperature applications. Hence the current work indicates that having crown ether structures with only nitrogens in place of oxygens in the crown ethers might be extremely efficient as PEMs in fuel cells.

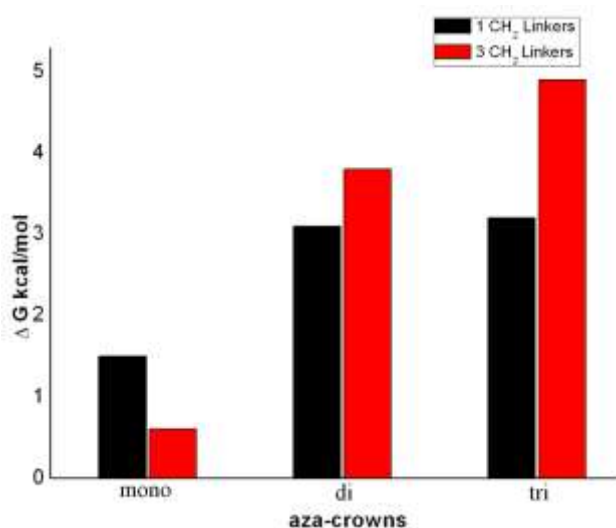


Figure 4.18 An overall picture of the proton transfer process through the different pendant group PEMs that have been considered.

4.5 Conclusion

There is a need to develop efficient polymer electrolyte membranes (PEMs) for fuel cells, membranes that can function effectively in the absence of water and other solvating media, and at elevated temperatures. Structures with nitrogen containing pendant groups on a polymer backbone represent one promising avenue¹⁷⁻²⁰ that has been explored as potential PEMs that can satisfy these criteria. However, such PEMs are likely to encounter high barriers, ranging from 8.0kcal/mol to 10.7 kcal/mol,¹⁷⁻²⁰ during the proton transfer process, due to the necessity for the pendant groups to rotate and reorient themselves during the proton transfer process. The current computational study proposes a new design of nitrogen containing pendant group PEMs that eliminates the need for the reorientation barrier during the proton transfer process. The pendant groups in question have (i) one, (ii) two and (iii) three

nitrogen atoms in 18-crown 6-ethers. Since nitrogen containing crown ethers have been prepared.⁴⁵⁻⁴⁷ Moreover, there exist synthetic strategies⁴⁸⁻⁵⁰ for post-functionalization reactions where a polymer backbone bearing a reactive group, such as $-\text{CH}_2\text{Cl}$ ⁵¹⁻⁵³ can react with a group on the crown ether (such as an amine) in order to create pendant crown ethers bound to a polymer backbone. This indicates that the experimental synthesis of the proposed PEMs would be a very feasible process. The possibility of proton transfer in such complexes has been comprehensively investigated with density functional theory (DFT). The results indicate that the proton transfer will be likely to take place with barriers significantly lower than those predicted for other pendant group PEMs. Indeed, the barriers indicate that the proposed PEMs would compare very favorably with all other PEMs that have been studied and reported in the literature. As such, the current work opens up promising new possibilities in the field of polymer electrolyte membrane fuel cells.

4.6 References

- (1) Kreuer, K.-D.; Paddison, S. J.; Spohr, E.; Schuster, M. *Chemical Reviews* **2004**, *104*, 4637-4678.
- (2) Kreuer, K.-D.; Rabenau, A.; Weppner, W. *Angewandte Chemie International Edition in English* **1982**, *21*, 208-209.
- (3) Kreuer, K.-D. *Chemistry of Materials* **1996**, *8*, 610-641.
- (4) Eikerling, M.; Kornyshev, A. A.; Kuznetsov, A. M.; Ulstrup, J.; Walbran, S. *The Journal of Physical Chemistry B* **2001**, *105*, 3646-3662.
- (5) Samuel, C. *Biochimica et Biophysica Acta (BBA) - Bioenergetics* **2006**, *1757*, 876-885.
- (6) Kreuer, K. D. *Journal of Membrane Science* **2001**, *185*, 29-39.
- (7) Noam, A. *Chemical Physics Letters* **1995**, *244*, 456-462.
- (8) Tuckerman, M. *J. Chem. Phys.* **1995**, *103*, 150.
- (9) Tuckerman, M.; Laasonen, K.; Sprik, M.; Parrinello, M. *The Journal of Physical Chemistry* **1995**, *99*, 5749-5752.
- (10) Carla, H.-W. *Journal of Membrane Science* **1996**, *120*, 1-33.
- (11) Li, Q.; He, R.; Jensen, J. O.; Bjerrum, N. J. *Chemistry of Materials* **2003**, *15*, 4896-4915.

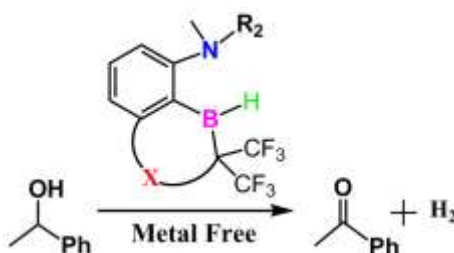
- (12) Kawada, A.; McGhie, A. R.; Labes, M. M. *The Journal of Chemical Physics* **1970**, *52*, 3121-3125.
- (13) Basch, H.; Krauss, M.; Stevens, W. J. *Journal of the American Chemical Society* **1985**, *107*, 7267-7271.
- (14) Goward, G. R.; Saalwachter, K.; Fischbach, I.; Spiess, H. W. *Solid State Nuclear Magnetic Resonance* **2003**, *24*, 150-162.
- (15) Goward, G. R.; Schuster, M. F. H.; Sebastiani, D.; Schnell, I.; Spiess, H. W. *The Journal of Physical Chemistry B* **2002**, *106*, 9322-9334.
- (16) Fischbach, I.; Spiess, H. W.; Saalwachter, K.; Goward, G. R. *The Journal of Physical Chemistry B* **2004**, *108*, 18500-18508.
- (17) Mangiatordi, G. F.; Butera, V.; Russo, N.; Laage, D.; Adamo, C. *Physical Chemistry Chemical Physics* **2012**, *14*, 10910-10918.
- (18) Benhabbour, S. R.; Chapman, R. P.; Scharfenberger, G.; Meyer, W. H.; Goward, G. R. *Chemistry of Materials* **2005**, *17*, 1605-1612.
- (19) Yamada, M.; Honma, I. *The Journal of Physical Chemistry B* **2004**, *108*, 5522-5526.
- (20) Mangiatordi, G. F.; Laage, D.; Adamo, C. *Journal of Materials Chemistry A* **2013**, *1*, 7751-7759.
- (21) Li, A.; Yan, T.; Shen, P. *Journal of Power Sources* **2011**, *196*, 905-910.
- (22) Tatara, W.; Wojcik, M. J.; Lindgren, J.; Probst, M. *The Journal of Physical Chemistry A* **2003**, *107*, 7827-7831.
- (23) Zhou, Z.; Liu, R.; Wang, J.; Li, S.; Liu, M.; Bredas, J.-L. *The Journal of Physical Chemistry A* **2006**, *110*, 2322-2324.
- (24) Subbaraman, R.; Ghassemi, H.; Zawodzinski Jr, T. *Solid State Ionics* **2009**, *180*, 1143-1150.
- (25) Mane, M. V.; Venkatnathan, A.; Ghatak, K.; Vanka, K. *The Journal of Physical Chemistry B* **2012**, *116*, 9803-9811.
- (26) Kreuer, K. D.; Fuchs, A.; Ise, M.; Spaeth, M.; Maier, J. *Electrochimica Acta* **1998**, *43*, 1281-1288.
- (27) Zhou, Z.; Li, S.; Zhang, Y.; Liu, M.; Li, W. *Journal of the American Chemical Society* **2005**, *127*, 10824-10825.
- (28) Junk Peter, C. In *Reviews in Inorganic Chemistry* **2001**; Vol. 21, p 93-124.
- (29) Ahlrichs, R.; Baer, M.; Haeser, M.; Horn, H.; Koelmel, C. *Chem. Phys. Lett.* **1989**, *162*, 165.

- (30) Perdew, J. P.; Burke, K.; Ernzerhof, M. *Physical Review Letters* **1996**, *77*, 3865.
- (31) Eichkorn, K.; Treutler, O.; O'hm, H.; Ha'sser, M.; Ahlrichs, R. *Chemical Physics Letters* **1995**, *240*, 283-289.
- (32) Sierka, M.; Hogekamp, A.; Ahlrichs, R. *J. Chem. Phys.* **2003**, *118*, 9136.
- (33) Adamo, C.; Barone, V. *The Journal of Chemical Physics* **1999**, *110*, 6158-6170.
- (34) Yamaguchi, M.; Ohira, A. *The Journal of Physical Chemistry A* **2012**, *116*, 10850-10863.
- (35) Leitao, E. M.; Stubbs, N. E.; Robertson, A. P. M.; Helten, H.; Cox, R. J.; Lloyd-Jones, G. C.; Manners, I. *Journal of the American Chemical Society* **2012**, *134*, 16805-16816.
- (36) Rao, L.; Ke, H.; Fu, G.; Xu, X.; Yan, Y. *Journal of Chemical Theory and Computation* **2008**, *5*, 86-96.
- (37) Rebolgar-Zepeda, A. M.; Campos-Hernandez, T.; Ramirez-Silva, M. T.; Rojas-Hernandez, A.; Galano, A. *Journal of Chemical Theory and Computation* **2011**, *7*, 2528-2538.
- (38) Lousada, C. M.; Johansson, A. J.; Brinck, T.; Jonsson, M. *Physical Chemistry Chemical Physics* **2013**, *15*, 5539-5552.
- (39) Li, Z.; Pan, Y. *Physical Review B* **2011**, *84*, 115112.
- (40) List, N. H.; Curutchet, C.; Knecht, S.; Mennucci, B.; Kongsted, J. *Journal of Chemical Theory and Computation* **2013**, *9*, 4928-4938.
- (41) Blancafort, L.; Williams, F. *The Journal of Physical Chemistry A* **2012**, *116*, 10607-10614.
- (42) Svozil, D.; Jungwirth, P. *The Journal of Physical Chemistry A* **2006**, *110*, 9194-9199.
- (43) Adamo, C.; Scuseria, G. E.; Barone, V. *The Journal of Chemical Physics* **1999**, *111*, 2889-2899.
- (44) Mangiatordi, G. F.; Hermet, J.; Adamo, C. *The Journal of Physical Chemistry A* **2011**, *115*, 2627-2634.
- (45) Alexandratos, S. D.; Stine, C. L. *Reactive and Functional Polymers* **2004**, *60*, 3-16.
- (46) Humphry-Baker, R.; Grätzel, M.; Tundo, P.; Pelizzetti, E. *Angewandte Chemie International Edition in English* **1979**, *18*, 630-631.

- (47) Jiang, J.; Higashiyama, N.; Machida, K.-i.; Adachi, G.-y. *Coordination Chemistry Reviews* **1998**, *170*, 1-29.
- (48) Durmaz, H.; Sanyal, A.; Hizal, G.; Tunca, U. *Polymer Chemistry* **2012**, *3*, 825-835.
- (49) Zeng, Q.; Cai, P.; Li, Z.; Qin, J.; Tang, B. Z. *Chemical Communications* **2008**, 1094-1096.
- (50) Li, Z.; Li, Q.; Qin, A.; Dong, Y.; Lam, J. W. Y.; Dong, Y.; Ye, C.; Qin, J.; Tang, B. Z. *Journal of Polymer Science Part A: Polymer Chemistry* **2006**, *44*, 5672-5681.
- (51) Tomoi, M.; Abe, O.; Takasu, N.; Kakiuchi, H. *Die Makromolekulare Chemie* **1983**, *184*, 2431-2436.
- (52) Warshawsky, A.; Kalir, R.; Deshe, A.; Berkovitz, H.; Patchornik, A. *Journal of the American Chemical Society* **1979**, *101*, 4249-4258.
- (53) Talanova, G. G.; Yatsimirskii, K. B.; Kravchenko, O. V. *Industrial & Engineering Chemistry Research* **2000**, *39*, 3611-3615.

CHAPTER 5

Computational Study of Metal Free Alcohol Dehydrogenation Employing Frustrated Lewis Pairs



ABSTRACT

The catalysis of acceptorless alcohol dehydrogenation (AAD) is an important area of research. Transition metal based systems are known to be effective catalysts for this reaction, but developing metal-free catalytic systems would lead to highly desirable cheaper and greener alternatives. With this in mind, the current computational study investigates design strategies that can lead to metal free frustrated Lewis pairs (FLPs) that can be employed for AAD catalysis. A careful study of thirty six different proposed FLP candidates reveals that several new FLPs can be designed from existing, experimentally synthesized FLPs that can rival or even be better than state-of-the-art transition metal based systems in catalyzing the alcohol dehydrogenation process.

5.1 Introduction

Alcohol dehydrogenation is often used to activate alcohols to the more reactive ketones or aldehydes.¹⁻⁴ Nowadays, the demand for renewable energy sources has led to significant interest⁵⁻⁸ in utilizing alcohol dehydrogenation for H₂ production from bio-mass or its fermentation products, usually employing transition metal catalysts.⁹⁻¹² A variety of transition metal catalysts such as rhodium, iridium and ruthenium have been reported¹³⁻²² for this process, with well known hydrogen acceptors such as O₂, H₂O₂ and acetones. Acceptorless alcohol dehydrogenation (AAD), on the other hand, is less common,^{1-4,11,23-25} but is useful, particularly in terms of H₂ production and atom economy. In this regard, the work of Yamaguchi, Fujita, and their co-workers^{26,27} is significant, because they have developed a new iridium metal complex which catalyzes alcohol dehydrogenation efficiently under mild conditions without requiring acceptors, thus being the most promising AAD catalyst developed to date.

The mechanism for the AAD catalysis by the iridium complex of Yamaguchi *et al.* has been computationally studied by Wang and coworkers.¹¹ As shown in Figure 5.1, the mechanism involves three steps: (i) ligand rotation leading to Ir-O bond cleavage to form the reactive intermediate *int.1*, (ii) hydrogen transfer from the alcohol substrate to form *int.3* (through transition state *TS1*) and (iii) the release of dihydrogen to regenerate the catalyst. They calculated the overall reaction free energy barrier height¹¹ for 1-phenylethanol dehydrogenation to be 30.0 kcal/mol.

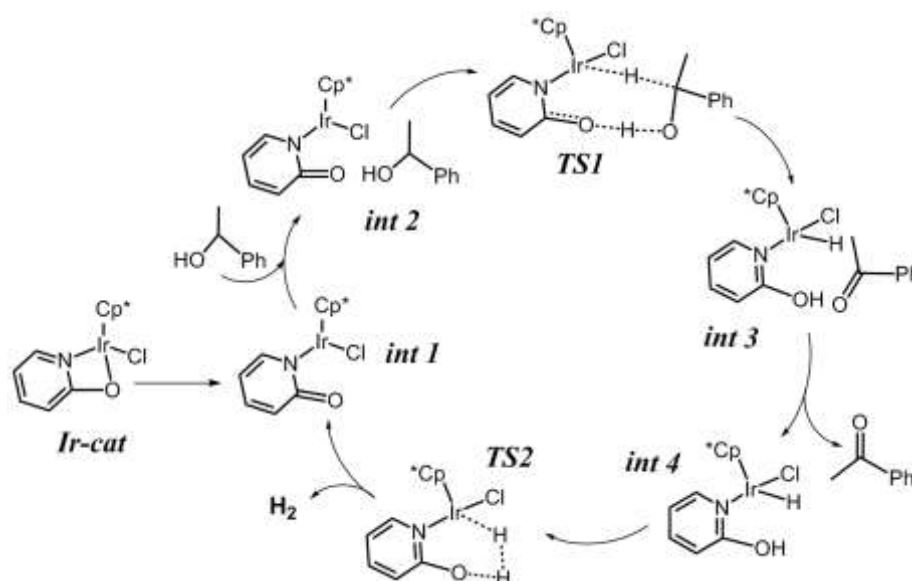


Figure 5.1 The catalytic cycle for alcohol dehydrogenation.

While the experimental and computational work on AAD catalysis, discussed above, is significant, it is notable for the fact that it involves a transition metal complex. Transition metal catalyzed reactions are not ideal because of the use of expensive transition metals, and the production of waste, high cost and toxicity. To overcome these disadvantages, the substitution of transition metal systems with Main Group systems is an attractive option, because this can lead to cheap and green catalyst systems. The recent work of Stephan and co-workers²⁸ is important in this context. They have introduced the concept of “frustrated Lewis pairs” (FLPs), which are complexes that contain a Lewis acidic and a Lewis basic center, sterically separated from bonding with each other, leading to latent Lewis acidity and basicity that can be exploited for small molecule activation.²⁸⁻³⁰ FLPs have been employed for the activation of dihydrogen,^{31,32} and amines.³³ Also, the hydrogenation of C=C,^{34,35} C=N,³⁶⁻³⁸ bulky imines^{37,39} and C=O⁴⁰ double bonds using FLPs has been reported. Furthermore, the dehydrogenation of alcohol to ketone,⁴¹ and the dehydrogenation of ammonia-borane^{33,42} by FLPs has also been demonstrated.

Coming to the topic under discussion: AAD, the FLP systems that may be important are phosphinoboranes, which have been studied experimentally^{28,37,38,43-45} and computationally.^{31,41,46-49} Indeed, computational studies have reported the dehydrogenation of alcohol through P/B cooperation in the (tBu)₂P=B(C₆F₅)₂ FLP.⁴¹ However, as will be shown in the section 5.3, the barriers in the dehydrogenation process with this system are higher than for the metal based iridium system¹¹ that has been discussed above. Now, in order to be truly effective, Main Group based systems need to have barriers that are similar to, or preferably lower, than the barriers obtained for metal systems. It is therefore imperative that other FLPs be considered that would be as effective (or more effective) than the existing metal-based system. An effective strategy in this context would be to design more sterically constrained FLPs that would have weaker interaction between the Lewis acidic and basic centers, leading to a lowering of the barriers for the alcohol dehydrogenation process, and thus to more catalytically efficient systems.

With this in mind, we have considered the N/B FLP system shown in Figure 5.2 below, which has been experimentally synthesized recently by Chernichenko *et*

al.^{50,51} In this FLP, **1**, and its variant, **2** (see Figure 5.2 below), there exists a dative bond between the nitrogen and the boron atoms, which is a weaker bond than the more covalent bond between P and B in the $(^t\text{Bu})_2\text{P}=\text{B}(\text{C}_6\text{F}_5)_2$ FLP. Furthermore, the coordination of each atom to the phenyl ring ensures greater steric hindrance in this case, which would lead to easier activation of the N-B bond. We have therefore decided to look at **1** and **2** as starting points of a thorough computational investigation into the possibility of employing these complexes, and introduced variations to these complexes, for the efficient dehydrogenation of alcohols. As many as thirty six different N/B complexes have been considered, and several promising candidates for the dehydrogenation of the alcohol 1-phenyl ethanol (the same alcohol that had been considered for the iridium based system)¹¹ have been identified. As will be shown in section 5.3, while **1**, **2** and several of their variants are predicted to not be as effective as the metal based system; our studies have unearthed some promising candidates that are predicted to be more effective than the metal based systems for the alcohol dehydrogenation catalysis process.

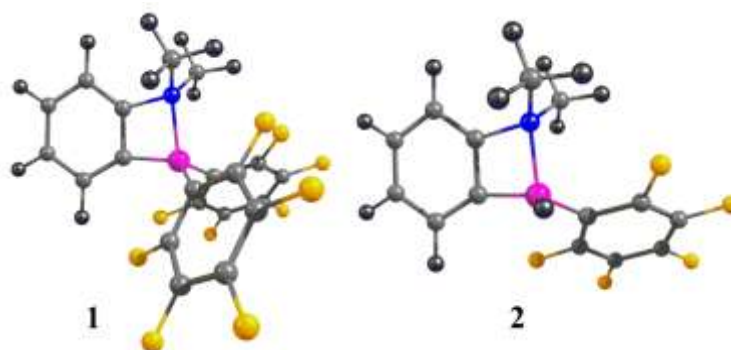


Figure 5.2 Main Group FLP complexes that have been reported experimentally; the color scheme is as follows: carbon-gray; nitrogen-blue; hydrogen-black; boron-pink; fluorine-yellow.

5.2. Computational Details

The geometry optimizations were carried out employing density functional theory (DFT) with the Turbomole 6.4 suite of programs.⁵² The Perdew, Burke, and Ernzerhof (PBE)⁵³ functional was used for the geometry optimization calculations. The triple- ζ basis set augmented by a polarization function (Turbomole basis set TZVP) was used for all the atoms. In the calculations involving the iridium catalyst, we have employed the def-TZVP basis set for the iridium atom. The resolutions of

identity (RI)⁵⁴ along with the multipole accelerated resolution of identity (marij)⁵⁵ approximations were employed for an accurate and efficient treatment of the electronic Coulomb term. In order to improve the calculation of the energy values, a further correction was made through single point B3-LYP calculations^{56,57} for the DFT (PBE)-optimized structures. Natural population analysis was done to obtain the NBO charges for certain cases described in section 5.3.3, where required, were done. Frequency calculations have been done at the DFT level in order to obtain the zero point energy, the internal energy and entropic contributions (calculated at 298.15 K). Hence, in addition to the ΔH values, ΔG values have also been reported. With regard to the transition states obtained during the investigations of the dehydrogenation process, care was taken to ensure that the obtained transition-state structures possessed only one imaginary frequency corresponding to the correct normal mode.

To check whether dispersion effects are important for these systems, we have done full optimizations of structures using Grimme's dispersion corrected functional, B97-D⁵⁸ (see section 5.3.3). Our calculations reveal that the dispersion corrections are not particularly significant for the systems that we have studied, and therefore, our TZVP/PBE/B3LYP approach is sufficiently robust to handle the newly proposed FLP systems.

5.3 Results and Discussion

The frustrated Lewis pair, **2**, which has been recently synthesized, can be employed for alcohol dehydrogenation. As shown in Figure 5.4 below, however, employing such a system would give rise to a barrier of 33.2 kcal/mol for the slowest (first step) of the reaction. This is in contrast to a barrier of 21.9 kcal/mol for the slowest (first) step of the reaction, if the iridium catalyst were to be employed (see Figure 5.5 below). It is therefore clear that **2** would not be an effective Main Group substitute for the iridium catalyst, which has been employed experimentally to dehydrogenate the alcohol.^{26,27} It is to be noted that the barriers for FLP **1**, discussed in the Introduction (section 5.1), are even higher than those calculated for **2** (see Figure 5.3), indicating that this would be even poorer at dehydrogenating the alcohol. However, beginning from **2** as the point of reference, one can modify and design new FLPs that may serve to be superior catalysts to **2**, and even rival the iridium based catalyst in dehydrogenating the alcohol.

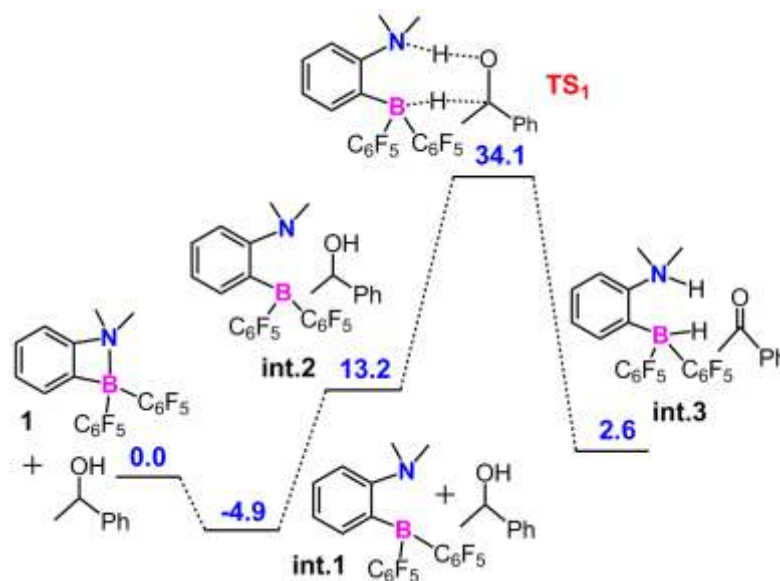


Figure 5.3 The free energy surface for the alcohol dehydrogenation reaction employing the recently synthesized metal free frustrated Lewis pair complex **1** at TZVP/PBE/B3LYP; all values are in kcal/mol.

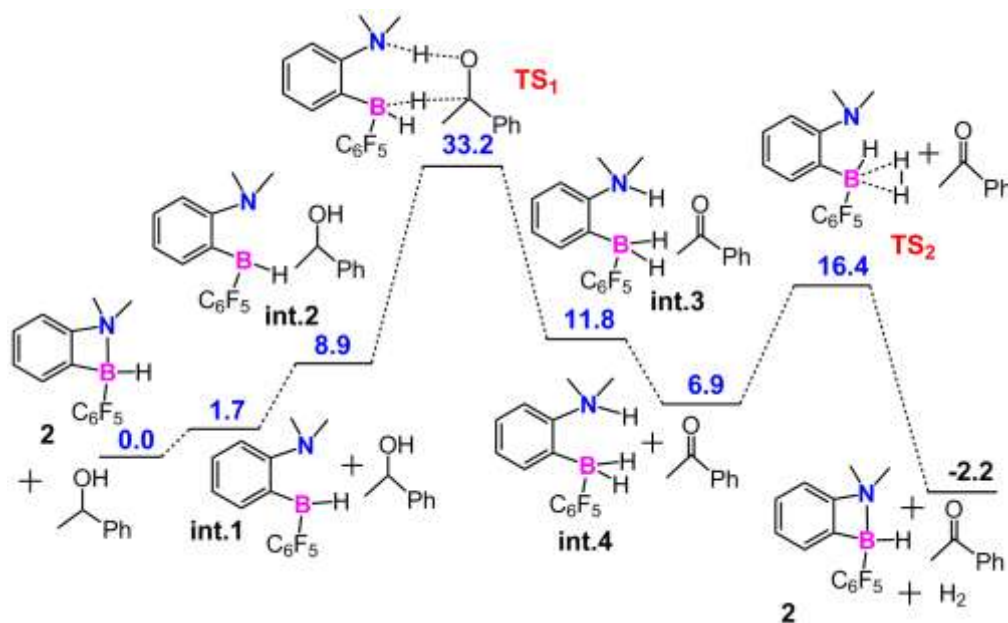


Figure 5.4 The free energy surface for the alcohol dehydrogenation reaction employing the recently synthesized metal free frustrated Lewis pair complex **2**; all values are in kcal/mol.

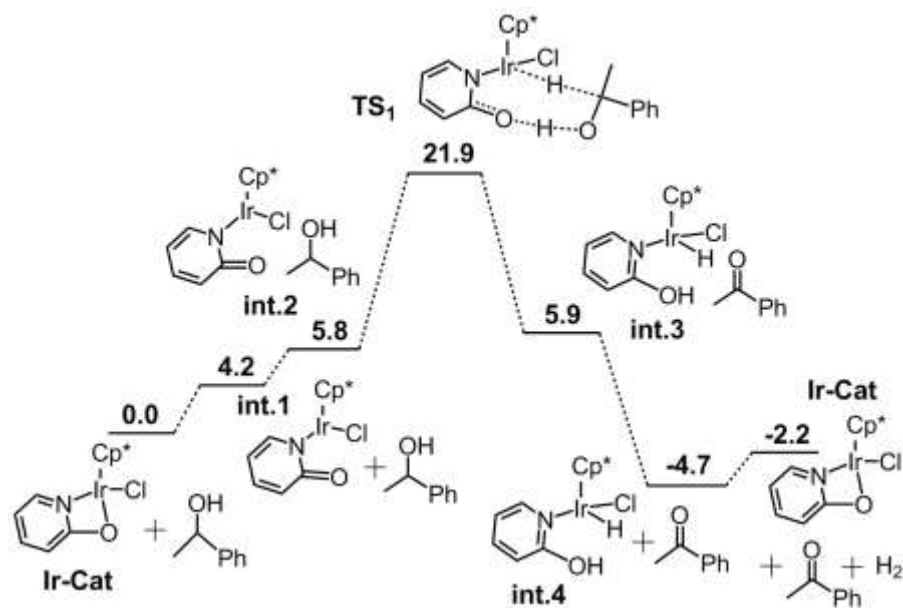


Figure 5.5 The free energy surface for the alcohol dehydrogenation reaction employing the recently synthesized iridium complex; all values are in kcal/mol.

With this in mind, we have designed four strategies for modifying **2**. As shown in Figure 5.6 below, the strategies are as follows:

Strategy I: Modify the functional groups on the nitrogen and boron of **2**. The groups modified are denoted as R₁, R₂ and R₃ respectively. As shown in Table 5.2 below, R₁ has been generally kept as the CH₃ group, while for R₂, the different groups that have been considered are: CH₃, C(CH₃)₃, CH(CH₂)₂, and the N(CH₃)₂ group, while for R₃, C₆F₅ and C(CH₃)₃ have been considered as the functional groups. Furthermore, all the corresponding cases with the hydrogens of the phenyl backbone of **2** replaced with fluorine atoms have also been considered.

Strategy II: Modify **2** by adding a linker, C(CF₃)₂-CF₂-CH₂-CH₂, between the boron and the backbone phenyl group (see Figure 5.6). As will be explained in a later section, the reason for adopting this strategy of “sewing” the boron and the backbone phenyl group together is to reduce the interaction between the boron and the nitrogen atoms, thereby sterically increasing the frustration in the FLP. Different R₂ groups have been considered for this case, including CH₃, C(CH₃)₃, CH(CH₂)₂, and the N(CH₃)₂ group. All the corresponding cases with the hydrogens of the phenyl backbone replaced with fluorine atoms have also been considered.

Strategy III: Modify **2** by adding the linker, $C(CF_3)_2-CF_2-CF_2-CF_2$, between the boron and the backbone phenyl group (see Figure 5.6). This is a variant of Strategy II, with the emphasis being on observing how having fluorines in place of hydrogens leads to a change in the alcohol dehydrogenation barrier. Different R_2 groups have been considered for this case, including CH_3 , $C(CH_3)_3$, $CH(CH_2)_2$, and the $N(CH_3)_2$ group.

Strategy IV: Modify **2** by adding a linker, $CF_2-CF_2-CF_2-CF_2$, between the boron and the backbone phenyl group (see Figure 5.6). Different R_2 groups have been considered for this case, including CH_3 , $C(CH_3)_3$, $CH(CH_2)_2$, and the $N(CH_3)_2$ group. All the corresponding cases with the hydrogens of the phenyl backbone replaced with fluorine atoms have also been considered. A possible synthetic strategy for making an FLP with a fluorinated backbone is shown in Figure 5.12.

Strategy	Complex	X = H	Complex	X = F	
I	3	$R_1 = CH_3 ; R_2 = C(CH_3)_3 ; R_3 = C_6F_5$	9	$R_1 = C(CH_3)_3 ; R_2 = CH_3 ; R_3 = C_6F_5$	
	4	$R_1 = C(CH_3)_3 ; R_2 = CH_3 ; R_3 = C_6F_5$	10	$R_1 = CH_3 ; R_2 = C(CH_3)_3 ; R_3 = C_6F_5$	
	5	$R_1 = CH_3 ; R_2 = CH(CH_3)_2 ; R_3 = C_6F_5$	11	$R_1 = CH_3 ; R_2 = CH(CH_3)_2 ; R_3 = C_6F_5$	
	6	$R_1 = CH_3 ; R_2 = N(CH_3)_2 ; R_3 = C_6F_5$	12	$R_1 = CH_3 ; R_2 = N(CH_3)_2 ; R_3 = C_6F_5$	
	7	$R_1 = CH_3 ; R_2 = CH_3 ; R_3 = C(CF_3)_3$	13	$R_1 = CH_3 ; R_2 = CH_3 ; R_3 = C(CF_3)_3$	
	8	$R_1 = CH_3 ; R_2 = N(CH_3)_2 ; R_3 = C(CF_3)_3$	14	$R_1 = CH_3 ; R_2 = N(CH_3)_2 ; R_3 = C(CF_3)_3$	
	II	15	$R_2 = CH_3$	19	$R_2 = CH_3$
		16	$R_2 = C(CH_3)_3$	20	$R_2 = C(CH_3)_3$
17		$R_2 = CH(CH_3)_2$	21	$R_2 = CH(CH_3)_2$	
18		$R_2 = N(CH_3)_2$	22	$R_2 = N(CH_3)_2$	
III	23	$R_2 = CH_3$	27	$R_2 = CH_3$	
	24	$R_2 = C(CH_3)_3$	28	$R_2 = C(CH_3)_3$	
	25	$R_2 = CH(CH_3)_2$	29	$R_2 = CH(CH_3)_2$	
	26	$R_2 = N(CH_3)_2$	30	$R_2 = N(CH_3)_2$	
IV	31	$R_2 = CH_3$	35	$R_2 = CH_3$	
	32	$R_2 = C(CH_3)_3$	36	$R_2 = C(CH_3)_3$	
	33	$R_2 = CH(CH_3)_2$	37	$R_2 = CH(CH_3)_2$	
	34	$R_2 = N(CH_3)_2$	38	$R_2 = N(CH_3)_2$	

Figure 5.6 The four strategies that have been employed for investigating the conversion of the existing catalyst system, **2**, to potential new complexes for alcohol dehydrogenation.

Before discussing the results obtained from the four strategies mentioned above, a point regarding the slowest step for the reaction cycle for the alcohol dehydrogenation catalysis is noted here. The complete catalytic cycle for the dehydrogenation of 1-phenylethanol has been shown in the Figures 5.4 and 5.5 above for the case of **2** and the iridium system respectively. As can be seen from the figures,

the cycle involves two steps, along with the respective barriers. The first step is the extraction of the hydrogens from the alcohol, leading to the formation of the ketone, while the second step involves the formation of the dihydrogen molecule, H₂, from the hydrogenated catalyst, thereby regenerating the catalyst (see Figure 5.4 above). As can be seen from Figure 5.4, the first barrier is 16.8 kcal/mol higher than the second barrier. This higher activation barrier for the first step in comparison to the second is seen to be the trend for a range of other different systems that we have considered. As shown in Table 5.1 below, the difference between the first and the second barriers is always significant (in the range 8.8-16.5 kcal/mol, see Table 5.1) for every case considered.

Table 5.1 The first and second barriers of the catalytic cycle for the dehydrogenation of 1-phenylethanol by a range of different FLP complexes considered in this study (all values are in kcal/mol).

Complex	$(\Delta G)^\ddagger$		Complex	$(\Delta G)^\ddagger$	
	TS ₁	TS ₂		TS ₁	TS ₂
8	27.9	16.8	29	28.4	16.9
15	30.2	18.9	30	17.5	3.9
18	21.7	10.2	31	24.3	15.5
19	30.0	16.4	34	22.0	10.4
22	23.9	7.4	35	21.9	12.5
25	36.8	16.3	38	21.5	9.7
26	18.3	3.7			

The reasons for this are two-fold:

- (i) The first barrier involves the interaction of two molecular species, i.e., it is an intermolecular reaction. This leads to a higher entropic cost for the reaction, thereby increasing the barrier.
- (ii) The crossing of the first barrier leads to an intermediate that is higher in energy than the reactant intermediate, while the crossing of the second barrier leads to an

intermediate that is lower in energy than the corresponding reactant intermediate. Thus, the favorability of the second reaction leads to a reduction in the second barrier.

Since all the different representative cases discussed in Table 5.1 have the second barrier lower than the first, it is clear that the rate determining step for the dehydrogenation reaction is the first step, involving the dehydrogenation of the 1-phenylethanol to the corresponding ketone. Therefore, only the first step has been considered for all the different cases that have been studied as modifications to **2** in the strategies I-IV. This has been done in order to reduce the computational cost of doing the full quantum chemical calculations for the many FLP complexes considered in the study.

The results from the different strategies adopted are discussed in the sections below.

5.3.1 Strategy I

The barriers (ΔG values) for the slowest (first) step of the reaction are shown in Table 5.2 for all the cases considered under Strategy 1. All the barriers for the alcohol dehydrogenation reaction are seen to be quite high, in the range 27.9 - 41.5 kcal/mol. Since the barriers are significantly higher than that for the iridium based system (21.9 kcal/mol), this indicates that these FLP complexes, if synthesized, would be significantly less effective than the iridium based system for the alcohol dehydrogenation. It is to be noted that for every case studied, its corresponding complex, where the hydrogens were replaced with fluorines, was also considered as a potential candidate for the alcohol dehydrogenation catalysis reaction. It is seen that this did not lead to any improvement in the barrier heights for any of the cases investigated (see Table 5.2).

It is to be noted that different conformations can be considered for the FLP complexes that have been studied under Strategy I. As shown in Figure 6 below, for the FLP complex **3**, the group R_1 is *cis* to the backbone phenyl group (denoted as “down $C(CH_3)_3$ group” in Figure 5.7 below), while for the FLP **4**, it is *trans* to the backbone phenyl group (denoted as “up $C(CH_3)_3$ group”). The calculations indicate that the “down” R_1 group case is the more energetically favorable conformer. In the cases of the FLPs **3** and **4**, the difference in energy between the two conformers is 1.7 kcal/mol, with the “down” conformer being more stable. The reason for this is steric:

having the $\text{C}(\text{CH}_3)_3$ group *cis* to the backbone phenyl increases the distance of this bulky group from the boron center, thereby making the conformer sterically more favorable. It is also observed that for **3**, the approach of the substrate alcohol is more favored in comparison to **4**, by 3.8 kcal/mol. The reason for this is that the undesired interaction between the substrate and the $\text{C}(\text{CH}_3)_3$ group is minimized in the “down conformer” in comparison to the “up”. As shown in Figure 5.7 below, the optimized structures of the reactant complexes of the two conformers with the substrate present shows that the distance between the oxygen of the incoming alcohol and the nitrogen center is significantly lower for the “down” conformer in comparison to the “up”. This indicates that putting the bulky group *cis* to the backbone phenyl or FLP complexes would yield lower barriers for the cases considered under Strategy I. Hence, for the other complexes that have been considered under this strategy, the bulkier group on the nitrogen has been kept *cis* to the phenyl ring, i.e. in the “down” conformers, as can be seen from Table 5.2 below.

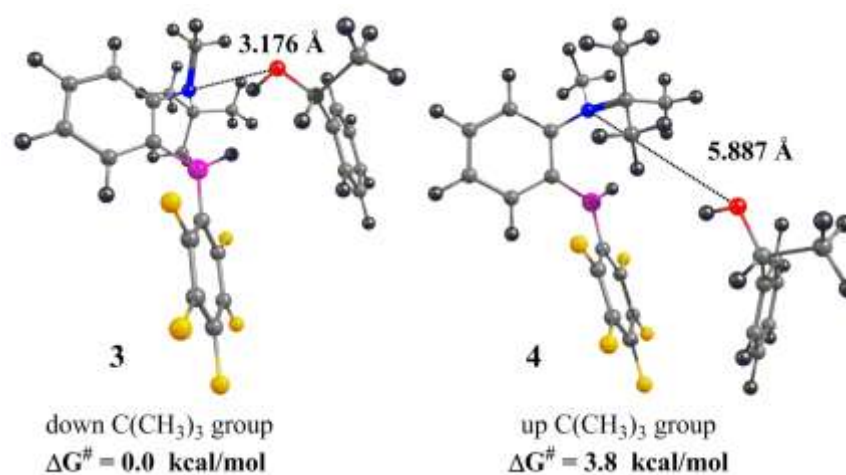
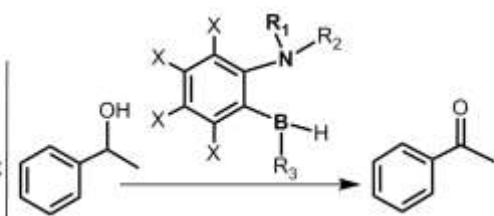


Figure 5.7 A comparison of the nitrogen-oxygen distance for two FLP cases: complexes **3** and **4**; the color scheme is as follows: carbon-gray; nitrogen-blue; hydrogen-black; boron-pink; fluorine-yellow.

These results indicate that changing the functional groups on the Lewis acidic boron and the Lewis basic nitrogen centers in the FLP is not enough to reduce the barrier for the alcohol dehydrogenation reaction, thereby implying that a different strategy has to be adopted in order to bring down the barrier. This is discussed in the next section, which discusses the results of employing Strategy II.

Table 5.2 The barrier heights (ΔG values) for the slowest step of the reaction of dehydrogenation of 1-phenylethanol by the newly designed discussed under Strategy I; all values are in kcal/mol.

Complex		Transition State (ΔG) [#]
	X = H	
3	R ₁ = CH ₃ ; R ₂ = C(CH ₃) ₃ ; R ₃ = C ₆ F ₅	31.7
4	R ₁ = C(CH ₃) ₃ ; R ₂ = CH ₃ ; R ₃ = C ₆ F ₅	35.5
5	R ₁ = CH ₃ ; R ₂ = CH(CH ₃) ₂ ; R ₃ = C ₆ F ₅	28.2
6	R ₁ = CH ₃ ; R ₂ = N(CH ₃) ₂ ; R ₃ = C ₆ F ₅	28.3
7	R ₁ = CH ₃ ; R ₂ = CH ₃ ; R ₃ = C(CF ₃) ₃	33.5
8	R ₁ = CH ₃ ; R ₂ = N(CH ₃) ₂ ; R ₃ = C(CF ₃) ₃	27.9
	X = F	
9	R ₁ = C(CH ₃) ₃ ; R ₂ = CH ₃ ; R ₃ = C ₆ F ₅	41.5
10	R ₁ = CH ₃ ; R ₂ = C(CH ₃) ₃ ; R ₃ = C ₆ F ₅	34.8
11	R ₁ = CH ₃ ; R ₂ = CH(CH ₃) ₂ ; R ₃ = C ₆ F ₅	36.9
12	R ₁ = CH ₃ ; R ₂ = N(CH ₃) ₂ ; R ₃ = C ₆ F ₅	33.3
13	R ₁ = CH ₃ ; R ₂ = CH ₃ ; R ₃ = C(CF ₃) ₃	41.2
14	R ₁ = CH ₃ ; R ₂ = N(CH ₃) ₂ ; R ₃ = C(CF ₃) ₃	31.5

5.3.2 Strategy II

The results from the previous section, where **2** was modified by putting different functional groups at the boron and nitrogen centers, suggests that this is not adequate to bring about the desired changes in the rate determining step for the alcohol dehydrogenation process. The reason the barrier heights are quite high for such cases is that there is a significant interaction between the Lewis acidic boron and the Lewis basic nitrogen centers. As can be seen from Figure 5.8 below, the distance between N and B is 1.764 Å in **2**. For the modifications discussed in Strategy I, this distance is increased only by about 0.059 Å for the best case, in terms of the greatest increase in the B-N bond distance, (for the case where R₁ = CH₃, R₂ = C(CH₃)₃ and R₃ = C₆F₅, complex **10**). Now, the slowest (first) step involves the addition of a hydrogen each at the nitrogen and the boron centers, which would occur at the cost of the interaction between the nitrogen and the boron in the FLP. Hence, any strategy that can lead to a decrease in the interaction between the N and the B centers would lead to a decrease in the barrier. This forms the basis for Strategy II, which involves the

linking of the boron and the backbone phenyl group. In doing this, the interaction between the boron and the nitrogen centers is reduced. The linker that has been employed to connect the boron and the phenyl carbon is $\text{C}(\text{CF}_3)_2\text{-CF}_2\text{-CH}_2\text{-CH}_2$. This linker has been chosen in order to maximize the withdrawal of electron density from the boron center: by putting fluorine atoms in place of hydrogens in the first two carbons attached to the boron.

Figure 5.9 below shows a comparison of the best case under Strategy I, in terms of the greatest increase in the B-N bond distance, with the worst case, among all the different linked cases studied in Strategy II, (the case where $\text{R}_1 = \text{CH}_3$, $\text{R}_2 = \text{C}(\text{CH}_3)_3$, complex **16**). What is observed is that the B-N distance is significantly increased by linking the boron to the phenyl backbone. The N-B distance is 2.566 Å in the worst Strategy II FLP case, while it is 1.823 Å in the best Strategy I FLP case. This decrease in interaction between the B and the N centers, i.e., the increase in steric frustration in the FLP in the Strategy II FLP cases should lead to greater interaction with the hydrogens of the 1-phenylethanol substrate, which could lead to a decrease in the dehydrogenation barrier.

This is indeed borne out by the calculations for all the different FLPs that have been considered in Strategy II, as shown in Table 5.3 below. In almost every case, the barriers have dropped significantly in comparison to the barriers that have been obtained for the complexes studied under Strategy I. Also, as had been done for all the cases studied under Strategy I, we have considered the effect of replacing the hydrogens of the backbone phenyl ring with fluorines for all the cases considered in Strategy II. The results, as shown in Table 5.3, indicate that this has only a marginal effect on the barriers in comparison to the corresponding non-fluorinated cases, with the barrier decreasing in two cases and increasing in the other two. This implies that fluorinating the backbone phenyl ring is unlikely to have a significant effect on the barrier heights for the alcohol dehydrogenation reaction for the cases considered under Strategy II as well.

A perusal of the results in Table 5.3 indicate that the most effective FLP among the ones considered in Strategy II is **18**: the case where $\text{R}_2 = \text{N}(\text{CH}_3)_2$. For this, the rate determining barrier has been found to be 21.7 kcal/mol. This compares very favorably with the barrier obtained for the iridium catalyst complex (21.9 kcal/mol). This

suggests that FLP complexes like **18** would be as effective as the highly efficient iridium complex in catalyzing the dehydrogenation of 1-phenylethanol.

The next section will discuss modifications to the linker connecting the boron center to the phenyl backbone.



Figure 5.8 A comparison of the boron-nitrogen distance for two cases: complexes **2** and **10**; the color scheme is as follows: carbon, gray; nitrogen, blue; hydrogen, black; boron, pink; fluorine, yellow.

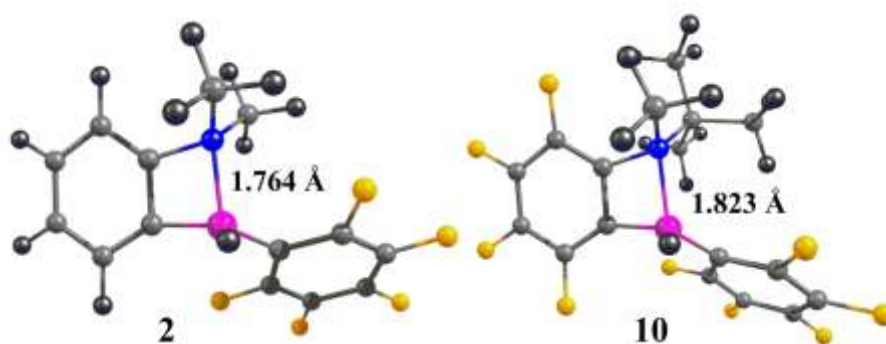
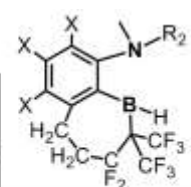


Figure 5.9 A comparison of the boron-nitrogen distance for two cases: complexes **10** and **16**; the color scheme is as follows: carbon, gray; nitrogen, blue; hydrogen, black; boron, pink; fluorine, yellow.

Table 5.3 The barrier heights (ΔG values) for the slowest step of the reaction of dehydrogenation of 1-phenylethanol by the newly designed discussed under Strategy II; all values are in kcal/mol.



Complex	Transition State (ΔG) [#]
X = H	
15	R ₂ = CH ₃ 30.2
16	R ₂ = C(CH ₃) ₃ 33.7
17	R ₂ = CH(CH ₃) ₂ 27.9
18	R ₂ = N(CH ₃) ₂ 21.7
X = F	
19	R ₂ = CH ₃ 29.6
20	R ₂ = C(CH ₃) ₃ 33.2
21	R ₂ = CH(CH ₃) ₂ 29.1
22	R ₂ = N(CH ₃) ₂ 23.9

5.3.3 Strategy III

The previous section discussed how connecting the boron and the phenyl backbone of **2** with the C(CF₃)₂CF₂-CH₂-CH₂ linker led to a significant decrease in the barrier height for the first step of the catalytic cycle, for almost all the cases considered. What is discussed in this section is the possibility of reducing the barriers even further by fluorinating all the hydrogens of the linker, i.e., by employing the linker C(CF₃)₂CF₂-CF₂-CF₂. The cases, otherwise, are the same as had been considered in Strategy II, in terms of the R₁, R₂ and R₃ groups. The values, collected in Table 5.5, show that the barrier increases marginally by about 0.6 – 1.6 kcal/mol in three cases (case **23** in comparison to case **15**; case **27** in comparison to case **19**; case **28** in comparison to case **20**). However, for the remaining five cases, the replacement of hydrogens with fluorine atoms is seen to lead to a decrease in the rate determining barrier heights. The most important cases in this regard are **26** and **30**, in which the barrier heights are reduced to 18.3 kcal/mol and 17.5 kcal/mol respectively.

An explanation for the slight increase in the barrier in some cases and the lowering of the barrier in the others when corresponding cases are considered between Strategies II and III is provided in Table 5.4 and Figure 5.10 below. An NBO charge analysis has been done for the nitrogen and the boron atoms in the transition state structures for the first transition state for the corresponding cases taken from Strategy II and Strategy III. It is seen that the charge difference between the N and the B atoms is almost the same between corresponding cases where the barrier is only slightly increased between the Strategies II and III (see Table 5.4, entries 1, 5 and 6). However, for the five Strategy III cases where the barriers are lowered, it is observed

that there is a marked reduction in the difference in the charge difference between the N and the B atoms (see Table 5.4, entries 2, 3, 4, 7 and 8). This indicates that the electrostatic interaction between the two atoms is reduced in these five Strategy III cases in comparison to their Strategy II counterparts, in the transition state structures. This would lead to greater ease of separation between the N and the B atoms, thereby reducing the barrier.

Table 5.4 The NBO charge analysis of the first transition state for different FLP complexes obtained from the Strategies II and III.

entry	complex	boron (B)	nitrogen (N)	Δ (B-N)	complex	boron (B)	nitrogen (N)	Δ (B-N)	difference (G) ^{#,a}
1	15	0.0646	-0.4153	0.4799	23	0.0244	-0.4292	0.4536	-0.9
2	16	0.1341	-0.4577	0.5918	24	0.0478	-0.4659	0.5137	0.9
3	17	0.1143	-0.4329	0.5472	25	0.0284	-0.4448	0.4732	1.1
4	18	0.0704	-0.2874	0.3578	26	-0.0339	-0.2981	0.2642	3.4
5	19	0.0210	-0.4177	0.4387	27	-0.0129	-0.4318	0.4189	-1.6
6	20	0.0542	-0.4564	0.5106	28	-0.0079	-0.4687	0.4608	-0.6
7	21	0.0605	-0.4342	0.4947	29	-0.0073	-0.4469	0.4396	0.7
8	22	0.0432	-0.3017	0.3449	30	-0.0748	-0.3016	0.2268	6.4

^aThis is the difference in the barrier height between the barrier obtained for the first transition state for the FLP in column 2 in comparison to the first transition state barrier for the corresponding FLP in column 6.

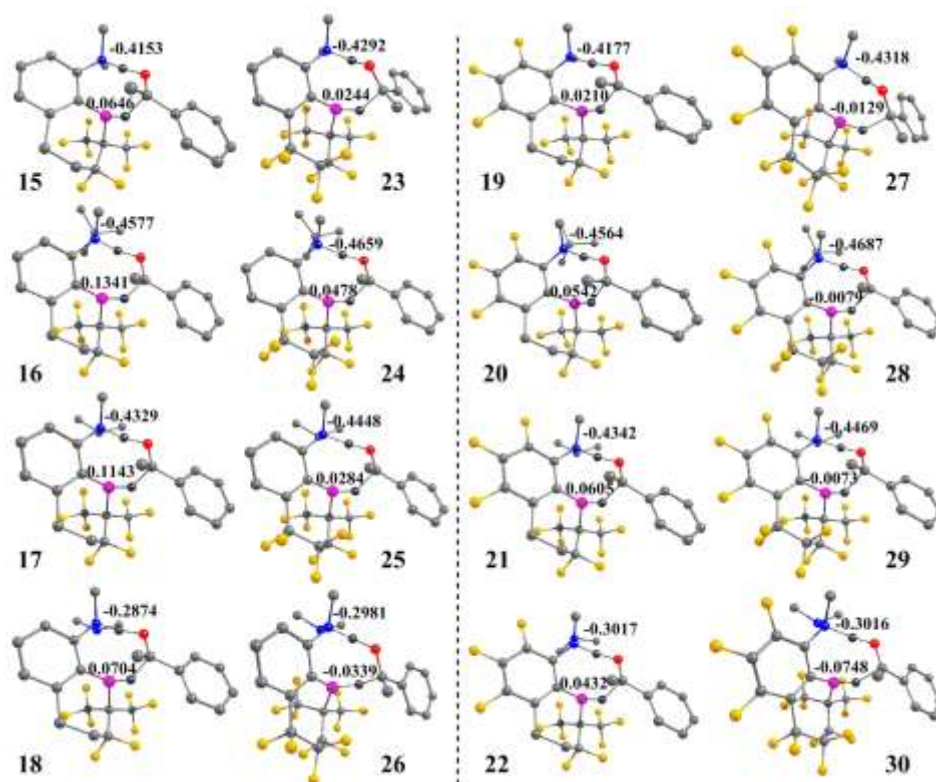


Figure 5.10 A comparison of the charges on the nitrogen (blue) and the boron (pink) atoms in the optimized transition state structures for corresponding structures taken from the Strategy II and Strategy III classes: the structures in the left (**15**, **16**, **17** and **18**; **19**, **20**, **21** and **22**) are from Strategy II and the structures to their right (**23**, **24**, **25** and **26**; **27**, **28**, **29** and **30**) are from Strategy III.

Among all the 36 cases that have been proposed and studied in this computational investigation, **30** represents the case that would be predicted to be the most efficient at doing the alcohol dehydrogenation catalysis. The complete catalytic cycle for the dehydrogenation of 1-phenylethanol by **30** is shown in Figure 5.11 below. As discussed earlier, the reactions subsequent to the first step proceed with very little further requirement of energy, with the second barrier being only 13.7 kcal/mol for the case of this FLP.

The values for the barrier heights for the slowest step for alcohol dehydrogenation for **26** and **30** are 3.6 kcal/mol and 4.4 kcal/mol lower than the corresponding barrier height for the iridium catalyst case. Hence, the current computational investigations provide a pointer to how non-metal based FLPs can be improved to make them significantly better than the state-of-the-art metal based systems at doing important chemical transformations.

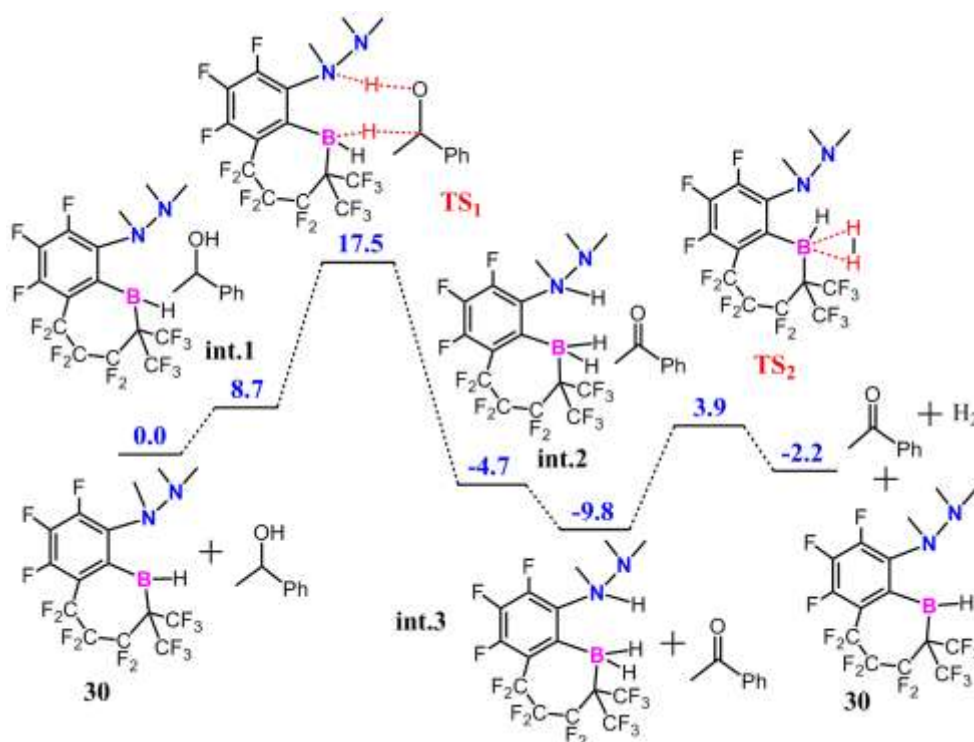
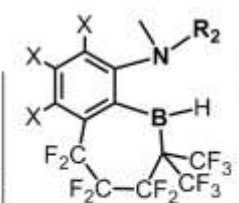


Figure 5.11 The free energy surface for the alcohol dehydrogenation reaction of employing the complex **30**; all values of free energies are given in kcal/mol.

Table 5.5 The barrier heights (ΔG values) for the slowest step of the reaction of dehydrogenation of 1-phenylethanol by the newly designed discussed under Strategy III; all values are in kcal/mol.

Complex		Transition State (ΔG) [#]
	<u>X = H</u>	
23	$R_2 = CH_3$	31.1
24	$R_2 = C(CH_3)_3$	32.8
25	$R_2 = CH(CH_3)_2$	26.8
26	$R_2 = N(CH_3)_2$	18.3
	<u>X = F</u>	
27	$R_2 = CH_3$	31.2
28	$R_2 = C(CH_3)_3$	33.8
29	$R_2 = CH(CH_3)_2$	28.4
30	$R_2 = N(CH_3)_2$	17.5

The calculations were conducted for the slowest (first) step of the reaction for FLP complexes **3**, **4**, **16**, **25**, and **30** by using B97-D functional. The results, as shown in Table 5.6 indicate that the values obtained by this TZVP/B97-D approach are quite similar to the corresponding values obtained by our reported TZVP/PBE/B3LYP approach. There is only a slight decrease observed in the barrier height when the TZVP/B97-D approach is employed: the barrier height decreases in the five cases by 1.5–2.8 kcal/mol, while the trends remain the same (see Table 5.6). Furthermore, as shown in Figures 5.12 the transition states for complexes **3** and **4**, the optimized geometries obtained from the TZVP/PBE/B3LYP and the TZVP/B97-D approaches are quite comparably similar.

Table 5.6 Comparing the barrier height of TS1 of dehydrogenation of 1-phenylethanol at B3-LYP and Grimme's B97-D functional Levels.

Entry	Complex	$TS_1(\Delta G)^\#$	
		PBE/B3-LYP	B97-D
1	3	31.7	29.5
2	4	35.5	33.9
3	16	33.7	31.2
4	25	26.8	24.0
5	30	17.5	14.8

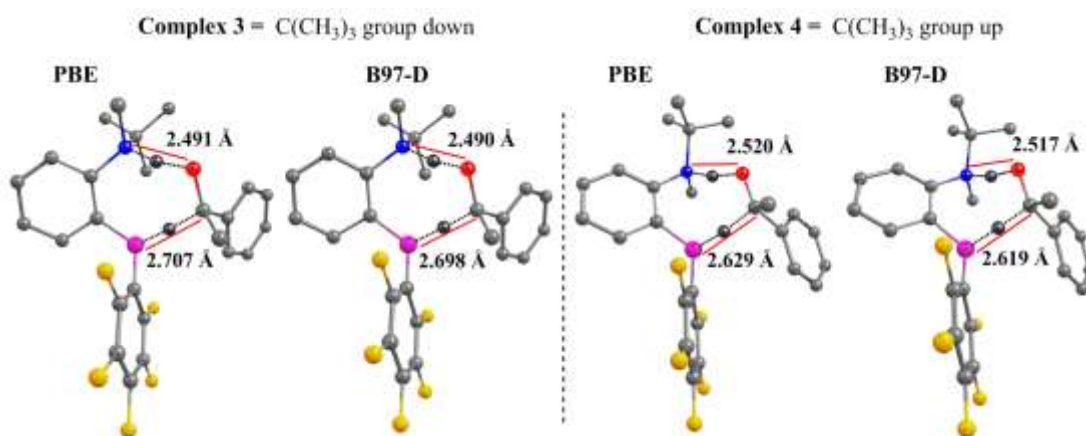


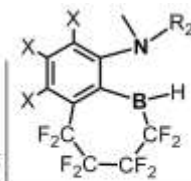
Figure 5.12 A comparison of the transition state for two FLP cases obtained from the TZVP/PBE/B3LYP and the TZVP/B97-D approaches: complexes **3** and **4**; the color scheme is as follows: carbon, gray; nitrogen, blue; hydrogen, black; boron, pink; fluorine, yellow.

5.3.4 Strategy IV

The last strategy that has been investigated is to reduce the size of the linker by replacing the $C(CF_3)_2CF_2-CF_2-CF_2$ linker employed in Strategy III with $CF_2-CF_2-CF_2-CF_2$. This replacement of the CF_3 groups in the carbon α to the boron with the smaller fluorine atoms has been done in order to reduce the possibility of steric interactions between the CF_3 groups with the hydrogens of the incoming alcohol substrate. That this change has a salutary effect on the barrier heights is evidenced by the results, collected in Table 5.6 below. The barrier heights are reduced to the range 21.5 kcal/mol – 28.9 kcal/mol for the eight cases considered. Indeed, the investigation

of these cases throws up three new possible FLPs: **38**, **35** and **34**, that have barrier heights for the slowest step (21.5 kcal/mol, 21.9 kcal/mol and 22.0 kcal/mol respectively) that are comparable to the corresponding barrier height for the iridium catalyst case (21.9 kcal/mol). This suggests that this strategy of employing a simpler linker can also lead to effective FLPs for alcohol dehydrogenation catalysis.

Table 5.6 The barrier heights (ΔG values) for the slowest step of the reaction of dehydrogenation of 1-phenylethanol by the newly designed discussed under Strategy IV; all values are in kcal/mol.



Complex	Transition State (ΔG) [#]
X = H	
31	24.3
32	27.0
33	25.8
34	22.0
X = F	
35	21.9
36	28.9
37	27.4
38	21.5

Overall, the current computational investigations indicate that one can design new FLPs beginning from an existing, experimentally synthesized, FLP, and introduce modifications that can increase the efficiency of the FLP substantially. As shown in the graph in Figure 5.15 below, out of the 36 cases investigated, there are six (**18**, **26**, **30**, **34**, **35**, **38**) that compare very favorably with the iridium catalyst, which is the state-of-the-art system present today for alcohol dehydrogenation catalysis.¹¹ It is to be noted that five of the six cases (**18**, **26**, **30**, **34**, **38**) feature an N-N bond in the FLP. It is likely that the presence of the nitrogen attached to the Lewis basic FLP nitrogen increases its Lewis basicity, and thereby leads to reduction in the barrier. Since N/B FLPs having an N-N substitution have not yet been reported, a synthetic route to making such complexes is shown in Figure 5.13 below, for the FLP case **34**. It is possible that such FLPs may also face decomposition pathways during the catalysis reaction, but such possibilities are beyond the scope of the current work.

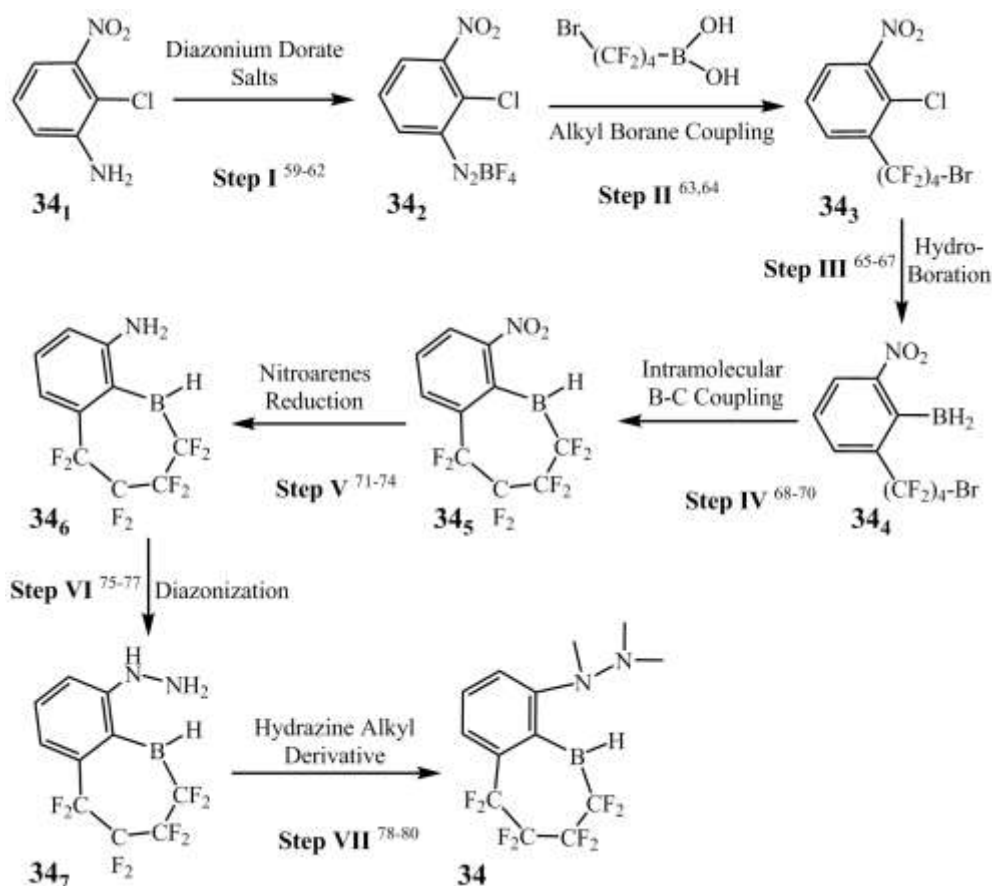


Figure 5.13 Proposed Synthesis of complex **34**.

The proposed synthetic route of the proposed compound **34** comprises a series of steps, which begins with the commercially available compound **34**₁. The **34**₁ will give diazonium-borate salt compound **34**₂ (step I)⁵⁹⁻⁶² followed by reaction with 4-bromo-1,1,2,2,3,3,4,4-octafluorobutylboronic acid to yield compound **34**₃ (step II).^{63,64} The hydro-boration of compound **34**₃ will generate compound **34**₄ (step III).⁶⁵⁻⁶⁷ The intramolecular B-C coupling as well as nitro-arenes reduction will be accomplished in the presence of a palladium based catalyst to yield compound **34**₅ and **34**₆ respectively (step IV⁶⁸⁻⁷⁰ and step V⁷¹⁻⁷⁴). The diazotization and hydrazine alkyl of compounds **34**₆ and **34**₇ will be form the final compound **34**₈ (step VI⁷⁵⁻⁷⁷ and step VII⁷⁸⁻⁸⁰).

The highly fluorinated chain would increase the electron deficiency on the boron center compared to a compound having a mixture of methylene and difluoromethylene groups, and having a more electron deficient boron centre would serve to decrease the energy barrier in the alcohol dehydrogenation reaction. This is why we have proposed highly fluorinated tethered FLP complexes like compound **34**.

This result also indicates the importance of modifying FLPs in order to increase the steric hindrance between the Lewis acid and base moieties in the FLP, thereby increasing their capacity to do new chemistry. The complete catalytic cycle for the dehydrogenation of 1-phenylethanol for the cases **18**, **26**, **34**, **35**, **38** are shown in the figure 5.14.

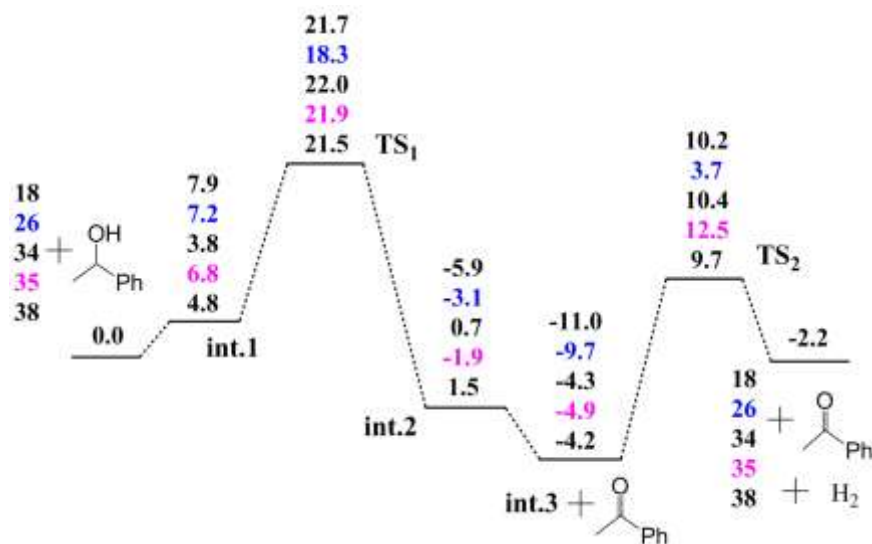


Figure 5.14 The free energy surface for the alcohol dehydrogenation reaction of employing the complexes **18**, **26**, **34**, **35**, **38**; all values of free energies are given in kcal/mol.

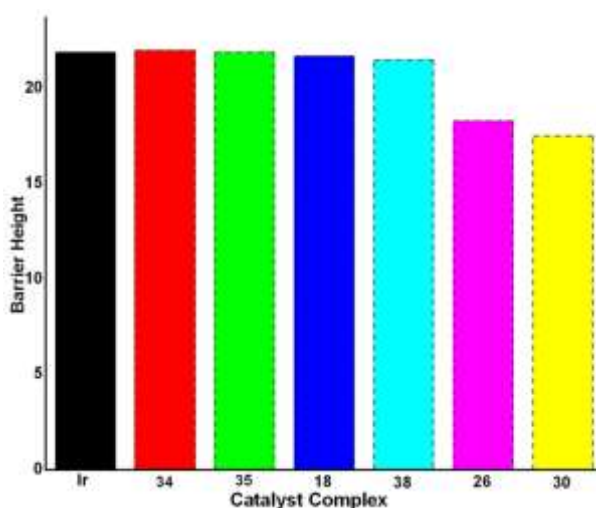


Figure 5.15 A comparison of the barrier heights for the slowest step of the alcohol dehydrogenation process for the six best FLP complexes obtained from the current study with the corresponding barrier height for the state-of-the-art iridium catalyst.

5.4 Conclusions

Full quantum chemical calculations have been done employing density functional theory (DFT) in order to test the possibility of designing new chemical systems that can do the important catalytic conversion of alcohols to the corresponding ketones. Specifically, metal free systems have been considered, based on the frustrated Lewis pairs (FLP) concept that has recently been developed.²⁸ Different strategies have been considered in order to design new FLPs beginning from an existing, experimentally synthesized, FLP⁵¹: a complex having a weak nitrogen-boron interaction that can be ruptured and regenerated during the alcohol dehydrogenation catalysis process. Careful investigations with thirty six proposed FLP complexes reveals that new FLPs can be designed with a weaker interaction between the nitrogen and boron centers, and thereby lead to systems that would be very effective at the alcohol dehydrogenation process. Indeed, there are several metal free FLP cases that have been identified through the current work that would have barriers comparable to or lower than the calculated barrier for the slowest step for the state-of-the art acceptorless alcohol dehydrogenation (AAD) metal catalyst present today.¹¹

The current work, therefore, provides insight into how one can substitute highly effective transition metal-based alcohol dehydrogenation catalyst systems with cheaper and greener metal-free catalysts, and should thus serve as a guide for experimentalists working in this important area of research.

5.5. References

- (1) Tojo, G.; Fernandez, M. *Springer: New York* **2006**.
- (2) Hudlicky, M. *American Chemical Society: Washington, DC* **1990**.
- (3) Watson, A. J. A.; Williams, J. M. J. *Science* **2010**, *329*, 635-636.
- (4) Fujita, K.-i.; Yamaguchi, R. *Synlett* **2005**, 560-571.
- (5) Nath, K.; Das, D. *Curr Sci* **2003**, *85*, 265-271.
- (6) Navarro, R. M.; Peña, M. A.; Fierro, J. L. G. *Chemical Reviews* **2007**, *107*, 3952-3991.
- (7) Piscina, P. R. d. l.; Homs, N. *Chemical Society Reviews* **2008**, *37*, 2459-2467.

- (8) Balat, H.; Kirtay, E. *International Journal of Hydrogen Energy* **2010**, *35*, 7416-7426.
- (9) Zhang, J.; Gandelman, M.; Shimon, L. J. W.; Rozenberg, H.; Milstein, D. *Organometallics* **2004**, *23*, 4026-4033.
- (10) van Buijtenen, J.; Meuldijk, J.; Vekemans, J. A. J. M.; Hulshof, L. A.; Kooijman, H.; Spek, A. L. *Organometallics* **2006**, *25*, 873-881.
- (11) Li, H.; Lu, G.; Jiang, J.; Huang, F.; Wang, Z.-X. *Organometallics* **2011**, *30*, 2349-2363.
- (12) Gunanathan, C.; Milstein, D. *Science* **2013**, *341*.
- (13) Marko, I. E.; Giles, P. R.; Tsukazaki, M.; Brown, S. M.; Urch, C. J. *Science* **1996**, *274*, 2044-2046.
- (14) Hayashi, M.; Kawabata, H. *Journal of Synthetic Organic Chemistry, Japan* **2002**, *60*, 137-144.
- (15) Sheldon, R. A.; Arends, I. W. C. E.; ten Brink, G.-J.; Dijkman, A. *Accounts of Chemical Research* **2002**, *35*, 774-781.
- (16) Sigman, M. S.; Jensen, D. R. *Accounts of Chemical Research* **2006**, *39*, 221-229.
- (17) Gligorich, K. M.; Sigman, M. S. *Chemical Communications* **2009**, 3854-3867.
- (18) Noyori, R.; Aoki, M.; Sato, K. *Chemical Communications* **2003**, 1977-1986.
- (19) Piera, J.; Bäckvall, J.-E. *Angewandte Chemie International Edition* **2008**, *47*, 3506-3523.
- (20) Gharah, N.; Chakraborty, S.; Mukherjee, A. K.; Bhattacharyya, R. *Inorganica Chimica Acta* **2009**, *362*, 1089-1100.
- (21) Almeida, M. L. S.; Beller, M.; Wang, G.-Z.; Bäckvall, J.-E. *Chemistry – A European Journal* **1996**, *2*, 1533-1536.
- (22) Hanasaka, F.; Fujita, K.-i.; Yamaguchi, R. *Organometallics* **2005**, *24*, 3422-3433.
- (23) Dobereiner, G. E.; Crabtree, R. H. *Chemical Reviews* **2009**, *110*, 681-703.
- (24) Hamid, M. H. S. A.; Williams, J. M. J. *Chemical Communications* **2007**, 725-727.
- (25) Nixon, T. D.; Whittlesey, M. K.; Williams, J. M. J. *Dalton Transactions* **2009**, 753-762.
- (26) Yamaguchi, R.; Ikeda, C.; Takahashi, Y.; Fujita, K.-i. *Journal of the American Chemical Society* **2009**, *131*, 8410-8412.

- (27) Fujita, K.-i.; Tanino, N.; Yamaguchi, R. *Organic Letters* **2007**, *9*, 109-111.
- (28) Welch, G. C.; Juan, R. R. S.; Masuda, J. D.; Stephan, D. W. *Science* **2006**, *314*, 1124-1126.
- (29) Stephan, D. W.; Erker, G. *Chemical Science* **2014**, *5*, 2625-2641.
- (30) Sajid, M.; Elmer, L.-M.; Rosorius, C.; Daniliuc, C. G.; Grimme, S.; Kehr, G.; Erker, G. *Angewandte Chemie International Edition* **2013**, *52*, 2243-2246.
- (31) Rokob, T. A.; Hamza, A.; Stirling, A.; Soós, T.; Pápai, I. *Angewandte Chemie International Edition* **2008**, *47*, 2435-2438.
- (32) Sumerin, V.; Schulz, F.; Nieger, M.; Leskelä, M.; Repo, T.; Rieger, B. *Angewandte Chemie International Edition* **2008**, *47*, 6001-6003.
- (33) Miller, A. J. M.; Bercaw, J. E. *Chemical Communications* **2010**, *46*, 1709-1711.
- (34) Zhao, L.; Lu, G.; Huang, F.; Wang, Z.-X. *Dalton Transactions* **2012**, *41*, 4674-4684.
- (35) Greb, L.; Oña-Burgos, P.; Schirmer, B.; Grimme, S.; Stephan, D. W.; Paradies, J. *Angewandte Chemie International Edition* **2012**, *51*, 10164-10168.
- (36) Zhao, L.; Li, H.; Lu, G.; Wang, Z.-X. *Dalton Transactions* **2010**, *39*, 4038-4047.
- (37) Chase, P. A.; Welch, G. C.; Jurca, T.; Stephan, D. W. *Angewandte Chemie International Edition* **2007**, *46*, 8050-8053.
- (38) Sumerin, V.; Schulz, F.; Atsumi, M.; Wang, C.; Nieger, M.; Leskelä, M.; Repo, T.; Pyykko, P.; Rieger, B. *Journal of the American Chemical Society* **2008**, *130*, 14117-14119.
- (39) Chase, P. A.; Jurca, T.; Stephan, D. W. *Chemical Communications* **2008**, 1701-1703.
- (40) Li, H.; Zhao, L.; Lu, G.; Huang, F.; Wang, Z.-X. *Dalton Transactions* **2010**, *39*, 5519-5526.
- (41) Privalov, T. *Chemistry – A European Journal* **2009**, *15*, 1825-1829.
- (42) Guo, Y.; He, X.; Li, Z.; Zou, Z. *Inorganic Chemistry* **2010**, *49*, 3419-3423.
- (43) Welch, G. C.; Stephan, D. W. *Journal of the American Chemical Society* **2007**, *129*, 1880-1881.
- (44) Spies, P.; Erker, G.; Kehr, G.; Bergander, K.; Frohlich, R.; Grimme, S.; Stephan, D. W. *Chemical Communications* **2007**, 5072-5074.

- (45) McCahill, J. S. J.; Welch, G. C.; Stephan, D. W. *Angewandte Chemie International Edition* **2007**, *46*, 4968-4971.
- (46) Guo, Y.; Li, S. *European Journal of Inorganic Chemistry* **2008**, *2008*, 2501-2505.
- (47) Guo, Y.; Li, S. *Inorganic Chemistry* **2008**, *47*, 6212-6219.
- (48) Stirling, A.; Hamza, A.; Rokob, T. A.; Papai, I. *Chemical Communications* **2008**, 3148-3150.
- (49) Staubitz, A.; Besora, M.; Harvey, J. N.; Manners, I. *Inorganic Chemistry* **2008**, *47*, 5910-5918.
- (50) Chernichenko, K.; Nieger, M.; Leskela, M.; Repo, T. *Dalton Transactions* **2012**, *41*, 9029-9032.
- (51) Chernichenko Konstantin, A. M., Imre Pa'pai, Martin Nieger, Markku Leskela, Timo Repo *Nature Chemistry* **2013**, *5*, 718-723.
- (52) Ahlrichs, R.; Baer, M.; Haeser, M.; Horn, H.; Koelmel, C. *Chem. Phys. Lett.* **1989**, *162*, 165.
- (53) Perdew, J. P.; Burke, K.; Ernzerhof, M. *Physical Review Letters* **1996**, *77*, 3865.
- (54) Eichkorn, K.; Treutler, O.; O'hm, H.; Ha'ser, M.; Ahlrichs, R. *Chemical Physics Letters* **1995**, *240*, 283-289.
- (55) Sierka, M.; Hogekamp, A.; Ahlrichs, R. *J. Chem. Phys.* **2003**, *118*, 9136.
- (56) Becke, A. D. *The Journal of Chemical Physics* **1993**, *98*, 5648-5652.
- (57) Lee, C.; Yang, W.; Parr, R. G. *Physical Review B* **1988**, *37*, 785-789.
- (58) Grimme, S. *Journal of Computational Chemistry* **2006**, *27*, 1787-1799.
- (59) Matheis, C.; Jouvin, K.; Goossen, L. J. *Organic Letters* **2014**, *16*, 5984-5987.
- (60) Darses, S.; Michaud, G.; Genêt, J.-P. *European Journal of Organic Chemistry* **1999**, *1999*, 1875-1883.
- (61) Doyle, M. P.; Bryker, W. J. *The Journal of Organic Chemistry* **1979**, *44*, 1572-1574.
- (62) Colas, C.; Goeldner, M. *European Journal of Organic Chemistry* **1999**, *1999*, 1357-1366.
- (63) Andrus, M. B.; Song, C. *Organic Letters* **2001**, *3*, 3761-3764.
- (64) Sengupta, S.; Bhattacharyya, S. *The Journal of Organic Chemistry* **1997**, *62*, 3405-3406.

- (65) Franz, D.; Bolte, M.; Lerner, H.-W.; Wagner, M. *Dalton Transactions* **2011**, 40, 2433-2440.
- (66) Seven, Ã. m.; Bolte, M.; Lerner, H.-W.; Wagner, M. *Organometallics* **2014**, 33, 1291-1299.
- (67) Lorbach, A.; Hubner, A.; Wagner, M. *Dalton Transactions* **2012**, 41, 6048-6063.
- (68) White, J.; Whiteley, C. G. *Synthesis* **1993**, 1993, 1141-1144.
- (69) Mikhailov, B. M.; Bubnov, Y. N.; Tsyban, A. V. *Journal of Organometallic Chemistry* **1978**, 154, 113-130.
- (70) Miyaura, N. *Bulletin of the Chemical Society of Japan* **2008**, 81, 1535-1553.
- (71) Cantillo, D.; Moghaddam, M. M.; Kappe, C. O. *The Journal of Organic Chemistry* **2013**, 78, 4530-4542.
- (72) Sabater, S.; Mata, J. A.; Peris, E. *Chemistry – A European Journal* **2012**, 18, 6380-6385.
- (73) Park, S.; Lee, I. S.; Park, J. *Organic & Biomolecular Chemistry* **2013**, 11, 395-399.
- (74) Sharma, S.; Kumar, M.; Kumar, V.; Kumar, N. *The Journal of Organic Chemistry* **2014**, 79, 9433-9439.
- (75) Coleman, G. H. *Organic Syntheses* **1922**, 2, 71-74.
- (76) Robinson, J. R.; Good, N. E. *Canadian Journal of Chemistry* **1957**, 35, 1578-1581.
- (77) Ohno, H.; Tanaka, H.; Takahashi, T. *Synlett* **2005**, 2005, 1191-1194.
- (78) Giumanini, A. G.; Chiavari, G.; Musiani, M. M.; Rossi, P. *Synthesis* **1980**, 1980, 743-746.
- (79) Bredihhin, A.; MÃœeorg, U. *Tetrahedron* **2008**, 64, 6788-6793.
- (80) Hisler, K.; Commeureuc, A. I. G. J.; Zhou, S.-z.; Murphy, J. A. *Tetrahedron Letters* **2009**, 50, 3290-3293.

CHAPTER 6

A Computational Study of the Hydrogenation of Unsaturated Substrates (C=O, C=N, C=C) Catalyzed by Frustrated Lewis Pairs

ABSTRACT

Catalytic hydrogenation of unsaturated compounds employing frustrated Lewis pair (FLPs) catalysts is an important area of research, because such catalysts offer a unique opportunity for the development of transition-metal-free hydrogenation. The aim of this chapter is to investigate the mechanism of metal-free catalytic hydrogenation by less frustrated and less sterically hindered FLPs, denoted as modified FLPs (MFLPs). The examination of a set of six MFLPs, for catalyzing various unsaturated compounds is investigated in detail by full quantum chemical calculations with density functional theory (DFT). In addition, a comparison of the turnover frequencies (TOFs) of FLPs and MFLPs shows that most of the cases having MFLPs would have a significantly higher TOF.

6.1 Introduction

Catalytic hydrogenation of unsaturated compounds is one of the most important reactions in chemical, industrial¹ and biological processes.² This process is facilitated by both homogeneous and heterogeneous transition metal (TM) catalysts.^{3,4} Unfortunately, transition metals are not only expensive but also require complete removal due to toxicity issues. To overcome the disadvantages of the traditional hydrogenation of unsaturated compounds, efforts have been directed to develop transition metal free hydrogenation catalysts. However, the direct reactions of molecular hydrogen with stable main group systems are quite rare and most of the reactions require harsh reaction conditions. The main-group hydride reagents (NaBH_4 and LiAlH_4)⁵ suffer various drawbacks for stoichiometric reduction, being plagued by tedious procedures and high cost, and also produce toxic chemical waste. For the reduction of organic compounds, a few strategies have been reported, such as for Hantzsch esters,⁶ the Birch reduction of arenes with sodium in ammonia,⁷ and the Meerwein–Ponndorf–Verley (MPV) transfer hydrogenation catalysis,⁸ but these procedures are stoichiometric and generate an equivalent of waste, and are more costly for production processes.

In this context, the major breakthrough towards the catalytic hydrogenation by “metal free” main group elements and Lewis acid-base pairs has been discovered by Stephan’s group in 2006.⁹ The combination of bulky Lewis acids and bulky Lewis bases, called Frustrated Lewis pairs (FLPs) has led to an important approach for the activation of molecular hydrogen and other small molecules. FLP chemistry has been employed for the hydrogenation of a wide range of unsaturated compounds, including imines,^{10,11} enamines,^{11,12} carbonyl compounds,¹³ nitriles,¹⁰ alkenes,^{14,15} alkynes,¹⁶ silylenol ethers,^{17,18} substituted olefins^{15,19,20} and aromatics,^{21,22}. Additionally, FLPs have been shown to dehydrogenate ammonia-borane^{23,24}, as well as alcohols.^{25,26} The heterolytic cleavage of H_2 is possible in the absence of the dative bond in imine-borane pairs and this type of hydrogenation of imines is much more valuable from a synthetic point of view. To date, the transition metal free catalytic hydrogenations of unsaturated compounds have been studied both experimentally²⁷⁻³⁰ and theoretically.³¹⁻³³ Stephan and co-workers have reported⁹ metal free reversible H_2 activation using a sterically encumbered Lewis acid and Lewis base, under mild

conditions, by the compound $(C_6H_2(CH_3)_3)_2P-C_6F_4-B(C_6F_5)_2$. Soon after the pioneering studies of the FLPs concept, the groups of Stephan's and Erker^{11,17,34,35} have developed several highly effective intramolecular P/B systems, while N/B systems have been explored by Repo and co-workers.³⁶⁻⁴⁰ From the theoretical point of view, the mechanism of the activation of molecular hydrogen and the hydrogenation of unsaturated compounds using FLP catalysts has been recently studied by Papai's^{16,30,33,41} and Privalov's^{25,32,42,43} groups respectively.

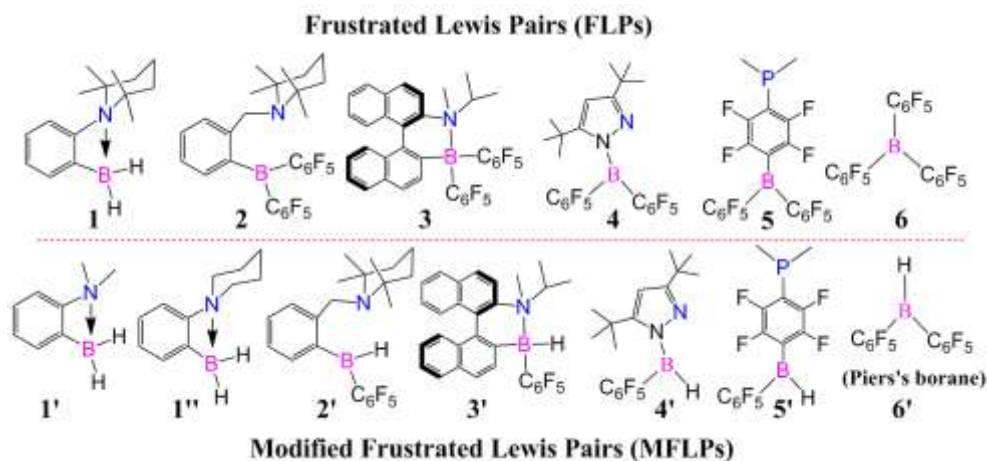


Figure 6.1 The reported and modifies FLPs catalysts used in this study for hydrogenation with H_2 .

Recently, Repo and co-workers⁴⁴ have studied with both experiment and theory the reversible activation of molecular hydrogen by using an intramolecular FLP catalyst *ansa*-aminoborane **1** (ortho-TMP- C_6H_4 - BH_2). The same group demonstrated exceptional reactivity in the asymmetric hydrogenation of imines and enamines with high stereoselectivities using the chiral bridged binaphthylaminoborane catalyst **3**.⁴¹ In 2008, Repo and Rieger reported⁴⁰ the efficient H_2 transfer to imines and other compounds by using *ansa*-aminoboranes **2** in catalytic amounts. As shown in Figure 6.1, **4** was synthesized by Tamm's group,⁴⁵ which was capable of activating H_2 in both a *cis* and a *trans* fashion. In the two step mechanism studied by Privalov,⁴⁵ the reduction of imines has been proposed to occur with the aid of a phosphonium borate complex (**5**), in which the proton transfer took place from phosphorus to nitrogen and the hydride was transferred from the boron to the carbon center of the imines. Oestreich's group⁴⁶ has reported a catalytic method for the hydrogenation of oximes to form hydroxylamines using **6** (shown in Figure 6.1).

Similarly, using **6** with 1,4-dioxane, Stephan's group has found an effective catalyst for the hydrogenation of ketones and aldehydes.

We present here a theoretical investigation, employing density functional theory (DFT), of the activation of molecular hydrogen by FLPs followed by the transfer of proton and hydride to the unsaturated (e.g. C=C, C=O, C=N) compounds to form the saturated product. We examine all the transition states and intermediates of the catalytic cycle of the newly designed catalysts that have been reported in the literature, and also show how subtle changes in the design of borane bound ligands can dramatically improve the performance of FLPs towards the hydrogenation process. We have focused mainly on the development of FLPs for hydrogenation catalysts. With this in mind, we have looked at the design of FLP catalysts in a counter-intuitive fashion by *decreasing* the frustration between the nitrogen or phosphorous and boron, thereby also decreasing the Lewis acidity and Lewis basicity, as well as the steric hindrance. Such catalyst design represents an introduction of hydrogen in place of the high electron deficient pentafluorophenyl backbone in the ligand framework. While decreasing the Lewis acidity at the boron center thus could affect the H₂ activation barrier, the hydride transfer from boron to carbon will be easily accomplished, which would result in a decrease in the activation barrier (the hydride transfer step). We have calculated all the catalytic cycles in the solvent phase, and have evaluated the efficiency of our modified catalyst to others, by comparing their relative turnover frequencies (TOFs) with the help of the 'energetic span model' (ESM), developed by Shaik and Kozuch.⁴⁷⁻⁴⁹

We have shown that such "modified FLPs" (MFLPs), shown in Figure 6.1, are a good choice of catalysts and that such species would be equally effective in other catalytic systems. The general outline of our concept is as shown in Figure 6.2, where the comparison of the barriers is illustrated for the hydrogenation of unsaturated compounds with a reported FLP that has a more electron rich center, with a modified frustrated Lewis pair catalyst (MFLP) that has a less electron deficient center. Also, we have demonstrated that dramatic changes can occur in the TOF if a less frustrated, less steric system were to be employed.

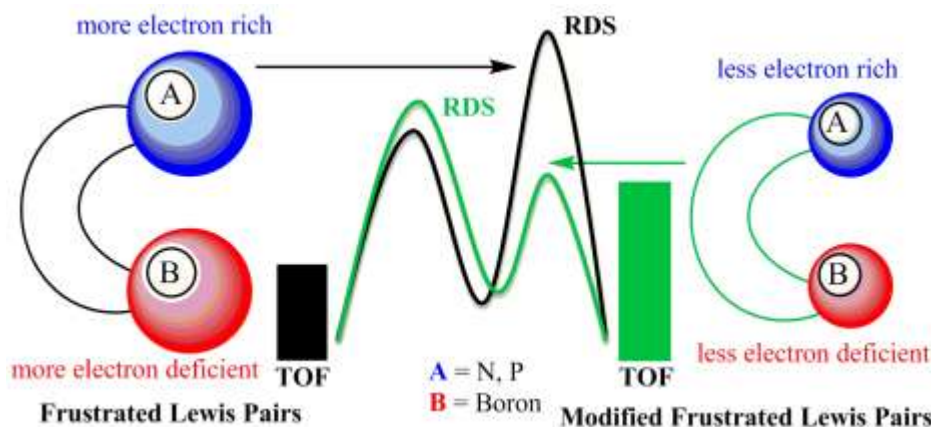


Figure 6.2 The general comparison of frustrated Lewis pairs (FLPs) with modified frustrated Lewis pairs (MFLPs) for the hydrogenation of unsaturated compounds.

6.2 Computational Details

The geometry optimizations were conducted employing density functional theory (DFT) with the Turbomole 6.4 suite of programs.⁵⁰ The Perdew, Burke, and Ernzerhof (PBE)⁵¹ functional was used for the geometry optimization calculations. The triple- ζ basis set augmented by a polarization function (Turbomole basis set TZVP) was used for all the atoms. The resolutions of identity (RI)⁵² along with the multipole accelerated resolution of identity (marij)⁵³ approximations were employed for an accurate and efficient treatment of the electronic Coulomb term. Solvent effects were accounted for as follows: we have done full geometry optimizations of all intermediates and transition states calculations using the COSMO model, with different solvents for the respective reactions. The solvents used in this study are toluene, diethyl ether, dichloromethane, 1,4-dioxane and benzene. Moreover, dispersion corrections (disp-3) were also included through these calculations.⁵⁴ To improve the calculation of the energy values, a further correction was made through single-point B3-LYP calculations^{55,56} for the DFT (PBE)-optimized structures. Frequency calculations were conducted at the DFT level to obtain the zero point energy, the internal energy, and entropic contributions (calculated at 298.15 K). With regard to the transition states obtained during the investigations of the hydrogenation process, care was taken to ensure that the obtained transition state structures possessed only one imaginary frequency corresponding to the correct normal mode. From Turbomole optimized geometries, refined energies of the hydrogenation reactions were obtained from single-point calculations, including the polarization

effects of solvent, which were considered by using the integral equation formalism: the polarizable continuum (IEFPCM)⁵⁷ solvent model calculations at the M062X/6-31+G* level using the Gaussian 09⁵⁸ program.

Described by Weinhold *et al.*, the second-order perturbation theory was applied in this study through the natural bond orbital (NBO)⁵⁹⁻⁶³ analysis using the NBO program as implemented in the Gaussian software package. On the basis of the NBO concept, the energetic importance of Lewis acid-base pairs for all the possible interactions between donor-acceptor orbitals was estimated. The donor-acceptor integrations give the estimate of the stabilization energy value $\Delta E^{(2)}$, which is calculated by the equation:

$$\Delta E^{(2)} = q_i \left[F(i, j)^2 / \varepsilon_i - \varepsilon_j \right]$$

where q_i is the donor orbital occupancy, ε_i and ε_j are the orbital energies of the donor and acceptor NBOs respectively and $F(i, j)$ are the off-diagonal NBO Fock matrix elements.

The efficiency of a catalytic cycle can be estimated through the determination of TOFs using the *AUTO*F program, which is based on the energetic span model (ESM) defined by Shaik and co-workers.⁴⁷⁻⁴⁹ According to this model, the TOF-determining transition state (TDTS) and intermediate (TDI) can be located from a catalytic cycle by the evaluation of the degree of TOF control (X_{TOF}).⁴⁷ This model has been employed to calculate the TOFs from the free energy profiles obtained for the different mechanisms discussed in this chapter.

6.3 Result and Discussion

In the present work, our main goal was the investigation of the catalytic hydrogenation of ketones, imines, oximes and enamines. Catalytic hydrogenation requires two reaction steps: first, H₂ cleavage and second, hydrogen transfer. The general idea behind this is the design of systems where the boron center would be less electrophilic, which would result in lower intrinsic Lewis acidity. In order to design new FLP catalysts, we have included six modified FLPs in our study. Figure 6.1 shows a list of modified FLPs containing *ansa*-amino borane (N/B) type of compounds (**1'**, **1''**, **2'**, **3'**), bifunctional pyrazolyborane (**4'**), P/B intramolecular FLP

(5') and a reported simple Lewis acid bis(pentafluorophenyl)borane [HB(C₆F₅)₂] (6'),^{64,65} called the Piers' borane, whereas Figure 6.3 lists seven (oxime, imine, ketone and enamine) reactants that were systematically hydrogenated in this study.

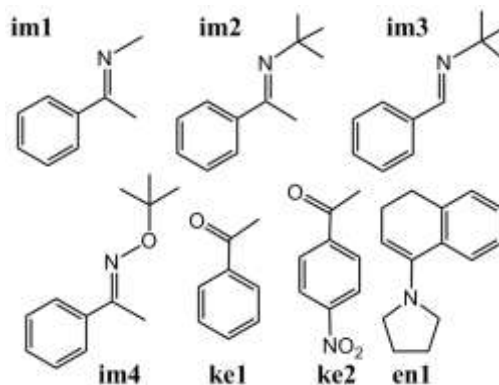


Figure 6.3 The unsaturated compounds employed in the hydrogenation reactions.

6.3.1 Hydrogen Splitting

The heterolytic cleavage of molecular hydrogen has been reported previously. These reported barriers had been calculated at a different level of theory with different solvents. We have therefore recalculated the barrier heights for the interaction of the FLP catalysts **1-5** with H₂ at the current level of theory with the solvent correction employed for the respective solvents. The calculated activation barriers are as follows: 11.1 kcal/mol, 10.7 kcal/mol, 22.2 kcal/mol and 21.0 kcal/mol for the catalysts **1**, **2**, **3** and **4** respectively. The results for the energy calculations have been included in the Table 6.1. Interestingly, while the pentafluorophenyl (C₆F₅) groups enhance the Lewis acidity of the FLP systems, the newly designed MFLPs for the less electron deficient systems are still highly reactive towards H₂ activation. Therefore, it is reasonable to conclude that the MFLPs also maintain their hydrogen-splitting capacity. The activation barriers of H₂ are 13.8 kcal/mol, 9.4 kcal/mol, 21.1 kcal/mol, 13.3 kcal/mol and 17.6 kcal/mol respectively for the MFLP catalysts **1'**, **1''**, **2'**, **3'**, **4'**. Except for the MFLP catalysts **1'** and **2'**, all other catalysts have a lower activation barrier in comparison to the corresponding FLP systems. In addition, we have also calculated the activation barrier of H₂ by **6** and modified **6'** catalysts. Experimental and theoretical reports have shown that, in the absence of the imine-borane dative bond, facile hydrogen splitting would occur. Therefore, we decided to investigate the non-covalent imine-borane and oxime-borane MFLP systems, which have a small

activation barrier of 15.2 kcal/mol and 14.3 kcal/mol respectively. The activation barrier of H₂ splitting is 20.8 kcal/mol for the MFLP catalyst **6'** with 1,4-dioxan as solvent.

Table 6.1 A comparison of the first transition state (H₂ splitting) activation barrier (ΔG^\ddagger , ΔE^\ddagger in kcal/mol) and the relative energies (ΔG , ΔE in kcal/mol) at the PBE/TZVP/B3LYP/TZVP and PBE/TZVP/M062X/6-31G* levels of theory, with solvent corrections.^[a]

Entry	FLP + H ₂	B3LYP		M06-2X	
		ΔG^\ddagger [ΔE^\ddagger]	ΔG [ΔE]	ΔE^\ddagger	ΔE
1.	1'	13.8 (5.0)	2.8 (-9.8)	3.3	-6.5
2.	1''	9.4 (0.1)	3.3 (-9.8)	0.6	-7.5
3.	2'	10.7 (0.7)	-12.1 (-28.1)	13.9	-10.1
4.	3'	13.3 (3.5)	5.1 (-6.5)	3.0	-3.8
5.	4'	17.6 (8.0)	-10.7 (-25.9)	7.3	-27.9
6.	6'-ox1	14.3 (5.2)	3.0 (-23.4)	6.1	-23.2
7.	6'-im2	15.2 (2.1)	-16.4 (-42.5)	2.4	-44.5
8.	6'-1,4-Dioxan	20.8 (16.7)	20.5 (-2.3)	21.8	0.1

^[a]The solvents are used are as follows: 1' and 1''= Dichloromethane; 2' = Benzene; 3' = Diethyl Ether; 4', 6'-ox1 and 6'-im2 = Toluene; 6'-1,4-Dioxan = 1,4-Dioxan.

6.3.2 Hydrogenation by B/N pairs

As shown in Figure 6.4, schematically describes the general catalytic cycle of the imine (or oxime) and ketone hydrogenation. On the basis of reported theoretical studies of hydrogenation reactions, the investigation for both the hydrogenation reactions involves three steps: i) molecular hydrogen activation to form the hydrogenated catalyst, ii) the transfer of hydrogens to the unsaturated compound to form the saturated product, and iii) the release of the product and regeneration of the

catalyst (see Figure 6.4). In all the intramolecular FLP catalysts (**1**, **2**, **3**, **4**), the hydride transfer is likely to be the rate determining step (TS3) for imine or oxime hydrogenation and for ketone hydrogenation, hydrogen transfer through the concerted mechanism is the rate determining step (TS2), in the catalytic cycle.

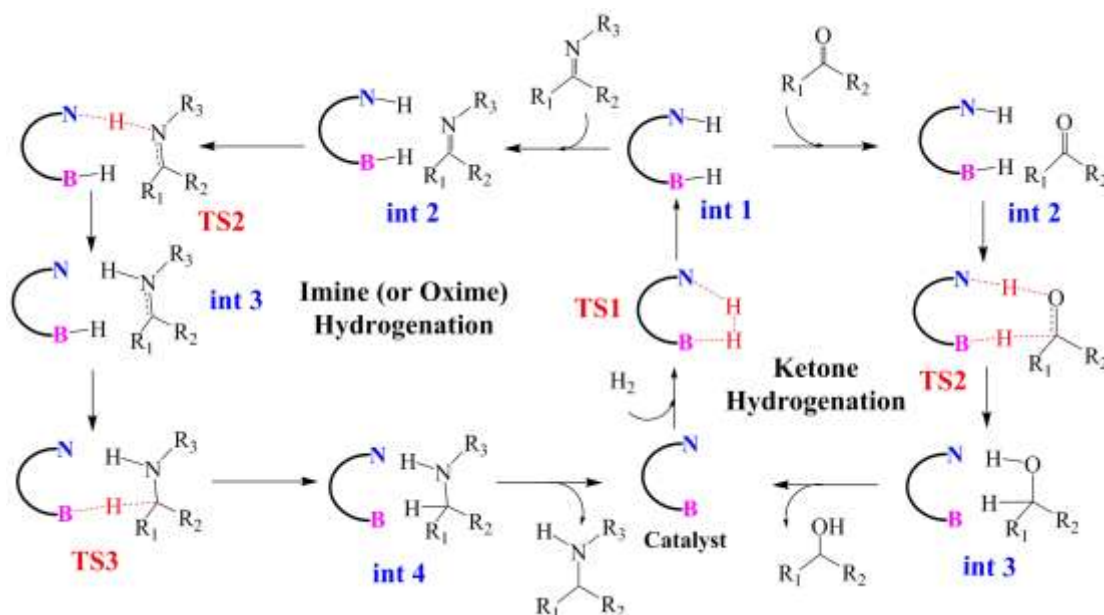


Figure 6.4 General catalytic cycles for imine and ketone hydrogenation by using MFLPs (**1'**, **1''**, **2'**, **3'**, **4'**).

In the intramolecular FLPs, there are four stable members in the heterocyclic ring, and there is a slight decrease in the steric hindrance of the acidic and basic units of the FLPs that form the dative bond. We have employed the modified FLP catalysts **1'** and **1''** for the hydrogenations of ketone and imine, having a common hydrogen splitting step. The solvent (dichloromethane, $\epsilon=8.93$) Gibbs free energy profile for (**1'**), and the complete catalytic cycle of acetophenone (ke1) and imine (im1) hydrogenation has been described in Figure 6.5. Both the hydrogenation reactions start with a common first step of di-hydrogen activation followed by transfer of hydrogen *via* the transition states TS_{ke} for ketone and TS_{im} (1-2) for imine. These then form the ketones and amines products and regenerate the catalysts **1'**. As shown in Figure 6.5, the hydrogen activation step has a barrier 13.8 kcal/mol, which is higher than the FLP catalyst **1** by 2.7 kcal/mol. For the ketone hydrogenations, the addition of acetophenone to the hydrogenated catalyst **1'** (**Int 2**) to form the second intermediate **Int_{ke}3** is followed by hydrogen transfer to the ketone by a concerted process having a barrier of 14.4 kcal/mol. The second step $TS_{ke}2$ is the rate

determining step for ketone hydrogenation to form 1-phenylethanol. As compared to the sterically hindered FLP **1**, the transition state of the rate determining step for **1'** is less by 10.7 kcal/mol. The complete energy profile of ketone hydrogenation by using **1** has been shown in the Figure 6.6.

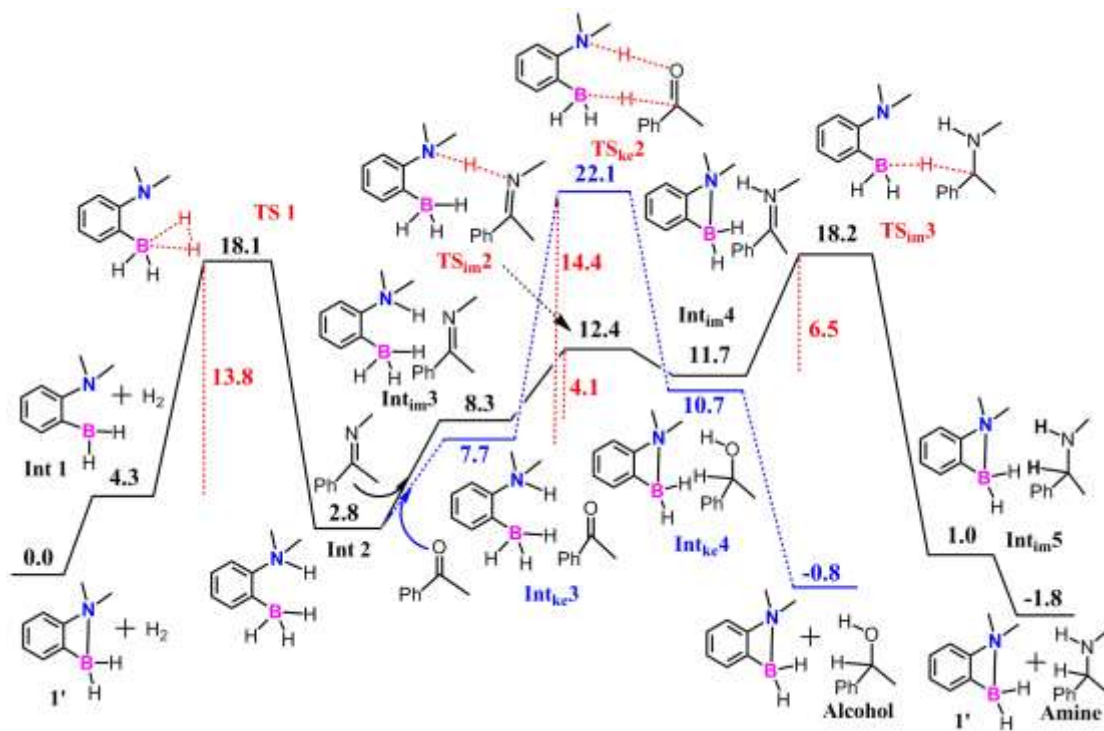


Figure 6.5 The Gibbs free energy profile for the imine (**im1**) and ketone (**ke1**) hydrogenation reaction employing modify frustrated Lewis pair complex **1'**; all values are in kcal/mol.

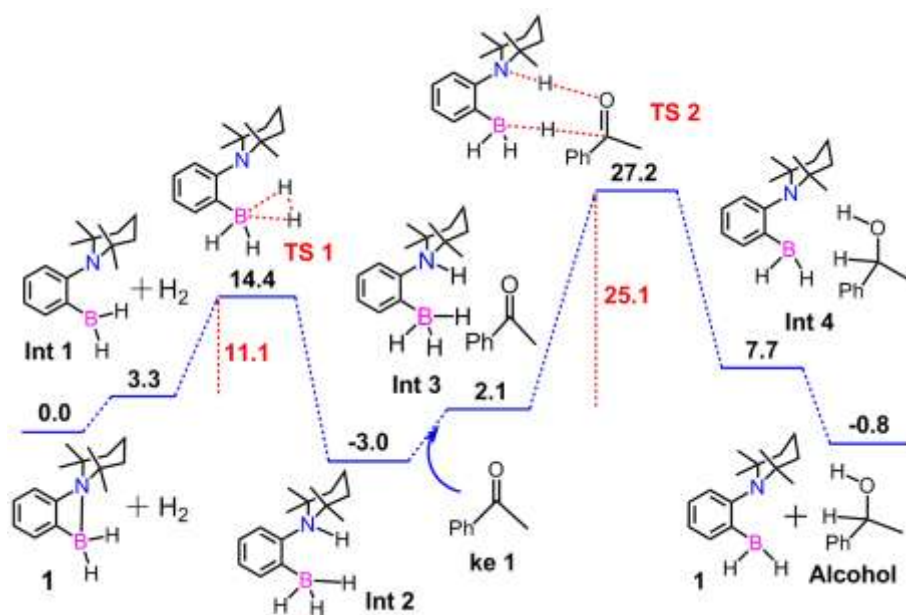


Figure 6.6 The Gibbs free energy profile for the ketone (**ke1**) hydrogenation reaction employing modify frustrated Lewis pair complex **1**; all values are in kcal/mol.

In the FLP-mediated imine hydrogenation, the processes usually take place in a stepwise fashion.^{25,32,33} The mechanisms of these proceed *via* the activation of hydrogen, then proton transfer to the nitrogen of imine, followed by hydride transfer from hydridoborate. After the first step activation of hydrogen, the transfer of the proton from N-H from **Int_{im3}** to the nitrogen of the imine to form **Int_{im4}** is endergonic by 3.4 kcal/mol in the dichloromethane solvent, with the corresponding barrier being only 4.1 kcal/mol. The last step involves the transfer of the hydride from the catalyst to the carbon of the imine to form the corresponding amine product. For this step, the barrier corresponding to the transition state **TS_{im3}** is 6.5 kcal/mol (seen Figure 6.5).

As illustrated, in the ansa-aminoboranes **2** and **3**, the Lewis acid and base are close to each other but do not form the B-N bond because of the highly hindered TMP (2,2,6,6-tetramethylpiperidino-1) and binaphthyl moieties. In our catalyst design, the idea was the introduction of less frustrated Lewis acid-base pairs at the boron center of the catalysts (**2'**, **3'**) in order to ensure the formation of the less stable boron-nitrogen bonds. Catalysts **2'** and **3'** have been modified by changing the functional group on the pentafluorophenyl (C₆F₅) group to the hydride, H, on the boron center of FLPs **2** and **3**. A comparison of the structures **2** and modified **2'** shows that the less hindered boron substituent causes lower stability of the intermediate formed. Therefore, the modified **2'** and **3'** activated H₂ produce an unstable hydrogenated product in comparison to the respective aminoboranes, **2** and **3**. For the imine (im1) hydrogenation reaction, the aminoborane **2** forms stable **2-H₂** and **3-H₂** adducts (-12.1 and -9.4 kcal/mol) compared to **2'-H₂** and **3'-H₂** (-0.4 and 5.1 kcal/mol).

We have attempted to gain further insight into the mechanism of hydrogen splitting by the modified **2'** and **3'** catalysts and the nature of the N-H, H-B dihydrogen bond interactions. The B-N dihydrogen distance of the optimized structure after hydrogen splitting in **2'**, **3'** MFLPs catalyst are 3.126 Å, 3.258 Å (as shown in figure 6.7) and for FLPs **2** and **3**, they are 3.281 Å and 3.293 Å respectively. These results suggest that there is a significant interaction between the boron and the nitrogen centers to gives a less frustrated system, upon going from **2** and **3** to **2'** and **3'** respectively. The imine (im1) forms an adduct **Int2** that is relatively unstable for

MFLP **2'** in comparison to the adduct **Int2** formed for FLP **2**. This is followed by proton and hydride transfer to the imine. The *ansa*-aminoborane **2** has a high hydride transfer barrier (21.6 kcal/mol) from the boron to the carbon center of imine, in comparison to the modified FLP **2'** (9.6 kcal/mol). The energy profile for imine hydrogenation reaction by using FLP **2'** is shown in Figure 6.8.

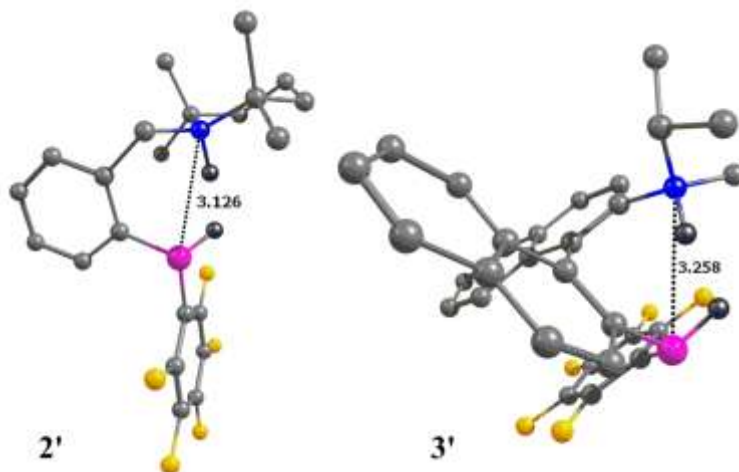


Figure 6.7 The boron-nitrogen distance for complexes **2'** and **3'**. Only the hydrogens involved are shown and the rest have been removed for the purpose of clarity. The B-N distances are shown in Å. The color scheme is as follows: carbon, gray; nitrogen, blue; hydrogen, black; boron, pink; fluorine, yellow.

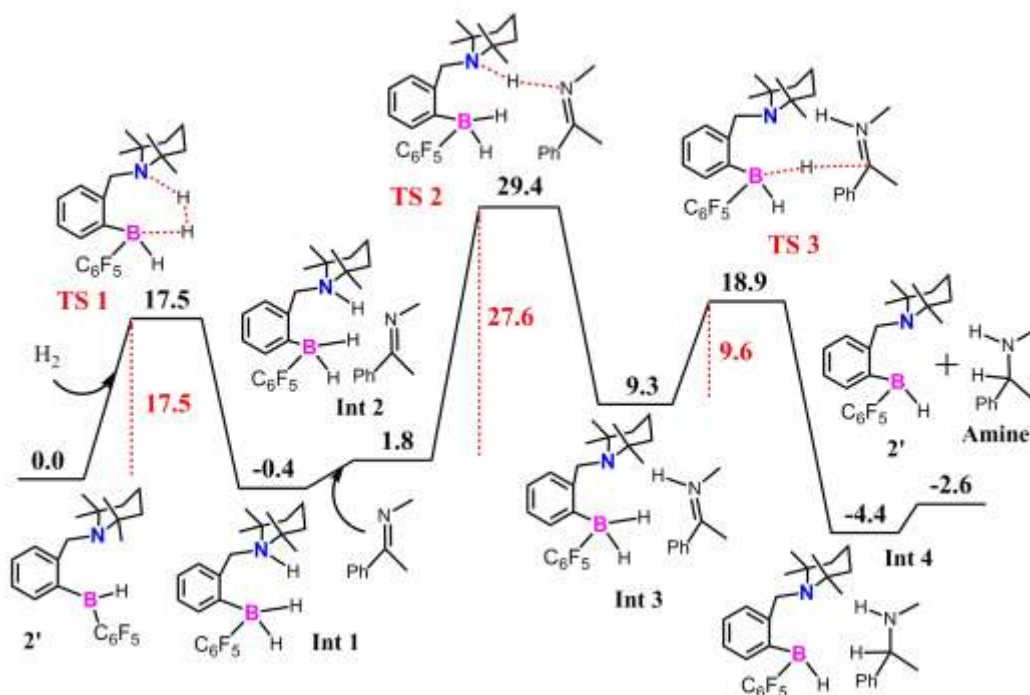


Figure 6.8 The Gibbs free energy profile for the imine (im1) hydrogenation reaction using modify frustrated Lewis pair complex **2'** with solvent; all values are in kcal/mol.

We have also carried out an NBO analysis (see Table 6.2), which provides information about electron donor-acceptor interactions. In this analysis, all possible interactions between filled (donor) and empty (acceptor) orbitals are examined and then their energies ($E^{(2)}$ values) are evaluated by second order perturbation theory. Table 6.2 shows a comparison of the transition states and intermediate structures of the full catalytic cycle for **2** and **2'**. In the transition state structures, the interactions of LP and σ with σ^* and LP* are important. An NBO analysis of the interactions between the H₂ and MFLP **2'** at the transition state (**TS1**) confirms that it has ineffective donor-acceptor interactions in comparison to FLP **2** (see Table 6.2, Entry 1). This result gives a high H₂ splitting barrier in MFLP **2'**. In **TS2**, the transfer of proton from nitrogen from **2'** to the nitrogen of imine leads to almost the same barrier as in **2**. In a last hydride transfer step (**TS3**), the donor-acceptor interactions was found to have a large stabilization energy $\sigma_{C8-H2} \rightarrow LP^*_{B3}$ and $LP^*_{B3} \rightarrow \sigma^*_{C8-H2}$ in MFLP **2'** in comparison to **2**, which resulted in a decrease in the activation barrier. These studies provide evidence that donor-acceptor interactions play a major role in the imine hydrogenation reaction. Figure 6.9 shows the selected one donor-acceptor interactions of intermediates and transition states for MFLP **2'**.

Table 6.2 Second-order perturbation stabilization energies ($E^{(2)}$ values in kcal/mol), for the intermediates and transition states for the reactions (for **2** and **2'**) as obtained by the NBO analysis.

Entry	Geo- metry	MFLP (2')		FLP (2)	
		Donor- Acceptor	$E^{(2)}$	Donor- Acceptor	$E^{(2)}$
1	TS1	$LP_{N4} \rightarrow \sigma^*_{H1-H2}$	9.90	$LP_{N4} \rightarrow \sigma^*_{H1-H2}$	9.97
		$\sigma_{H1-H2} \rightarrow LP^*_{B3}$	15.90	$\sigma_{H1-H2} \rightarrow LP^*_{B3}$	19.85
2	Int1	$\sigma_{B3-H1} \rightarrow \sigma^*_{N4-H2}$	16.81	$\sigma_{B3-H1} \rightarrow \sigma^*_{N4-H2}$	26.07
3	Int2	$LP_{N5} \rightarrow \sigma^*_{C6-H7}$	1.50	$LP_{N5} \rightarrow \sigma^*_{C6-H7}$	1.31
				$LP_{F9} \rightarrow \sigma^*_{C9-H10}$	1.17

4	TS2	$\pi_{C8-N5} \rightarrow LP^*_{H2}$	19.93	$\pi_{C8-N5} \rightarrow LP^*_{H2}$	16.05
		$LP_{N4} \rightarrow LP^*_{H2}$	271.03	$LP_{N4} \rightarrow LP^*_{H2}$	269.52
		$LP_{N5} \rightarrow LP^*_{H2}$	127.67	$LP_{N5} \rightarrow LP^*_{H2}$	125.24
5	Int3	$\sigma_{B3-H1} \rightarrow \sigma^*_{N5-H2}$	22.97	$\sigma_{B3-H1} \rightarrow \sigma^*_{N5-H2}$	11.29
6	TS3	$\sigma_{C8-H2} \rightarrow LP^*_{B3}$	129.57	$\sigma_{C8-H2} \rightarrow LP^*_{B3}$	114.47
		$LP^*_{B3} \rightarrow \sigma^*_{C8-H2}$	254.06	$LP^*_{B3} \rightarrow \sigma^*_{C8-H2}$	165.97

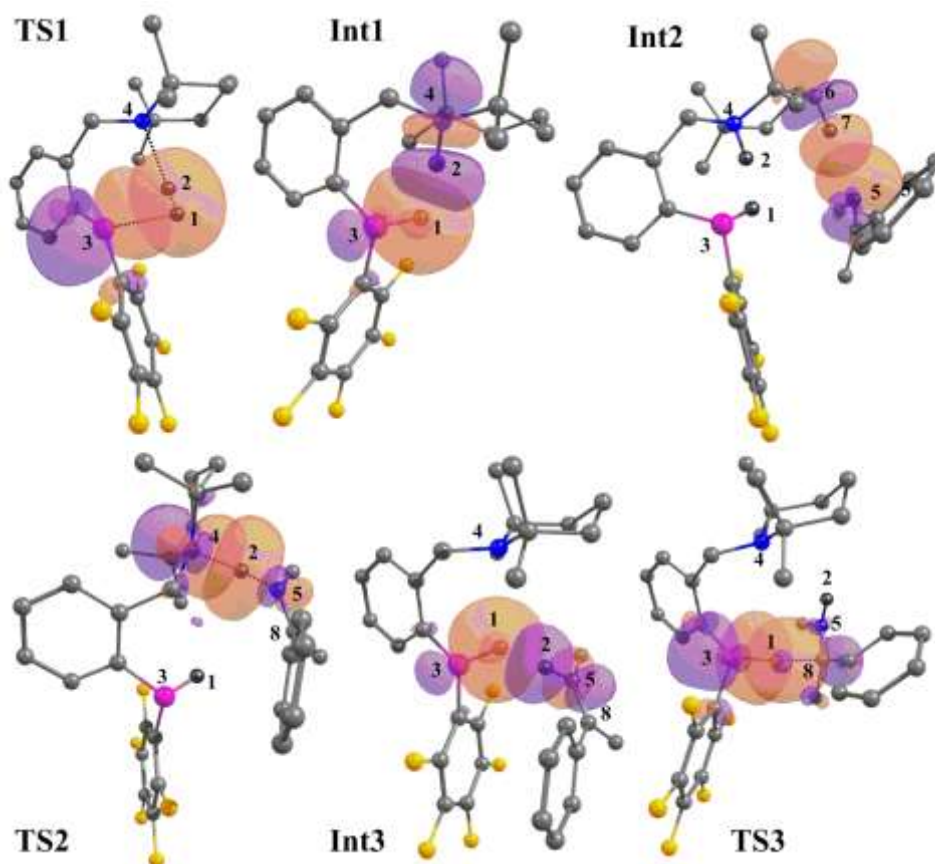


Figure 6.9 The selected NBOs donor-acceptor interaction diagram of three intermediate and three transition state structures for the imine (**im1**) hydrogenation using the MFLP **2'**.

Recently, Du's group⁶⁶⁻⁶⁸ has introduced the asymmetric hydrogenation of imines and enamines through a binaphthyl backbone. We have modified the recently developed⁴¹ chiral bridged binaphthyl backbone aminoborane **3'** catalyst for the hydrogenation of imine (**im1**) and enamine (**en1**). We have also determined the free energy profile (with diethyl ether as solvent) as reported by Repo *et al.*,⁴¹ for the

hydrogenation of enamines, as well as the full catalytic cycle of **3** (see Figure 6.10). Calculations with the modified chiral aminoborane catalyst (**3'**), indicated a decrease in the barrier height of the hydrogen splitting and the hydride transfer barrier (see Figure 6.11). In the second step, the proton transfer from the nitrogen to the carbon of enamine has a barrier of 17.4 kcal/mol, i.e. it is the rate limiting step. In MFLP **3'**, the hydride transfer barrier decreases considerably, from 26.5 kcal/mol (in the FLP **3** case) to 3.0 kcal/mol. These results indicated that the barrier heights decrease but comparing the overall reaction cycle is not helpful for the hydrogenation of enamine, if the TOFs are compared.

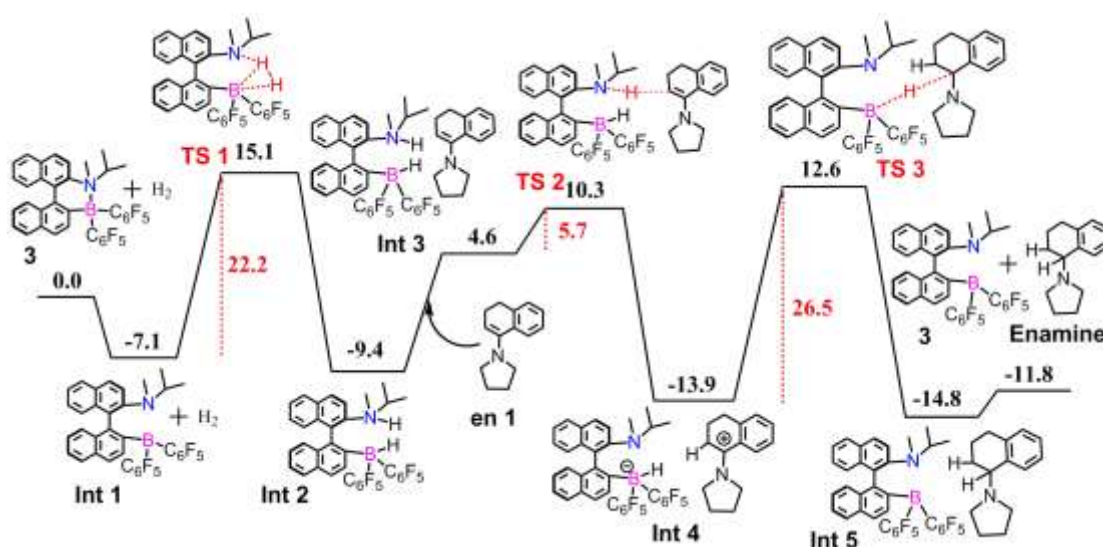


Figure 6.10 The Gibbs free energy profile for the enamine (**en1**) hydrogenation reactions, employing the modified frustrated Lewis pair complex **3**; all values are in kcal/mol.

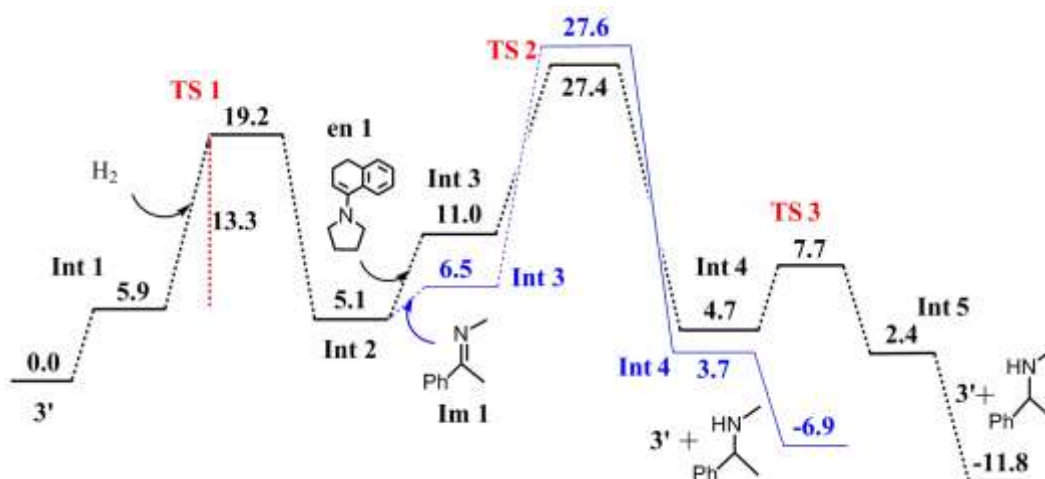


Figure 6.11 The Gibbs free energy profile for the imine (**im1**) and enamine (**en1**) hydrogenation reactions, employing the modified frustrated Lewis pair complex **3'**; all values are in kcal/mol.

For the hydrogenation of imine (**im1**) by MFLP **3'**, only two transition states were obtained. The first transition state is for H₂ splitting, which is common for the hydrogenation of imines and enamines, while **TS2** is for the proton transfer to the imine, which is the rate limiting step (see Figure 6.11), while the hydride transfer step is a barrierless process.

The FLP containing bifunctional pyrazolylborane **4** was reported for the heterolytic cleavage of dihydrogen (H₂). We have employed the modified FLP catalyst **4'**, having a less frustrated boron center. The hydrogenation of ketone (**ke1**) was studied for the case of **4'**. In the hydrogenation of **ke1**, the H₂ splitting transition state (**TS1**) barrier found to be 17.6 kcal/mol and the hydrogen transfer to ketone (**TS2**) was found to have a barrier of 28.0 kcal/mol when the MFLP **4'** was employed. The second step is the rate-determining step in both cases **4** and **4'**. It is interesting to note that for this case – for the hydrogenation of ketone, the rate determining step remains the same in both the catalytic systems (**4** and **4'**), and the only change is seen for the H₂ splitting barrier, which was decreased by 3.4 kcal/mol in the case of **4'**. The energy profiles for the complete catalytic cycles for **4** and **4'** are given in Figure 6.12.

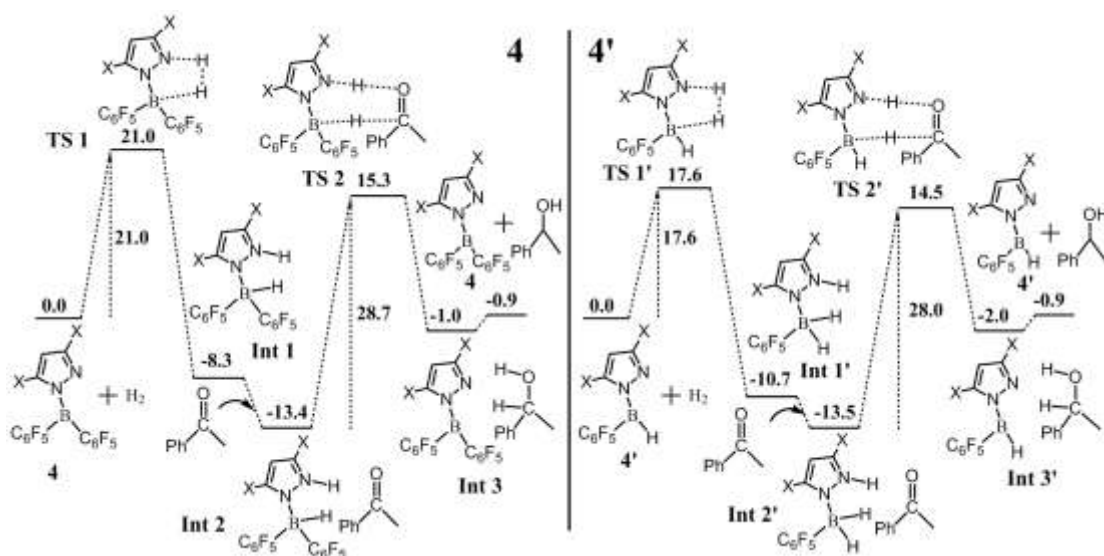


Figure 6.12 The Gibbs free energy profile for the ketone (**ke1**) hydrogenation reactions, employing the modified frustrated Lewis pair complex **4** and **4'**; all values are in kcal/mol.

We have further compared the FLPs with the MFLPs with the help of turnover frequency (TOF) calculations using the energetic span model (ESM). The basis of the ESM is the correct assumption that the TOF depends not only upon the highest energy transition state but also on other, more stable intermediates with respect to the reactants and products. It is notable that when the ESM is employed, the calculated (Turnover Determining Intermediate) TDI and the (Turnover Determining Transition State) TDTS may be different for the different catalysts employed. A perusal of the mechanistic cycles of different FLPs and also modified FLP catalysts shows that the TDI and TDTS are different for each of the reaction pathways. Table 6.3 shows the TOF comparison of the FLPs catalysts (**1**, **2**, **3**, **4**) with the modified FLPs (**1'**, **2'**, **3'**, **4'**).

Table 6.3 The absolute and relative (MFLP/FLP) turnover frequency (TOF) values obtained for FLP **1-4** and MFLP **1'-4'** catalysts with respective reactants imine, ketone and enamine. All the TOF values are in h⁻¹.

Reactant (reduction of)	MFLP	TOF (hour) ⁻¹	FLP	TOF (hour) ⁻¹	Relative TOF (MFLP/FLP)
Imine (im1)	1'	2.59 x 10 ²	1	5.03 x 10 ⁻¹¹	5.15 x 10 ¹²
	2'	1.55 x 10 ⁻⁶	2	7.04 x 10 ⁻¹²	2.20 x 10 ⁵
	3'	6.42 x 10 ⁻⁵	3	1.40 x 10 ⁻⁵	4.59
Ketone (ke1)	1'	5.11 x 10 ⁻¹	1	1.16 x 10 ⁻⁶	4.41 x 10 ⁵
	4'	8.52 x 10 ⁻⁶	4	5.83 x 10 ⁻⁹	1460
Enamine (en1)	3'	8.99 x 10 ⁻⁵	3	8.21 x 10 ⁻⁴	- 0.11

6.3.3 Hydrogenation by HB(C₆F₅)₂ and P/B FLP pairs

To date, heterolytic hydrogen splitting and hydrogenation of oxime ethers, imines and ketones have been reported by using the Lewis acid B(C₆F₅)₃.^{15,19,27,33,46,69-74} Also the Lewis acid borane species such as HBAr^F₂ (Ar^F=2,4,6-tris(trifluoromethyl)phenyl)⁷⁵ and the Piers's borane^{19,76} HB(C₆F₅)₂ with the

combination of tri-tert-butylphosphine ($t\text{Bu}_3\text{P}$) and chiral diene can act as FLP catalysts.^{66,68,77,78} This has been employed for the activation of H_2 and a highly enantioselective hydrogenation of silyl enol ethers⁶⁸ and imines.⁶⁶ Herein, our aim was to investigate whether the less frustrated $\text{HB}(\text{C}_6\text{F}_5)_2$ systems were useful for the splitting of molecular hydrogen and for catalytic reductions, with ketone or imine or oxime ethers. To this end, we have compared the full catalytic cycle for the electron deficient $\text{B}(\text{C}_6\text{F}_5)_3$ with the less deficient $\text{HB}(\text{C}_6\text{F}_5)_2$ (**6'**) catalysts with basic partners. We have considered three cases for the hydrogenation: the first hydrogenation of the oxime ether (**ox1**) and the second hydrogenation of imine (**im2**), and the third hydrogenation of 4'-nitroacetophenone (**ke2**) with 1,4-dioxan, by the modified **6'** FLP. These reactions were carried out by using toluene as solvent for the hydrogenation of oxime and imine and 1,4-dioxan as solvent for the hydrogenation of ketone.

The first step involves H_2 splitting by the oxime (**ox1**) and imine (**im2**) with a modified borane to form oxime-hydridoborate [**6'-H**][**H-oxi**]⁺ and imine-hydridoborate [**6'-H**][**H-Im**]⁺ ionic complexes having barriers of 14.4 kcal/mol (**TS_{oxi1}**) and 13.0 kcal/mol (**TS_{im1}**) respectively. After formation of the ionic intermediates, the hydrogenation of the oxime ether and imine can easily occur by hydride transfer from hydridoborane. The hydride transfer transition state barriers [8.9 kcal/mol (**TS_{oxi2}**) and 6.5 kcal/mol (**TS_{im2}**)] are lower than the H_2 splitting barriers in both the cases. In the overall reaction, the formation of the hydroxylamine and amine is an exergonic process when the modified $\text{HB}(\text{C}_6\text{F}_5)_2$ FLP (see Table 6.4) is employed. It is important to note that the overall rate of the reaction (i.e., the TOF) is decided at the H_2 splitting step for both the cycles. A catalytic turnover frequency calculation done for each catalytic cycle is shown in Table 6.4, entry 6; for both methods PBE/TZVP/B3LYP/TZVP and PBE/TZVP/M062X/6-31+G* for the hydrogenation of imine and oxime using MFLP **6'**.

In the third case, for ketone hydrogenation in the presence of Lewis acid **6'** attached to one of the oxygen atoms of the 1,4-dioxan, the formation of the complex intermediate **Int1** was seen to have higher free energy in comparison to the fully dissociated reactant species. The H_2 splitting on the **Int1** gives the hydridoborane and protonated 1,4-dioxan (**Int2**) via the transition state **TS1**. The activation free energy barrier for H_2 splitting is 20.8 kcal/mol being lower than the $\text{B}(\text{C}_6\text{F}_5)_3$ in the 1,4-dioxan transition state **TS1**. This shows that the MFLP **6'** can activate H_2 readily in

comparison to FLP **6**. The addition of ketone to the **Int2** was seen to be endergonic by 5.1 kcal/mol, but the proton transfer from 1,4-dioxan to the oxygen atom of 4'-nitroacetophenone has a barrier height of only 0.5 kcal/mol. The turnover frequency for this catalytic cycle of hydrogenation of ketone with 1,4-dioxan as solvent for **6'** is $8.04 \times 10^{-4} \text{ h}^{-1}$, which is relatively higher than the FLP **6** by 18.2 h^{-1} . All the optimized transition state structures for the hydrogenation of oxime, imine and ketone in 1,4-dioxan with **6'** catalyst are shown in Figure 6.13 below.

Table 6.4 The relative free energies ΔG (B3LYP/TZVP) and electronic energy ΔG (M06-2X/6-31+G*) for the hydrogenation of imine and oxime by the modified molecule (**6'**) in toluene, and the absolute turnover frequency (TOF) in h^{-1} . All values are in kcal/mol.

Entry	MFLPs 6'	B3LYP/TZVP (ΔG)		M06-2X/6-31+G* (ΔE)	
		Imine	Oxime	Imine	Oxime
1	Int1 + H ₂	-10.3	-5.0	-18.8	-16.7
2	TS1	4.9	9.4	-16.3	-10.6
3	Int2	-16.4	3.0	-44.5	-23.2
4	TS2	-10.9	11.9	-38.3	-15.3
5	Product	-20.1	-8.6	-41.1	-28.3
6	TOF	1.59×10^5	1.97×10^3	6.33×10^{11}	3.43×10^{10}

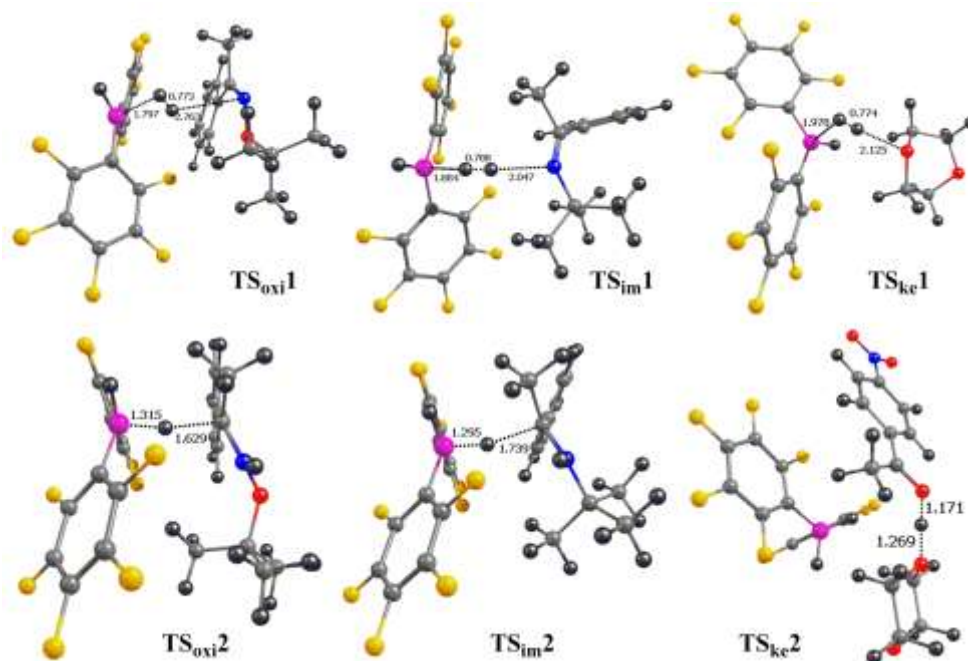


Figure 6.13 Optimized structures of the first and second transition states for the hydrogenation of **6'** to the oxime and imine, with toluene as solvent, and ketone, with 1,4-dioxan as the solvent. The transition states are denoted as TS_{oxi} for oxime, TS_{im} for imine and TS_{ke} for ketone; the key atom-atom distances are in Å. The color scheme is as follows: carbon-gray; nitrogen-blue; oxygen-red; hydrogen-black; boron-pink; fluorine-yellow.

The experimentally^{10,79} proposed two step hydrogenation of imines by the bifunctional phosphonium borate (**5**, see in figure 6.1) complexes has been studied through computational methods by Privalov.³² We have done the calculation by our methods for the **5** and modified **5'** catalysts with a sterically encumbered and electron-rich imine (*t*BuN=CPh(H)), with toluene employed as the solvent. Our aim was to decrease the rate determining step barrier. To this end, we have compared the energies of FLP **5** with the MFLP **5'**. The comparison indicates that the transition state TS2 is the rate determining step when **5** is used as the catalyst – the same as reported earlier.³² The first step is the proton transfer to the imine to form the iminium ion, having a barrier ΔG (ΔE) of 3.9 (3.5) kcal/mol, which is almost the same (ΔE) as compared to the catalyst **5**. The corresponding ΔG (ΔE) values are 0.8 (3.4) kcal/mol]. We have demonstrated that the less electron deficient boron center plays an important role in the second transition state. However, the formation of intermediate is an exergonic process in both catalysts. The second barrier, corresponding to hydride transfer to the carbon center of the corresponding iminium ion was large in **5** [ΔG

(ΔE) = 8.5 (7.4) kcal/mol] compares to the modified FLP **5'** [ΔG (ΔE) = 2.3 (0.3) kcal/mol]. The calculations were also done by another Gaussian method with single point (ΔE) calculations at the M062X/6-31+G* level. Such calculations also showed the same trend as calculated at the B3LYP level of theory. The proton transfer to nitrogen of imine (**TS1**) barrier was found to be 4.6 kcal/mol and the barrier for the second transition state (**TS2**) hydride transfer to carbon of imine was found to be only 1.3 kcal/mol. The overall exergonicity of the imine reduction is increased when the MFLP is employed. Figure 6.14 shows the energy profile for the hydrogenation of **im3** using **5'**, which has been calculated at B3LYP and M062X levels of theory. The three optimized intermediates and the two transition state structures are given in Figure 6.15 below.

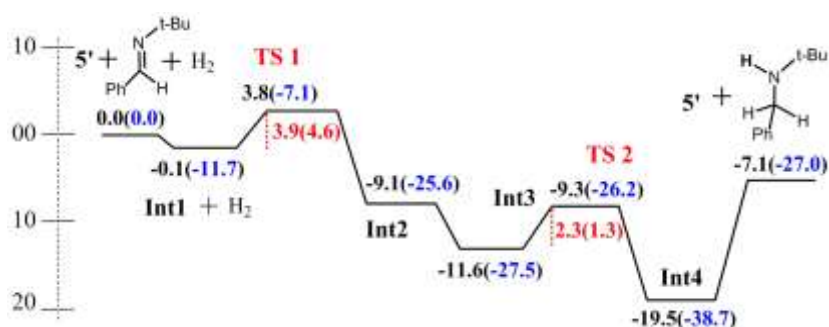


Figure 6.14 The energy profile for the reaction **5'** + **im3** + H_2 in toluene. The relative ΔG (ΔE) energies are calculated by single point B3LYP/TZVP and M06-2X/6-31+G* (in parentheses) levels respectively, with toluene as the solvent. All values are in kcal/mol.

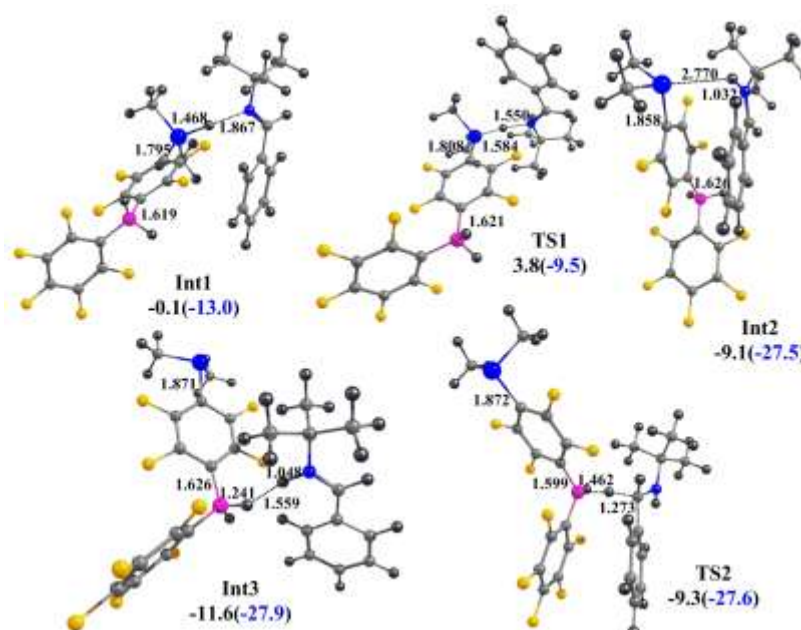


Figure 6.15 Optimized structures of the intermediates and the transition states for the hydrogenation of imine (**im3**) by hydrogenation of **5'**, with toluene employed as the solvent. The key atom-atom distances are in Å. The color scheme is as follows: carbon, gray; nitrogen, blue; oxygen, red; hydrogen, black; boron, pink; fluorine, yellow.

6.4 Conclusion

We have demonstrated that the electronic modification on both the Lewis acid and the Lewis base in FLPs provides less frustrated and less steric hindrance, leading to what we have denoted as modified FLPs or MFLPs. This approach was exemplified by the hydrogenation of unsaturated compounds, which have been studied by using a set of six MFLPs. This calculation has been studied with the aid of full quantum chemical calculations by employing density functional theory (DFT) with the solvent model (COSMO) to understanding the role of MFLPs on the heterolytic splitting of H₂ heterolytic and the hydrogenation of unsaturated compounds such as imines, ketones and enamines. The hydrogen activation with the mediation of MFLPs was seen to have better kinetics and thermodynamics in comparison to that of the other FLPs. Among the FLPs employed, the hydride transfer was observed to be the rate limiting step, but in the case of the MFLPs catalyst, for most of the cases, the molecular hydrogen splitting step and in a few cases, the proton transfer step was seen to be the rate limiting step. The change in the reaction mechanism can be attributed to the change in electronic nature and in the steric hindrance of the Lewis acids-bases. Importantly, a comparison of the turnover frequencies of FLPs and MFLPs, except for the case of enamine hydrogenation, showed that all cases having MFLPs had higher TOF, in the range of 4.59 h⁻¹ to 5.15 x 10¹² h⁻¹. Our results therefore provide important new insights into the mechanism of MFLPs mediated, heterolytic splitting of molecular hydrogen and the catalytic hydrogenation of unsaturated compounds.

6.5 References

- (1) Spindler, F.; Blaser, H.-U.; Vries, J. G. d.; Elsevier, C. J. In *The Handbook of Homogeneous Hydrogenation*; Wiley-VCH: Weinheim, Germany: 2007.
- (2) Siegbahn, P. E. M.; Eldik, R. v. In *Advances in Inorganic Chemistry*; Academic Press: 2004; Vol. Volume 56, p 101-125.
- (3) Kubas, G. J. *Chemical Reviews* **2007**, *107*, 4152-4205.

- (4) Berke, H. *ChemPhysChem* **2010**, *11*, 1837-1849.
- (5) Smith, M. B.; March, J. in *March's Advanced Organic Chemistry, Wiley Interscience, New York, 5th edn*, **2001**, pp. 1197–1204 and pp. 1544–1564.
- (6) Hantzsch, A. *Chemische Berichte* **1881**, *14*, 1637-1638.
- (7) Birch, A. J. *Journal of the Chemical Society* **1944**, 430-436.
- (8) Meerwein, H.; Schmidt, R. *Justus Liebigs Annalen der Chemie* **1925**, *444*, 221-238.
- (9) Welch, G. C.; Juan, R. R. S.; Masuda, J. D.; Stephan, D. W. *Science* **2006**, *314*, 1124-1126.
- (10) Chase, P. A.; Welch, G. C.; Jurca, T.; Stephan, D. W. *Angewandte Chemie International Edition* **2007**, *46*, 8050-8053.
- (11) Spies, P.; Schwendemann, S.; Lange, S.; Kehr, G.; Fröhlich, R.; Erker, G. *Angewandte Chemie International Edition* **2008**, *47*, 7543-7546.
- (12) Farrell, J. M.; Hatnean, J. A.; Stephan, D. W. *Journal of the American Chemical Society* **2012**, *134*, 15728-15731.
- (13) Li, H.; Zhao, L.; Lu, G.; Huang, F.; Wang, Z.-X. *Dalton Transactions* **2010**, *39*, 5519-5526.
- (14) Zhao, L.; Lu, G.; Huang, F.; Wang, Z.-X. *Dalton Transactions* **2012**, *41*, 4674-4684.
- (15) Greb, L.; Oña-Burgos, P.; Schirmer, B.; Grimme, S.; Stephan, D. W.; Paradies, J. *Angewandte Chemie International Edition* **2012**, *51*, 10164-10168.
- (16) Chernichenko Konstantin, A. M., Imre Pa'pai, Martin Nieger, Markku Leskela, Timo Repo *Nature Chemistry* **2013**, *5*, 718-723.
- (17) Erker, G.; Stephan, D. W. In *Topics in Current Chemistry*; Springer Berlin Heidelberg: **2013**; Vol. 332, p 85-110.
- (18) Stephan, D. W. *Organic & Biomolecular Chemistry* **2012**, *10*, 5740-5746.
- (19) Wang, Y.; Chen, W.; Lu, Z.; Li, Z. H.; Wang, H. *Angewandte Chemie International Edition* **2013**, *52*, 7496-7499.
- (20) Greb, L.; Daniliuc, C.-G.; Bergander, K.; Paradies, J. *Angewandte Chemie International Edition* **2013**, *52*, 5876-5879.
- (21) Zhong, G.; Chan, B.; Radom, L. *Journal of the American Chemical Society* **2007**, *129*, 924-933.

- (22) Segawa, Y.; Stephan, D. W. *Chemical Communications* **2012**, *48*, 11963-11965.
- (23) Miller, A. J. M.; Bercaw, J. E. *Chemical Communications* **2010**, *46*, 1709-1711.
- (24) Guo, Y.; He, X.; Li, Z.; Zou, Z. *Inorganic Chemistry* **2010**, *49*, 3419-3423.
- (25) Privalov, T. *Chemistry – A European Journal* **2009**, *15*, 1825-1829.
- (26) Mane, M. V.; Rizvi, M. A.; Vanka, K. *The Journal of Organic Chemistry* **2015**, *80*, 2081-2091.
- (27) Mahdi, T.; Stephan, D. W. *Journal of the American Chemical Society* **2014**, *136*, 15809-15812.
- (28) Hounjet, L. J.; Stephan, D. W. *Organic Process Research & Development* **2014**, *18*, 385-391.
- (29) Stephan, D. W. *Accounts of Chemical Research* **2015**, *48*, 306-316.
- (30) Erős, G.; Mehdi, H.; Pápai, I.; Rokob, T. A.; Király, P.; Tárkányi, G.; Soós, T. *Angewandte Chemie International Edition* **2010**, *49*, 6559-6563.
- (31) Rokob, T. A.; Bako, I.; Stirling, A.; Hamza, A.; Papai, I. *Journal of the American Chemical Society* **2013**, *135*, 4425-4437.
- (32) Privalov, T. *Dalton Transactions* **2009**, 1321-1327.
- (33) Rokob, T. A.; Hamza, A.; Stirling, A.; Papai, I. *Journal of the American Chemical Society* **2009**, *131*, 2029-2036.
- (34) Xu, B.-H.; Kehr, G.; Fröhlich, R.; Wibbeling, B.; Schirmer, B.; Grimme, S.; Erker, G. *Angewandte Chemie International Edition* **2011**, *50*, 7183-7186.
- (35) Axenov, K. V.; Kehr, G.; Frohlich, R.; Erker, G. *Journal of the American Chemical Society* **2009**, *131*, 3454-3455.
- (36) Sumerin, V.; Chernichenko, K.; Nieger, M.; Leskelä, M.; Rieger, B.; Repo, T. *Advanced Synthesis & Catalysis* **2011**, *353*, 2093-2110.
- (37) Schulz, F.; Sumerin, V.; Heikkinen, S.; Pedersen, B.; Wang, C.; Atsumi, M.; Leskela, M.; Repo, T.; Pyykko, P.; Petry, W.; Rieger, B. *Journal of the American Chemical Society* **2011**, *133*, 20245-20257.
- (38) Sumerin, V.; Schulz, F.; Nieger, M.; Atsumi, M.; Wang, C.; Leskela, M.; Pyykko, P.; Repo, T.; Rieger, B. *Journal of Organometallic Chemistry* **2009**, *694*, 2654-2660.

- (39) Sumerin, V.; Schulz, F.; Nieger, M.; Leskelä, M.; Repo, T.; Rieger, B. *Angewandte Chemie International Edition* **2008**, *47*, 6001-6003.
- (40) Sumerin, V.; Schulz, F.; Atsumi, M.; Wang, C.; Nieger, M.; Leskelä, M.; Repo, T.; Pyykko, P.; Rieger, B. *Journal of the American Chemical Society* **2008**, *130*, 14117-14119.
- (41) Lindqvist, M.; Borre, K.; Axenov, K.; Kotai, B.; Nieger, M.; Leskela, M.; Papai, I.; Repo, T. *Journal of the American Chemical Society* **2015**, *137*, 4038-4041.
- (42) Nyhlen, J.; Privalov, T. *Dalton Transactions* **2009**, 5780-5786.
- (43) Nyhlén, Jonas; Privalov, T. *Journal of Molecular Catalysis A: Chemical* **2010**, *324*, 97-103.
- (44) Chernichenko, K.; Kótai, B.; Pápai, I.; Zhivonitko, V.; Nieger, M.; Leskelä, M.; Repo, T. *Angewandte Chemie International Edition* **2015**, *54*, 1749-1753.
- (45) Theuergarten, E.; Schluns, D.; Grunenber, J.; Daniliuc, C. G.; Jones, P. G.; Tamm, M. *Chemical Communications* **2010**, *46*, 8561-8563.
- (46) Mohr, J.; Oestreich, M. *Angewandte Chemie International Edition* **2014**, *53*, 13278-13281.
- (47) Kozuch, S.; Shaik, S. *Accounts of Chemical Research* **2011**, *44*, 101-110.
- (48) Kozuch, S.; Shaik, S. *Journal of the American Chemical Society* **2006**, *128*, 3355-3365.
- (49) Uhe, A.; Kozuch, S.; Shaik, S. *Journal of Computational Chemistry* **2011**, *32*, 978-985.
- (50) Ahlrichs, R.; Bar, M.; Haser, M.; Horn, H.; Kolmel, C. *Chemical Physics Letters* **1989**, *162*, 165-169.
- (51) Perdew, J. P.; Burke, K.; Ernzerhof, M. *Physical Review Letters* **1996**, *77*, 3865.
- (52) Eichkorn, K.; Treutler, O.; O`hm, H.; Ha`ser, M.; Ahlrichs, R. *Chemical Physics Letters* **1995**, *240*, 283-289.
- (53) Sierka, M.; Hogeckamp, A.; Ahlrichs, R. *J. Chem. Phys.* **2003**, *118*, 9136.
- (54) Grimme, S. *Journal of Computational Chemistry* **2006**, *27*, 1787-1799.
- (55) Becke, A. D. *The Journal of Chemical Physics* **1993**, *98*, 5648-5652.
- (56) Lee, C.; Yang, W.; Parr, R. G. *Physical Review B* **1988**, *37*, 785-789.

- (57) Tomasi, J.; Mennucci, B.; Cammi, R. *Chemical Reviews* **2005**, *105*, 2999-3094.
- (58) Frisch, M. J.; Trucks, G. W.; Schlegel, H. B.; Scuseria, G. E.; Robb, M. A.; Cheeseman, J. R.; Scalmani, G.; Barone, V.; Mennucci, B.; Petersson, G. A.; Nakatsuji, H.; Caricato, M.; Li, X.; Hratchian, H. P.; Izmaylov, A. F.; Bloino, J.; Zheng, G.; Sonnenberg, J. L.; Hada, M.; Ehara, M.; Toyota, K.; Fukuda, R.; Hasegawa, J.; Ishida, M.; Nakajima, T.; Honda, Y.; Kitao, O.; Nakai, H.; Vreven, T.; Montgomery, J. A.; Peralta, J. E.; Ogliaro, F.; Bearpark, M.; Heyd, J. J.; Brothers, E.; Kudin, K. N.; Staroverov, V. N.; Kobayashi, R.; Normand, J.; Raghavachari, K.; Rendell, A.; Burant, J. C.; Iyengar, S. S.; Tomasi, J.; Cossi, M.; Rega, N.; Millam, J. M.; Klene, M.; Knox, J. E.; Cross, J. B.; Bakken, V.; Adamo, C.; Jaramillo, J.; Gomperts, R.; Stratmann, R. E.; Yazyev, O.; Austin, A. J.; Cammi, R.; Pomelli, C.; Ochterski, J. W.; Martin, R. L.; Morokuma, K.; Zakrzewski, V. G.; Voth, G. A.; Salvador, P.; Dannenberg, J. J.; Dapprich, S.; Daniels, A. D.; Farkas; Foresman, J. B.; Ortiz, J. V.; Cioslowski, J.; Fox, D. J. In *Gaussian 09, Revision B.01*, Gaussian, Inc., Wallingford CT Wallingford CT, 2009.
- (59) Reed, A. E.; Curtiss, L. A.; Weinhold, F. *Chemical Reviews* **1988**, *88*, 899-926.
- (60) Reed, A. E.; Weinhold, F.; Curtiss, L. A.; Pochatko, D. J. *The Journal of Chemical Physics* **1986**, *84*, 5687-5705.
- (61) Reed, A. E.; Weinhold, F. *The Journal of Chemical Physics* **1983**, *78*, 4066-4073.
- (62) Foster, J. P.; Weinhold, F. *Journal of the American Chemical Society* **1980**, *102*, 7211-7218.
- (63) Reed, A. E.; Weinstock, R. B.; Weinhold, F. *The Journal of Chemical Physics* **1985**, *83*, 735-746.
- (64) Parks, D. J.; von H. Spence, R. E.; Piers, W. E. *Angewandte Chemie International Edition in English* **1995**, *34*, 809-811.
- (65) Parks, D. J.; Piers, W. E.; Yap, G. P. A. *Organometallics* **1998**, *17*, 5492-5503.
- (66) Liu, Y.; Du, H. *Journal of the American Chemical Society* **2013**, *135*, 6810-6813.
- (67) Zhang, Z.; Du, H. *Angewandte Chemie International Edition* **2015**, *54*, 623-626.
- (68) Wei, S.; Du, H. *Journal of the American Chemical Society* **2014**, *136*, 12261-12264.

-
- (69) Holthausen, M. H.; Colussi, M.; Stephan, D. W. *Chemistry – A European Journal* **2015**, *21*, 2193-2199.
- (70) Stephan, D. W. *Dalton Transactions* **2009**, 3129-3136.
- (71) Hounjet, L. J.; Bannwarth, C.; Garon, C. N.; Caputo, C. B.; Grimme, S.; Stephan, D. W. *Angewandte Chemie International Edition* **2013**, *52*, 7492-7495.
- (72) Paradies, J. *Angewandte Chemie International Edition* **2014**, *53*, 3552-3557.
- (73) Privalov, T. *European Journal of Inorganic Chemistry* **2009**, *2009*, 2229-2237.
- (74) Scott, D. J.; Fuchter, M. J.; Ashley, A. E. *Journal of the American Chemical Society* **2014**, *136*, 15813-15816.
- (75) Lu, Z.; Cheng, Z.; Chen, Z.; Weng, L.; Li, Z. H.; Wang, H. *Angewandte Chemie International Edition* **2011**, *50*, 12227-12231.
- (76) Nikonov, G. I.; Vyboishchikov, S. F.; Shirobokov, O. G. *Journal of the American Chemical Society* **2012**, *134*, 5488-5491.
- (77) Chen, D.; Wang, Y.; Klankermayer, J. *Angewandte Chemie International Edition* **2010**, *49*, 9475-9478.
- (78) Ghattas, G.; Chen, D.; Pan, F.; Klankermayer, J. *Dalton Transactions* **2012**, *41*, 9026-9028.
- (79) McCahill, J. S. J.; Welch, G. C.; Stephan, D. W. *Angewandte Chemie International Edition* **2007**, *46*, 4968-4971.

Chapter 7

Summary

The present thesis has addressed two aspects that are significant in dihydrogen chemistry: fuel cells and frustrated Lewis pairs (FLPs).

The key findings of this thesis are as follows:

- The third chapter has focused on newly proposed proton exchange membranes (PEMs) that can perform significantly in the absence of water at high temperatures. The recently synthesized and characterized zero-dimensional doped N-cage structures have the potential to be excellent PEMs in fuel cells. This potential has been examined through full quantum mechanical calculations with DFT and MP2 methods. The results indicate that the hydrogenated N-cage system doped with 1,2,3- triazole would be likely to perform in a highly efficient manner as a PEM. Therefore, the effectiveness of the proposed fuel cell membrane would also be high at higher temperatures.
- What is essential for efficiency in the PEM is the reorientation barrier in certain type of pendant group PEMs, which was the focal point of the fourth chapter. What has been proposed in this chapter is a new design of nitrogen containing pendant group PEMs on a polymer backbone that can satisfy these criteria. The results indicate that the proton transfer will be likely to take place with barriers significantly lower than those predicted for other pendant group PEMs. The current work thus opens up promising new possibilities in the field of PEM fuel cells.
- In the last few years, the chemistry of FLPs has been developed at a spectacular pace. The reactions discovered with FLPs have opened up new

avenues in small molecule activation and hydrogenation-dehydrogenation reactions. Computational studies have allowed the establishment of effective mechanistic studies to aid the experimental breakthroughs. Our quantum chemical calculations have been conducted by employing density functional theory (DFT) to test the possibility of designing new catalysts that can do the important hydrogen splitting and the catalytic conversion of hydrogenation-dehydrogenation reactions to the corresponding products. Specifically, transition-metal free catalysts have been considered, based on the FLP concept. 36 proposed FLP complexes have been proposed and studied, revealing new FLPs that can be designed with a weaker interaction between the nitrogen and boron centers, which can thereby lead to systems that would be very effective at the alcohol dehydrogenation process. Also, we have demonstrated that the electronic modification on FLPs provides lower frustration and less steric hindrance, denoted as modified FLPs (MFLPs). This approach is shown to be highly effective for the heterolytic splitting of H₂ and the hydrogenation of unsaturated compounds such as imines, ketones and enamines. Finally, these results indicate that the newly designed FLPs can be even better than transition metal based systems at important chemical transformations.